UNIVERSIDADE FEDERAL DE SANTA CATARINA
CENTRO TECNOLÓGICO
PROGRAMA DE PÓS-GRADUAÇÃO EM ENGENHARIA MECÂNICA

Maria Fernanda Possebon Mazer

THEORETICAL ANALYSIS OF REFRIGERANTS AND CARBON DIOXIDE BINARY BLENDS FOR COMBINED SPACE AND WATER HEATING HEAT PUMP CYCLES

Florianópolis
2023

Maria Fernanda Possebon Mazer

THEORETICAL ANALYSIS OF REFRIGERANTS AND CARBON DIOXIDE BINARY BLENDS FOR COMBINED SPACE AND WATER HEATING HEAT PUMP CYCLES

Dissertação do Programa de Pós-Graduação em Engenharia Mecânica do Centro Tecnológico da Universidade Federal de Santa Catarina para a Obtenção do Título de Mestre em Engenharia Mecânica.
Orientador: Prof. Alexandre Kupka da Silva, Ph. D.
Coorientadora: Dra. Olivia Carolina da Rosa

Florianópolis
2023

Ficha de identificação da obra elaborada pelo autor,
através do Programa de Geração Automática da Biblioteca Universitária da UFSC.

MAZER, MARIA FERNANDA POSSEBON
THEORETICAL ANALYSIS OF REFRIGERANTS AND CARBON DIOXIDE BINARY BLENDS FOR COMBINED SPACE AND WATER HEATING HEAT PUMP CYCLES / MARIA FERNANDA POSSEBON MAZER ; orientador, ALEXANDRE KUPKA DA SILVA, coorientadora, OLIVIA CAROLINA DA ROSA, 2023.
96 p.

2. BOMBA DE CALOR. 3. CO2. 4. MISTURAS. 5. REFRIGERANTES. I. DA SILVA, ALEXANDRE KUPKA. II. DA ROSA, OLIVIA CAROLINA. III. Universidade Federal de Santa Catarina. Programa de Pós-Graduação em Engenharia Mecânica. IV. Título.

Maria Fernanda Possebon Mazer

THEORETICAL ANALYSIS OF REFRIGERANTS AND CARBON DIOXIDE BINARY BLENDS FOR COMBINED SPACE AND WATER HEATING HEAT PUMP CYCLES

O presente trabalho em nível de Mestrado foi avaliado e aprovado, em 26 de Junho de 2023, pela banca examinadora composta pelos seguintes membros:

Professor Joaquim Manoel Gonçalves, Dr.

Professor Louis Gosselin, PhD.

Certificamos que essa é a versão original e final do trabalho de conclusão que foi julgado adequado para obtenção do título de Mestra em Engenharia Mecânica.

Documento assinado digitalmente
Henrique Simas
Data: 22/09/2023 06:58:20-0300
CPF: ***.194.639-**
Verifique as assinaturas em https://v.ufsc.br

Prof. Henrique Simas, Dr. Eng.
Coordenador do Curso

Documento assinado digitalmente
Alexandre Kupka da Silva
Data: 21/09/2023 18:47:21-0300
CPF: ***.190.189-**
Verifique as assinaturas em https://v.ufsc.br

Prof. Alexandre Kupka da Silva, Ph. D.
Orientador

Florianópolis, 26 de Junho de 2023.

Dedico esse trabalho à minha vó (in memoriam).

ACKNOWLEDGEMENTS

Agradeço ao Prof. Alexandre Kupka da Silva por me acolher em seu laboratório e concordar em ser meu orientador ao longo dessa jornada de formação acadêmica. Sua orientação e apoio foram essenciais para o meu crescimento profissional e pessoal.

Expresso minha gratidão especial à Olivia Carolina da Rosa, cujo apoio constante durante o desenvolvimento deste trabalho foi certamente como um farol, iluminando meu caminho ao longo do mestrado.

Gostaria de estender meus agradecimentos ao corpo técnico do LEPTEN, Allan e Rosângela. Agradeço também aos meus colegas Adriano, Bruno, Ederson, Luiz e Thais, cuja convivência no laboratório foi enriquecedora e proporcionou um ambiente colaborativo e estimulante.

À banca examinadora, composta pelo Prof. Joaquim Gonçalves e pelo Prof. Louis Gosselin, expresso meu sinceros agradecimentos pelo tempo dedicado à leitura e avaliação criteriosa deste trabalho.

Quero dedicar um agradecimento especial à minha família e às pessoas queridas que estiveram ao meu lado ao longo dessa jornada. À minha mãe e ao meu irmão, sou grato por seu amor, apoio incondicional e compreensão durante os desafios e momentos de dedicação intensa ao mestrado.

Ao meu companheiro, Willian, que contribuiu diretamente para a realização desse trabalho e por estar ao meu lado, me encorajando, celebrando minhas conquistas e oferecendo seu ombro amigo nos momentos desafiadores.

Não posso deixar de expressar minha gratidão ao povo brasileiro, representado pela CAPES, pelo apoio financeiro fundamental na execução deste trabalho. Sua contribuição foi essencial para a realização desta pesquisa e meu desenvolvimento acadêmico ao longo de toda a minha vida.

RESUMO

O setor residencial representa uma parcela significativa do consumo de energia em todo o mundo. Uma opção para atender às exigências técnicas e ambientais de aquecimento de ambientes e água quente nesse setor é o uso de misturas de CO_2 como refrigerante em ciclos baseados em compressão. No entanto, embora não-inflamável e com baixo impacto ambiental, o CO_2 apresenta baixo efeito refrigerante específico e grandes perdas de estrangulamento nos dispostivos de expansão. Misturas que incluem um refrigerante de baixo GWP e CO_2 podem melhorar o desempenho desses ciclos enquanto atendem aos requisitos ambientais. Portanto, este estudo avalia o desempenho de um sistema combinado de bomba de calor que fornece aquecimento do ambiente e água quente destinados para regiões de climas frios usando misturas binárias de CO_2 e outros refrigerantes. Por meio de um modelo numérico desenvolvido para representar a bomba de calor, foram testadas três configurações de ciclo com diferentes demandas representadas por razões de aquecimento de ambiente para água quente e frações de massa de CO_2. A configuração da bomba de calor com a melhor faixa de desempenho dispunha de três *gas coolers*: um *gas cooler* de baixa temperatura que pré-aquecia a água, um *gas cooler* intermediário que aquecia o ambiente e um *gas cooler* de alta temperatura que aquecia a água já pré-aquecida à temperatura de operação. As bombas de calor dedicadas principalmente ao aquecimento de ambientes se beneficiaram de misturas com baixas frações de massa de CO_2 (≈10%), enquanto as bombas de calor que atendiam principalmente ao aquecimento de água obtiveram melhor desempenho com elevadas frações mássicas de CO_2 (≈90%). Nessa configuração combinada, aproximadamente 87% das misturas analisadas apresentaram um coeficiente de desempenho mais alto do que os fluidos puros, indicando uma melhoria nas bombas de calor de CO_2. O impacto da fonte de calor também foi considerado, utilizando um modelo computacional para avaliar o desempenho da bomba de calor para diferentes razões de aquecimento de ambiente para água quente e temperaturas da fonte de calor. A mistura com 10% de CO_2 e 90% de R32 obteve os melhores valores de COP em toda a faixa de temperaturas reduzidas de fonte de calor em comparação com as outras misturas analisadas. Além disso, por meio de análise de escala, a capacidade de aquecimento da bomba de calor foi normalizada por unidade de volume específico na entrada do compressor e pela condutância térmica global (UA_{total}) do ciclo. Misturas ricas em CO_2 apresentaram a melhor capacidade de aquecimento volumétrico devido às maiores densidades do fluido natural em baixas temperaturas. Isso indica que as misturas de refrigerante com CO_2 requerem menos volume varrido pelo compressor para produzir a mesma quantidade de calor em comparação com outras misturas. Além disso, este estudo identificou dois fatores opostos relacionados à operação de bomba de calor com temperaturas de evaporação reduzidas: a adição de CO_2, que reduz o tamanho da planta, e a adição de refrigerante que melhora o desempenho (COP).

Palavras-chave: CO_2. Misturas. Bomba de calor. Refrigerantes.

RESUMO EXPANDIDO

Introdução

O setor residencial tem uma parte cada vez mais proeminente nas emissões globais de CO_2 e, à medida que a população do mundo cresce, a demanda por consumo de energia doméstica também cresce. A maioria dos edifícios ainda é aquecida predominantemente pela combustão de combustíveis fósseis, principalmente gás natural. Isso contribui significativamente para a acumulação de gases de efeito estufa na atmosfera, e a atual escassez de energia destaca ainda mais a necessidade de transição para métodos de aquecimento mais acessíveis, confiáveis e de impacto ambiental reduzido. Nesse contexto, as bombas de calor são uma forma eficiente e sustentável de fornecer aquecimento, pois são de três a cinco vezes mais eficientes do que as caldeiras a gás natural. As bombas de calor podem contribuir para reduzir os impactos ambientais melhorando a eficiência energética dos sistemas de aquecimento residencial. No entanto, certos refrigerantes podem levar à liberação de gases de efeito estufa. Historicamente, as bombas de calor e dispositivos de refrigeração têm utilizado HFCs como refrigerantes, adotados como substitutos aos refrigerants que destroem a camada de ozônio, eliminados pelo Protocolo de Montreal.

O dióxido de carbono é proposto como um fluido refrigerante potencial devido à sua não inflamabilidade, acessibilidade a partir de processos industriais e baixos níveis de GWP (potencial de aquecimento global). No entanto, seu uso ainda é limitado em virtude dos custos e eficiência do sistema. O CO_2 é uma opção viável para sistemas de aquecimento de água domésticos, que permite um desempenho eficiente de compressão e transferência de calor e, por consequência, valores elevados de COP. Além disso, a produção de água em temperaturas mais altas do que as tradicionais (80 °C em vez de 60 °C) não causa grandes reduções no COP, ou seja, a operação com CO_2 permite uma gama de aplicações, ao contrário de sistemas tradicionais que são restritos a temperaturas de 55 °C.

Recentemente, determinadas misturas de refrigerantes têm ganhado popularidade como uma opção viável para bombas de calor. Misturas zeotrópicas, que apresentam temperatura variável (*glide*) durante a mudança de fase, são particularmente vantajosas devido aos efeitos de transferência de calor no perfil de temperaturas nos trocadores de calor, reduzindo irreversibilidades. Além disso, novas misturas criadas variando a composição de componentes individuais oferecem vantagens em termos de restrições técnicas e ambientais em relação a componentes puros.

Objetivos

Diante dos desafios relacionados à promoção de novos fluidos refrigerantes para aplicações de bombas de calor, este trabalho propõe identificar misturas de fluidos orgânicos e sintéticos (com baixo impacto no efeito estufa e nenhum impacto na depleção da

camada de ozônio) com CO_2. O objetivo geral é analisar o ciclo de uma bomba de calor combinada que opera com várias misturas de fluidos, incluindo fluidos supercríticos. Para alcançar este objetivo, os seguintes objetivos específicos devem ser alcançados:

- Avaliar e otimizar um ciclo de bomba de calor operando com CO_2, refrigerantes de baixo GWP e zero ODP (potencial de depleção da camada de ozônio) e misturas destes, em uma bomba de calor dedicada ao aquecimento do ambiente e água.
- Avaliar os impactos da adição de CO_2 aos refrigerantes no desempenho da bomba de calor e em outros parâmetros de projeto, como o tamanho da planta térmica.
- Normalizar e avaliar o COP e a capacidade de aquecimento obtidos partir do desempenho dos fluidos analisados.
- Avaliar a influência da demanda de aquecimento, concentração da mistura e temperatura da fonte de calor no desempenho da bomba de calor.

Métodos

Um modelo computacional foi utilizado para avaliar o desempenho de um sistema em diferentes demandas de aquecimento de ambiente e água quente, bem como em diferentes temperaturas da fonte de calor, simulando diversas condições de clima frio. Esta dissertação explorou o uso de uma bomba de calor combinada para aquecimento do ambiente e água quente, utilizando misturas binárias de CO_2 e vários refrigerantes, considerando frações mássicas de CO_2 na mistura ($\dot{x}_{CO_2}$) variando de 0 a 1.

Para isso, um modelo computacional foi desenvolvido para representar o ciclo de refrigeração, baseado na operação em regime permanente e nos princípios da primeira lei da termodinâmica. A simulação compreendeu quatro variáveis independentes, e algumas simplificações foram feitas para facilitar os cálculos. O compressor foi modelado com base em uma eficiência isentrópica fixa de 70%, o dispositivo de expansão foi considerado isentálpico e todos os trocadores de calor (*gas coolers* e evaporador) foram discretizados em uma malha unidimensional para permitir um cálculo detalhado do perfil de temperatura. A rotina implementada baseou-se na maximização do COP do sistema, sujeita a restrições de *pinch point* nos trocadores de calor. Foram consideradas três configurações de sistemas (AB, BC e ABC) baseadas no número de *gas coolers* em cada ciclo. Na configuração AB, um *gas cooler* de baixa temperatura foi usado para aquecer a água quente doméstica e um *gas cooler* de alta temperatura para aquecimento do ambiente, enquanto a configuração BC foi o oposto. Na configuração ABC, três *gas coolers* foram usados, sendo que o *gas cooler* de baixa temperatura pré-aquecia a água para o *gas cooler* de alta temperatura, enquanto um *gas cooler* de temperatura intermediária rejeitava calor para o sistema de aquecimento do ambiente.

A verificação do modelo numérico proposto foi realizada em três etapas: verificação do tamanho da malha do trocador de calor, verificação da configuração combinada do ciclo da bomba de calor operando com fluido puro e verificação da operação da bomba de calor com misturas de refrigerante. O procedimento para verificar a independência da malha considerou diversos tamanhos de malha e adotou o critério de erro absoluto inferior a 0,4 K. Assim, uma malha unidimensional de 150 e de 200 elementos foram selecionadas para o evaporador e o *gas cooler*, respectivamente. A verificação do ciclo de bomba de calor combinada associada à configuração do ciclo, assim como a verificação quanto ao uso de mistura de refrigerante foram realizadas comparando os resultados numéricos do modelo aqui desenvolvido com dados existentes na literatura. A figura de mérito escolhida para este procedimento de verificação foi o COP, e nenhum erro relativo maior que 5% foi obtido, demonstrando a precisão do modelo.

Após a realização de um estudo exploratório sobre os efeitos da composição da mistura e das configurações do ciclo, foi realizado um estudo complementar para investigar o efeito da temperatura da fonte de calor em bombas de calor combinadas. Este estudo considerou o ciclo ABC, previamente identificado como a alternativa mais adequada para uma ampla faixa de demandas de calor. Além disso, para essa análise foram consideradas três misturas binárias de CO_2: com R32, R290 e R1234yf; bem como a operação de fluido puro com R410A. As composições da mistura foram limitadas aos valores de $\dot{x}_{CO_2}$ de 0,1 e 0,9. Visto que esse estudo considerou temperaturas reduzidas da fonte de calor, o fluido secundário no evaporador foi alterado para uma solução aquosa de água e propilenoglicol (mistura 0,5/0,5) devido às limitações do ponto de congelamento da água. Dessa forma, a utilização da mistura anti-congelante no evaporador teve de ser validada. Os resultados foram comparados com dados publicados na literatura, e as figuras de mérito de COP e capacidade de aquecimento volumétrico foram consideradas para o procedimento de verificação. As divergências observadas entre os resultados da capacidade de aquecimento volumétrico não foram maiores que 0,31%, enquanto o erro relativo entre os resultados de COP oscilou de -0,12% a 0,6%, garantindo a adequação do modelo de bomba de calor combinada para temperaturas reduzidas da fonte de calor.

Resultados e discussões

O desempenho de um sistema de bomba de calor combinada que fornece tanto aquecimento de ambiente quanto água quente utilizando misturas binárias de CO_2 e outros refrigerantes foi avaliado. Foram testadas três configurações de ciclo, com diferentes proporções de demandas de aquecimento de ambiente e água quente, assim como frações de massa de CO_2. A primeira configuração analisada (AB) utiliza o *gas cooler* de alta temperatura (B) para o sistema de aquecimento do ambiente e o *gas cooler* de baixa temperatura (A) para o aquecimento da água. Os resultados demonstraram que essa configuração é indicada para operações que demandam o aquecimento de água. Já a

configuração BC, em que o *gas cooler* de baixa temperatura é dedicado ao aquecimento do ambiente (B) e o de alta temperatura (C) para a produção de água quente, apresentou elevados valores de COP para condições de operação focadas no aquecimento do ambiente. Enquanto a confguração ABC, que inclui três *gas coolers*, sendo que o *gas cooler* de baixa temperatura (A) pré-aquece a água, o *gas cooler* intermediário (B) aquece o espaço e o *gas cooler* de alta temperatura (C) aquece a água já pré-aquecida para a temperatura de operação, apresentou a melhor faixa de desempenho.

A análise da influência da concentração de mistura demonstrou que misturas com concentrações 0,5/0,5 reduzem o COP do sistema devido a valores elevados de *glide*. Enquanto os fluidos de trabalho com traços reduzidos de misturas (próximos de 10%) apresentam valores de COP superiores quando comparados aos seus respectivos fluidos puros. Tal comportamento ocorre devido aos valores de *glide* moderados observados nesse intervalo de concentrações, que favorece a redução das irreversibilidades no trocadores de calor.

Em relação à influência da demanda de calor, as bombas de calor que são principalmente dedicadas ao aquecimento do ambiente se beneficiam de misturas com baixas frações de massa de CO_2 (cerca de 10%), enquanto àquelas destinadas principalmente ao aquecimento de água apresentam melhor desempenho para altas frações de massa de CO_2 (cerca de 90%). Nesta configuração combinada ABC, cerca de 87% das misturas analisadas apresentaram um coeficiente de desempenho mais alto do que os fluidos puros, o que indica uma melhoria no desempenho das bombas de calor com CO_2.

Essa dissertação também considerou o impacto da fonte de calor, utilizando um modelo computacional para avaliar o desempenho da bomba de calor multi-propósito em diferentes proporções de aquecimento do ambiente e água quente e temperaturas da fonte de calor.

Os resultados mostraram que a mistura CO_2(0,1)/R32(0,9) apresentou os melhores valores de COP em temperaturas reduzidas de fonte de calor em comparação a outras misturas. A adição de CO_2 aumentou o desempenho da bomba de calor para razões de aquecimento menores (em que a demanda pela produção de água quente é dominante), mas prejudicou o COP para razões de aquecimento maiores e temperaturas mais baixas da fonte de calor. Portanto, o uso de misturas ricas em CO_2 deve ser restrito à produção de água quente e temperaturas de evaporação mais elevadas.

A razão de pressão entre a linha de sucção e descarga e a pressão de evaporação foram analisadas para várias misturas. Resultados demonstraram a forte correlação entre a pressão de sucção e a temperatura da fonte de calor. Misturas ricas em CO_2 apresentaram valores reduzidos de razão de pressão, devido ao baixo ponto de ebulição do dióxido de carbono.

Uma análise de escala foi realizada indiretamente por meio da normalização da figura de mérito da capacidade aquecimento da bomba de calor $\dot{Q}_{heat}$ pelo volume específico

do fluido de trabalho na entrada do compressor e pela condutância térmica total do ciclo $(UA)_{total}$. Os resultados demonstraram que as misturas ricas em CO_2 apresentaram capacidade de aquecimento volumétrica elevada, devido, em partes, ao aumento de densidade do CO_2 em baixas temperaturas. Ademais, as misturas ricas em CO_2 também demonstraram valores superiores de capacidade de aquecimento normalizados por $(UA)_{total}$.

Considerações finais

Os resultados deste trabalho mostram que a adição de CO_2 para misturas de trabalho em bombas de calor multi-propósito pode aumentar a eficiência do sistema para condições de demanda em que a produção de água quente é predominante. O exposto ocorre especialmente para misturas compostas majoritariamente por dióxido de carbono (90%) e para condições de operação com temperaturas de evaporação elevadas, caracterizando uma solução adequada técnica ambientalmente. Porém, em relação a condições de temperatura de evaporação reduzidas, as misturas ricas em CO_2 (90%) reduzem o COP do sistema quando comparadas à operação com misturas ricas em outros fluidos refrigerantes.

Além da avaliação da eficiência do sistema, uma análise técnica considerando critérios de projeto de bombas de calor demonstrou os benefícios da utilização de misturas binárias de CO_2 em temperaruras de evaporação reduzidas. A análise considerou o volume do compressor e o tamanho total dos trocadores de calor requeridos pelo sistema em relação à capacidade de aquecimento entregue pelos fluidos de trabalho. As misturas ricas em CO_2 apresentaram os melhores resultados e foram observados dois fatores contrastantes relacionados a operação de bomba de calor com temperaturas de evaporação reduzidas: a adição de CO_2, que reduz o tamanho da planta, e a adição de refrigerante, que melhora o desempenho (COP).

Por fime, sugere-se que uma análise quantitativa de custos e uma análise multi-objetivo que considera tanto o COP do sistema como a escala do mesmo UA) para trabalhos futuros.

Palavras-chave: CO_2. Misturas. Bomba de calor. Refrigerantes.

ABSTRACT

The residential sector accounts for a considerable share of energy consumption worldwide. An alternative to meet the technical and environmental requirements of space heating and hot water demanded by this sector uses CO_2 mixtures as a refrigerant in compression-based cycles. However, while CO_2 is not flammable and has low environmental impact, it performs poorly due to its low specific refrigerating effect and large throttling losses. Differently, mixtures with low-GWP refrigerant and CO_2 could enhance the performance of these cycles while meeting environmental requirements. Therefore, this study evaluates the performance of a combined heat pump system that provides both space heating and hot water in cold climates using binary mixtures of CO_2 and other refrigerants. Through an in-house routine, three cycle configurations were tested, with different ratios of space heating to hot water demands and CO_2 mass fractions. The heat pump configuration with the best performance range had three gas coolers, where the low-temperature gas cooler preheated the water, the intermediate equipment heated the space, and the high-temperature gas cooler heated the already preheated water to the operating temperature. Heat pumps primarily dedicated to space heating benefit from mixtures with low mass fractions of CO_2 ($\approx$10%), whereas heat pumps primarily dedicated to water heating perform better for high mass fractions of CO_2 ($\approx$90%). In this combined configuration, about 87% of the mixtures analyzed had a higher coefficient of performance than pure fluids, indicating an improvement in CO_2 heat pumps. The impact of the heat source was also considered, and a computational model was used to evaluate the performance of the heat pump at different ratios of space heating to domestic hot water and heat source temperatures. The R32 mixture offered the best coefficient of performance (COP) values throughout the range of reduced heat source temperatures compared to other mixtures. Adding CO_2 to mixtures reduces COP, particularly when the temperature of the heat source is low. A scale analysis was performed by normalizing the heat pump capacity per unit of specific volume at the compressor inlet and the total UA of the cycle. CO_2-rich mixtures exhibited the best volumetric heating capacity due to the higher densities of the natural fluid at low temperatures. This indicates that refrigerant mixtures with CO_2 require less compressor swept volume to produce the same amount of heat compared to other fluid alternatives. In addition, this study has identified two opposing factors when dealing with the operation of a heat pump with reduced evaporating temperatures: the addition of CO_2, which reduces the size of the site, and the addition of refrigerant, which improves the performance (COP).

Keywords: CO_2 mixtures. Cold climates. Refrigerants. Heat pump.

LIST OF FIGURES

LIST OF TABLES

LIST OF SYMBOLS

Nomenclature

A	Area	m^2
UA	Global conductantce	W/K
Q	Heat	J
$\dot{Q}$	Heat transfer rate	W
$\dot{m}$	Mass flow rate	kgs^{-1}
$\dot{x}$	Mass fraction	-
N	Number of elements in the mesh	-
p	Pressure	Pa
$\dot{W}$	Power	W
x	Quality	-
r_{heat}	Space to water heating ratio	-
i	Specific enthalpy	J/kg
c_p	Specific heat at constant pressure	J/kg k
T	Temperature	K
W	Work	J

Greek alphabet and symbols

η	Efficiency	%

Acronyms

COP	Coefficient of Performance
GWP	Global Warming Potential
LMTD	Logarithmic Mean Temperature Difference
ODP	Ozone Depleting Potencial
PP	Pinch Point
TFC	Total Final Consumption
VHE	Volumetric heating effect

Subscripts

comp	Compression
cond	Condenser
crit	Critical
high	Discharge

DW	Domestic Water
evap	Evaporator
gc	Gas cooler
HS	Heat Source
heat	Heating
in	Inlet
isen	Isentropic
out	Outlet
pp	Pinch point
ref	Refrigerant
sat	Saturation
SH	Space Heating
low	Suction

CONTENTS

1 INTRODUCTION

As the global population expands and economies become increasingly industrialized, demand for energy is rising at a rapid rate, with a corresponding increase in CO_2 emissions (IEA, 2023). According to the International Energy Agency, energy demand has steadily increased annually (Figure 1.1a) (IEA, 2021). The residential sector has an increasingly prominent part in global CO_2 emissions, and as world population increases, so does the demand for energy in household consumption (MUZAYANAH *et al.*, 2022). For instance, buildings constitute the largest sectoral share of final consumption and related carbon emissions in the European Union, approximately 38%. This is mainly due to the demand for residential space and water heating, which together account for almost 80% of residential energy consumption (Figure 1.1b) (EUROSTAT, 2022).

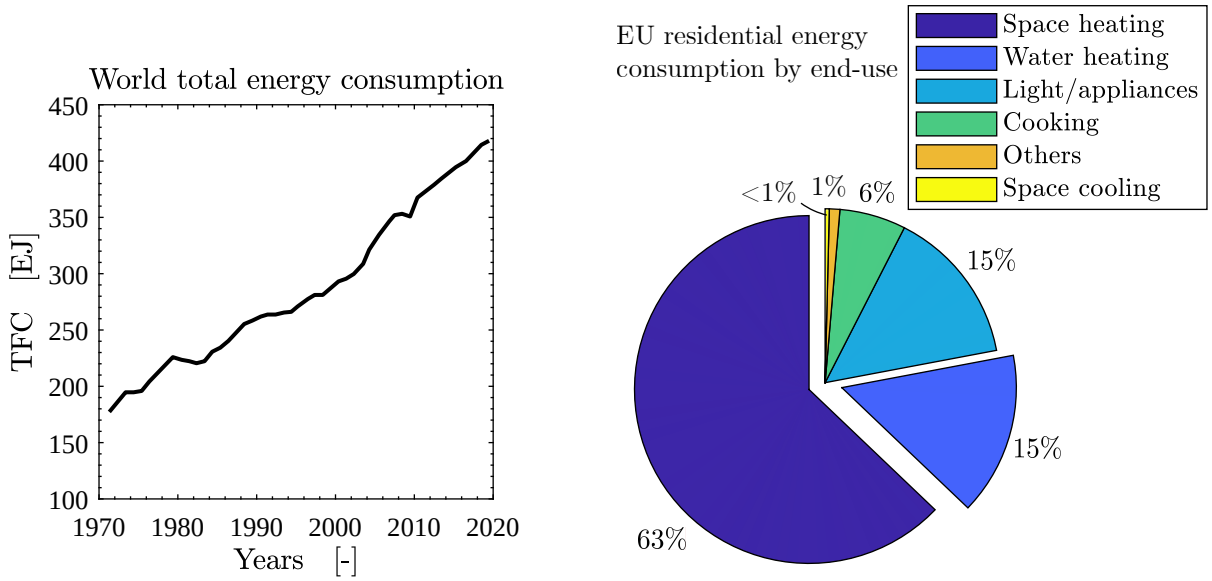

(a) (b)

Figure 1.1 – (a) Growth of the world energy consumption over the years 1971-2019. Total Final Consumption (TFC) in exaJoules. Adapted from IEA (2021). (b) The end-use shares of residential energy in Europe for the year of 2020. Adapted from Eurostat (2022)

Additionally, in emerging markets such as China, which alone represents approximately 21% of the world's energy demand (IEA, 2021), the residential sector can account for up to 18% of the nation's total final energy consumption (YAN, 2018). Public buildings and urban dwellings are the main drivers of energy demand in buildings. Of the final energy used in buildings in 2017, around 40% was used for heating and cooling, 27% for cooking and hot water, and 33% for other purposes. The China Energy Efficiency Report indicates that improving the energy efficiency of buildings is a crucial step in reducing energy consumption in the country (YAN, 2018).

The majority of buildings globally, such as residences, offices, schools, and factories, are still heated predominantly through the combustion of fossil fuels, primarily natural

gas (IEA, 2022). This contributes significantly to the accumulation of greenhouse gases in the atmosphere, and the current energy shortage further highlights the necessity of transitioning to more affordable, reliable, and environmentally friendly methods of heating (IEA, 2022).

In this context, heat pumps are an efficient and sustainable way of providing heating, as they are three to five times more energy efficient than natural gas boilers (IEA, 2022). Heat pumps can contribute to reducing environmental impacts by improving the energy efficiency of residential heating systems. However, the use of specific refrigerants may lead to the release of greenhouse gases. Historically, heat pumps and refrigeration devices have utilized *HFCs*[1] as refrigerants, which were adopted as a means of replacing ozone-depleting substances phased out by the *Montreal Protocol*[2] (IEA, 2022).

Within this scope, CO_2 has been proposed as a potential refrigerant fluid due to its non-flammability, availability from industrial processes (ANDRESEN, 2009) and low *GWP*[3] levels (KIM, 2004). However, efficiency and costs of the CO_2-based systems limit its widespread use (NEKSÅ, 2002). CO_2 has been proven to be a viable option for domestic water heating systems, due to its efficient compression, efficient heat transfer performance, and compatibility of heat pump systems (NEKSÅ, 2002). Besides, the production of water at higher temperatures than the traditional ones (80 °C instead of 60 °C) does not cause great reductions in COP, that is, the operation with CO_2 allows a wider range of applications, unlike traditional systems that are restricted to temperatures of 55 °C (NEKSÅ, 2002).

Recently, certain refrigerant mixtures have gained popularity as a viable option for heat pumps (PAN *et al.*, 2011; WANG *et al.*, 2019; ZHANG *et al.*, 2017). Zeotropic mixtures, which exhibit a varying temperature during phase change, are particularly advantageous due to the increased heat transfer and temperature glide effects (CHANG *et al.*, 2000). Furthermore, new mixtures created by varying the composition of individual components offer advantages in terms of technical and environmental restrictions over pure components (RADERMACHER; HWANG, 2005).

Given the heavy dependence of the global energy scenario on the heating demand of buildings, which has a direct effect on the environment, it is imperative to find solutions for residential heating that can improve energy efficiency and reduce the use of refrigerants that damages the environment. Thus, the analysis of systems with heat pumps interests particularly because of their impact on global energy consumption, which represents an

[1] *HFCs*: Hydrochlorofluorocarbon, a family of synthetic compounds containing hydrogen, chlorine, fluorine, and carbon.

[2] *Montreal Protocol*: an international agreement designed to protect the earth's ozone layer from the damaging effects of human-produced chemicals. It was adopted in 1987 and has since been ratified by 197 countries.

[3] *GWP*: Global Warming Potential is a measure of the total energy, in terms of carbon dioxide equivalent, that a gas has over a given period of time. GWP is used to compare the relative impact of different gases on climate change and is expressed as a multiple of the impact of CO_2.

opportunity to observe solutions that both reduce environmental damage and present performance comparable to those of traditional refrigerants.

1.1 OBJECTIVES

Aiming to outcome the aforementioned challenges, this work proposes to identify mixtures of organic and synthetic fluids (with low impact on the greenhouse effect and no impact on the depletion of the ozone layer) with CO_2 for this application. The main objective is to analyze the thermodynamic cycle of a combined heat pump that operates with several fluid mixtures, including supercritical fluids. To achieve this objective, the following specific objectives should be met:

i) Evaluate and optimize a heat pump cycle dedicated to space and water heating operating with CO_2, low GWP and zero *ODP*[4] refrigerants and mixtures of these.

ii) Assess the impacts of CO_2 addition to refrigerants on the heat pump performance and other design parameters such as the plant size.

iii) Normalize and evaluate the coefficient of performance (COP) and the heating capacity of the analyzed fluids.

iv) Evaluate the influence of heating demand, mixture concentration, and heat source temperature on the heat pump performance.

1.2 STRUCTURE OF THE DOCUMENT

This master thesis is organized into five chapters. Chapter 2 presents a review of thermodynamic concepts related to water heat pumps modeling and their fundamentals, investigations regarding refrigerant mixtures and CO_2 use, and water heat pump configurations. Chapter 3 is based on a manuscript that is currently under review for publication and details the major findings of the investigation of combined heat pump configurations and the effects of heating demand and mixture composition on several figures of merit. Chapter **??** is also based on a manuscript that is in preparation for submission and presents the discussions and the main results related to the performance of a combined heat pump operation with CO_2-binary mixtures using reduced heat source temperatures. Lastly, Chapter 5 outlines the conclusion and suggestions for future works.

[4] *ODP*: Ozone Depletion Potential is a measure of the potential of a chemical to contribute to the depletion of the Earth's ozone layer.

2 THEORETICAL FOUNDATION AND LITERATURE REVIEW

The approach for the literature review has two main objectives. Firstly, it lays the groundwork for the proposed research, providing evidence of the research problem's significance, demonstrating how this study contributes to the existing knowledge. Secondly, it involves summarizing the existing body of work and pinpointing the areas of knowledge that this study intends to address.

In this chapter, a general description of basic concepts related to heat pump operation and definitions used throughout this master thesis is provided as well as a brief review of fundamental works about heat pumps focused on CO_2 and mixture applications, describing relevant aspects and contributions to the field.

Section 2.1 details the historical use of refrigerants in the industry. Section 2.2 describes the thermodynamic concepts of heat pump systems, mixture behaviour, supercritical phenomena, and their relationship with ideal thermodynamic cycles. Finally, Section 2.3 presents a review of the state-of-the-art, briefly describing their major contributions to the field.

2.1 HISTORICAL AND ENVIRONMENTAL ASPECTS

In theory, any substance can reach the liquid phase at the required evaporating temperature that is volatile enough could be employed as a refrigerant. But, at a practical level, several factors must be addressed when choosing a reasonable candidate for the refrigeration system (GOSNEY, 1982). As history shows, these factors have changed with time and the most adequate choice of a working fluid is usually limited to flammability issues, toxicity, chemical stability, behavior with oils and cost (GOSNEY, 1982; GRASSI, 2018).

Originally, natural substances were used to cool food and other items for being readily available and for presenting low price and adequate thermal conductivity values (OLIVEIRA, 2013). With the introduction of synthetic refrigerants in the 1930s, the refrigeration industry was revolutionized. These new synthetic refrigerants (*CFCs*)[1] offered greater efficiency and safety related to flammability issues (CUBE *et al.*, 1981).

The environmental impacts of CFCs were only discovered in the late 1970s, when it was found that these synthetic refrigerants contributed to ozone depletion and global climate change (OLIVEIRA, 2013). In response, the international community developed protocols such as the Montreal Protocol in 1987, which aimed to reduce and eventually eliminate the use of ozone-depleting substances. The transition away from these substances — which was not immediate — was done with the employment of HFCs, with an interim period where *HCFCs*[2] were used (MONTAGNER, 2013).

[1] *CFCs*: Chlorofluorocarbons, a group of synthetic compounds with chlorine, fluorine, and carbon atoms.
[2] *HCFCs*: Hydrochlorofluorocarbons, a group of chemicals that were widely used in the refrigeration

While hydrofluorocarbons (HFCs) have since been adopted as replacement refrigerants, they still contribute to the greenhouse effect and climate change. Thus, due to growing concerns about anthropogenic emissions of greenhouse gases, several international agreements, such as the Kyoto Protocol and the Kigali amendment have been proopsed with the goal to reduce greenhouse gas emissions, including those from HFCs, which contribute to global climate change (RADERMACHER; HWANG, 2005).

Aiming at attending the environmental legislation, the refrigeration industry put aside CFCs and HCFCs to embrace HFCs and hydrofluoroolefins (*HFOs*)[3] which have a much lower ODP and GWP. As the refrigeration industry continues to move away from ozone-depleting substances and towards more sustainable refrigerants, the environmental impacts of refrigeration continue to be reduced. Thus, the refrigeration industry has always been challenged on fluid selection, international compliance and restrictions based on safety, and environmental issues have been pushing the industry towards system improvement.

2.2 THERMODYNAMIC FUNDAMENTALS

Vapor compression systems are the most commonly employed, because of their favorable construction and operating characteristics, and they can be found in both domestic refrigerators and large industrial facilities (MONTAGNER, 2013). In this thermodynamic cycle, the refrigerant absorbs the heat from a heat source (and, consequently cooling it) at the evaporator by pumping away the vapor with the assistance of a compressor. The fluid is then compressed to a higher pressure and flows into the condenser, where heat is rejected. In order to maintain the different pressure levels in the evaporator and condenser an expansion device is applied, so after the condenser the fluid must flow through this device and return to the evaporator. This vapour compression cycle is claimed by Evan Perkins and sometimes it is called the Evans-Perkins cycle (GOSNEY, 1982). A heat pump device is a refrigerator used as a heating machine, where the figure of interest is the heat rejected in the condenser. Another possible classification of heat pumps and refrigerators are related to the heat sources that the working fluid interacts with. The heat sources or sinks can be the atmospheric air, water from a river nearby, the ground (i.e., geothermal heat pumps) (GRASSI, 2018). In this work discussions are limited to water-to-water heat pumps, in which water is used as the secondary fluid in the heat exchangers (evaporator, condenser and gas cooler).

The performance of a refrigeration plant is measured by a COP (coefficient of performance) and for a basic vapour-compression cycle it is defined by the ratio of the refrigerating capacity (rate of heat transfer) by, generally, the compressor work (power

industry as a substitute for CFCs due to their lower ozone depletion potential. However, they still have a negative impact on the ozone layer and are also potent greenhouse gases.

[3] *HFOs*: hydrofluoroolefins are substitutes for less environmentally friendly refrigerants such as CFCs and HCFCs.

delivered to the system) (GOSNEY, 1982). Since this work is focused on water and space heating the term COP will be associated with the refrigerant capacity of the condenser (or gas cooler) as the useful effect as described by the equation:

$$COP = \frac{\dot{Q}_{heat}}{\dot{W}_{comp}}. \tag{2.1}$$

2.2.1 Lorenz cycle

In situations where the temperature change of secondary fluids is constrained by heat sources/sinks, using a refrigerant that can adapt to these temperature variations becomes more suitable. This principle — that can be achieved by employing a mixture of refrigerants — was first proposed by Lorenz (GOSNEY, 1982) and it addresses the entropy production in the heat exchangers aiming at maximizing the system performance (RADERMACHER; HWANG, 2005).

Figure 2.1 shows a hypothetical temperature-entropy diagram of a Carnot cycle (a) and a Lorenz cycle (b) applied to the same heat sources/sinks of a given fluid. Processes 8-1 and 4-5 represent, respectively, the heat addition (evaporation) and the heat rejection (condensation). The heat source and sink temperature (dashed-line) is superimposed on the diagram just to compare the temperature differences with the refrigerant.

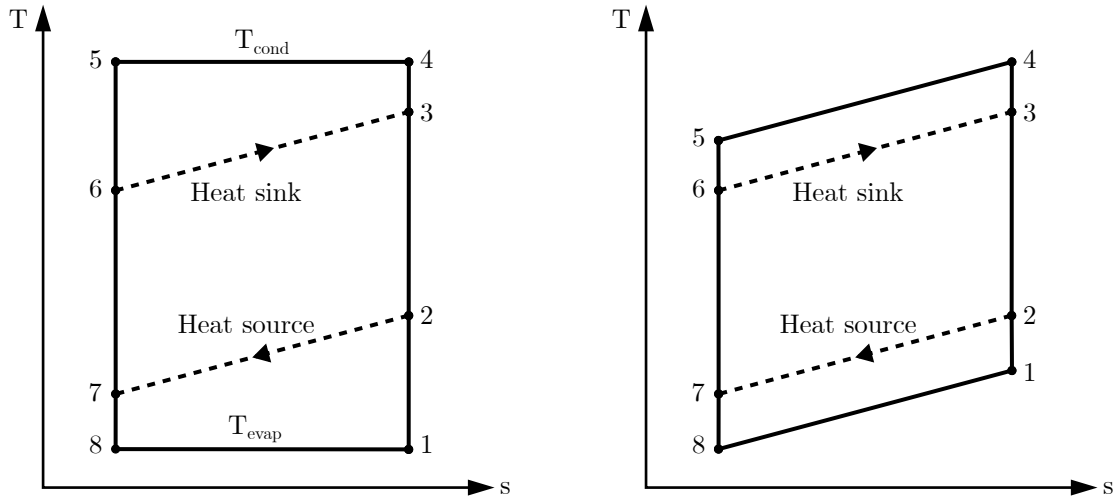

Figure 2.1 – Comparison Carnot cycle (a) vs. Lorenz cycle (b) operating between the same heat source/sink external conditions. Adapted from Radermacher and Hwang (2005).

If both the heat sink and heat source are fixed (that is usually the case in water heat pumps due to design restrictions) one can observe that for a pure fluid that holds a constant temperature during condensation and evaporation (Carnot cycle Figure 2.1a), the evaporating and condensing temperatures of the cycle are also fixed. This heat transfer

limitation is related to *pinch point*[4] restrictions that will be discussed latter. In turn, the Lorenz cycle focuses on this issue and, ideally, the refrigerant matches the secondary fluid temperature profile throughout evaporation and condensation. Consequently, both temperature curves become parallel and the pinch point issue is avoided. In this particular case, the Lorenz cycle compared to the Carnot cycle might help reduce entropy generation in the heat exchangers of the cycle. Furthermore, since the heat source and heat sink have fixed temperatures, not only the use of a refrigerant that changes its temperature during the course of evaporation and condensation can reduce the mean temperatures of the cycle, but can also enhance the system efficiency by reducing the difference between the suction and discharge pressures (RADERMACHER; HWANG, 2005).

2.2.2 Mixture of refrigerants

For simplicity, this text focuses on the fundamental behavior of glide and how it affects working fluids during constant-pressure processes. More information on mixing thermodynamics and fluid properties can be found at Radermacher and Hwang (2005).

As pointed out in the previous Subection 2.2.1, a Lorenz cycle could be achieved by using a mixture of refrigerants, which relates to a distinct behavior presented when two pure components are mixed. The concentration of each component within the binary mixture is, then, represented by its mass fraction, expressed as:

$$\dot{x}_A = \frac{\text{mass of component [A]}}{\text{mass of components [A] and [B]}}, \tag{2.2}$$

where $\dot{x}_A$ equals to zero means that component [A] is absent from the formula and $\dot{x}_A = 1$ is the pure fluid [A].

This distinct behaviour presented by mixtures is illustrated with a temperature-concentration diagram of a mixture at constant pressure, as shown in Figure 2.2 for a binary mixture of CO_2 and R32 at the 1 MPa constant pressure. This diagram shows both the bubble and dew point line; bellow the bubble line is subcooled liquid, above the dew line is super-heated vapor, and the envelope enclosed by these two is the two-phase region. At $\dot{x}$ values of 0 and 1, the temperature represents the normal boiling points of the two components of the mixture R32 and CO_2, respectively. Figure 2.2 depicts a constant pressure evaporation process at a given composition $\dot{x}_1$. As temperature increases the first vapor bubble is formed with a mass fraction of $\dot{x}_{1'}$ which is in thermal equilibrium with the liquid phase at point 1. As the mixture is heated, point 2 is reached and evaporation is complete. Here, the vapor has the same mass fraction at the beginning of the process ($\dot{x}_1 \equiv \dot{x}_2$) and the last liquid droplet to evaporate has the mass fraction $\dot{x}_{2'}$. In summary, it is interesting to observe that during the constant pressure evaporation process of a mixture

[4] *pinch point*: in the heat transfer field is defined as the minimum temperature difference between the refrigerant and the secondary fluid.

the saturation temperature is not constant. Changes from T_1 to T_2, this temperature difference ΔT is called glide. Generally, temperature glide is expected to be higher for mixtures whose pure components present great differences between their boiling points. Besides, the glide is also affected by mixture composition, as $\dot{x}$ values are closer to 0 and 1 glide is usually smaller than for $\dot{x}$ intermediate values.

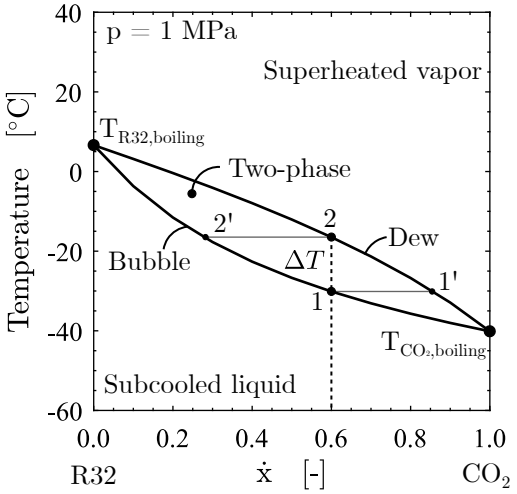

Figure 2.2 – T- $\dot{x}$ diagram of CO_2/R32 mixture. Data from Lemmon *et al.* (2013).

Mixtures with behavior similar to Figure 2.2 are called *zeotropic* mixtures because in phase equilibrium the mass fractions of the vapor and liquid phase ($\dot{x}$) are always different (RADERMACHER; HWANG, 2005). They are created to have properties that are different from the individual components (SÁNCHEZ *et al.*, 2018). Other fluids may not exihibit glide when mixed together, these mixtures are referred as *azeotropic* and during phase change and, at a certain pair of pressure and temperature values, the mass fractions of vapor and liquid are identical.

When the temperature profiles of the secondary fluid heat source and sink are overlaid on the T-h diagram along with the refrigeration cycle, the advantages of zeotropic mixtures become evident. Figure 2.3 illustrates the T-h diagram of a cycle operating at 400 kPa evaporating pressure and 1600 kPa condensing pressure for both pure R22 and the zeotropic mixture R22/R114 (50/50 % mass basis). In this diagram, the cycle 1234 represents the refrigeration cycle (4-1: evaporation, 1-2: compression, 2-3: condensation, 3-4: isenthalpic expansion), while the lines 1'-4' and 2'-3' represent the temperature profiles of the heat source and heat sink.

By comparing the temperature difference between the refrigerant and the secondary fluid for the two refrigerants, as shown in Figure 2.3, the advantages of zeotropic mixtures become apparent. In the case of R22, the temperature of saturated vapor during the condensation process is closest to the temperature of the secondary fluid (Figure 2.3a) resulting in a potential heat exchange pinch-point (RADERMACHER; HWANG, 2005). Additionally, R22 exhibits nonuniform approach temperatures during the evaporation pro-

cess, whereas R22/R114 demonstrates nearly uniform and smaller approach temperatures during both the evaporation and condensation processes (Figure 2.3b) (RADERMACHER; HWANG, 2005). Consequently, the approach temperatures at the inlet and outlet of the heat exchangers for R22 are larger compared to those of R22/R114. Larger approach temperatures imply higher irreversible losses associated with heat exchange. Therefore, zeotropic mixtures that have temperature glides properly matched with the secondary fluids experience fewer irreversible losses compared to pure refrigerants (RADERMACHER; HWANG, 2005).

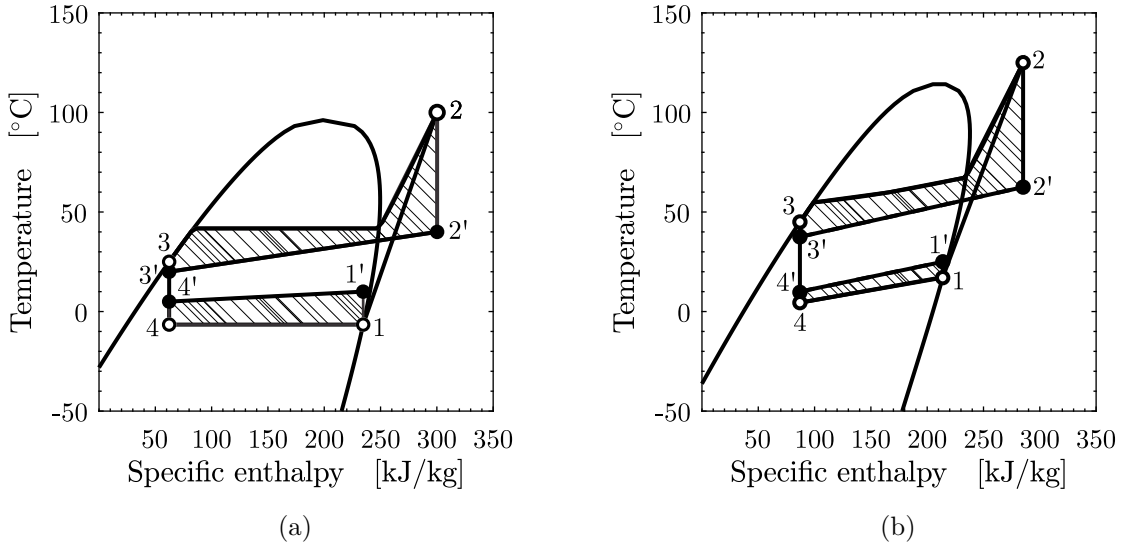

Figure 2.3 – Comparison temperature-enthalpy diagrams of a heat pump cycle with pure R22 (a) and the zeotropic mixture R22/R114 (50/50 %). Adapted from Radermacher and Hwang (2005).

2.2.3 Supercritical phenomena

The gas cooling process of a supercritical fluid can closely resemble the Lorenz cycle, thanks to the presence of non-linear gliding temperatures in the supercritical region (LIU *et al.*, 2021). To achieve this, the incorporation of supercritical fluids into the cycle is necessary. In this regard, a possible classification of refrigerating cycles is related to the presence of supercritical states, if the cycle has no supercritical states than it is called *subcritical*, if all thermodynamic states are in the supercritical region, it is called *supercritical*, and if there are some states placed in and others outside the supercritical region, it is considered a *transcritical* cycle.

Supercritical phenomena occur when pressure and temperature exceed the critical point, causing the fluid to no longer be distinguishable between two distinct phases (BEJAN, 2006). As a result, the fluid presents thermal and physical properties that are characteristic of both a liquid and a gas. This sharp variation of properties near the critical point renders supercritical fluids advantages for heat transfer applications, as shown by

Hall (1971), like the specific heat at constant pressure that increases considerably near the critical point.

Unlike the conventional subcritical cycle, where the thermodynamics states of the working fluid take place below the critical point and heat is transferred through condensation and evaporation processes, transcritical cycles operate between the supercritical and subcritical regions (LECOMPTE *et al.*, 2019). For example, in a transcritical heat pump, evaporation still occurs below the critical point and heat is transferred from the heat source to the refrigerant through a phase-changing process. However, after the compression process, the working fluid discharge pressure increases above the critical pressure and heat rejection occurs in the supercritical state as a single-phase cooling (*gas cooling*), and so the *gas cooler* replaces the condenser (AUSTIN; SUMATHY, 2011). For some fluids with low critical temperatures, the operation within a transcritical cycle is necessary, as a control stategy for the optimal discharge pressure. Temperature and pressure are independent variables in the supercritical region, which differs for conventional subcritical systems, that have suction and discharge pressure levels based on the evaporating and condensating temperatures (GOSNEY, 1982; AUSTIN; SUMATHY, 2011). Additionally, the heat transfer in the gas cooler varies greatly compared to the typical condensing process, since the mechanism is no longer latent heat, but sensible cooling. This singularity allows great temperature differences between the inlet and outlet of the gas cooler and, for heat sinks with temperature change, it matches better the temperature of the refrigerant and the secondary fluid (AUSTIN; SUMATHY, 2011).

Still referencing Austin and Sumathy (2011), some heating applications can take advantage of the distinctive features of the transcritical cycle. One such example is heating applications that necessitate a significant temperature rise. Unlike the condensing process, where heat is rejected through sensible cooling, the transcritical cycle exhibits a greater temperature difference (referred to as temperature glide) between the inlet and outlet temperatures. As a result, the transcritical cycle proves more advantageous for heating applications that require a substantial increase in temperature.

A comparison of the temperature profiles on the heat rejection process between pure refrigerant, zeotropic mixture and supercritical fluid is shown in Figure 2.4. The temperature-enthalpy diagram illustrates the process of heat rejection during subcritical cycles (pure and refrigerant mixture): beginning with desuperheating, followed by condensation, and then subcooling. In subcritical operation, pure fluids maintain a constant temperature, whereas zeotropic mixtures exhibit glide. The diagram also reveals how using mixtures and supercritical fluids can help match the temperature of the working fluid and the heat sink, by emulating the Lorenz cycle. Furthermore, the pinch point in a supercritical heat exchanger may not necessarily be located at the hot or cold end, but instead can be internal, demonstrating the importance of accurately assessing pinch point restriction.

2.2.4 Pinch point and heat exchanger design

To transfer heat from/to the working fluid in the vapor-compression cycle, heat exchangers are employed aiming at maximizing the total heat transfer. Ideally, the maximum feasible coefficient of performance would be achieved when no temperature difference is observed between the refrigerant fluid and the secondary fluids at the condenser and evaporator (GOSNEY, 1982). However, in practical terms, it is impossible to give out heat with no temperature difference due to the large size of the required heat exchangers. A very important parameter in heat exchanger design is the pinch point, which corresponds to the location of the minimum temperature difference of refrigerant and secondary fluid along the heat exchanger (NELLIS; KLEIN, 2009). As mentioned previously, the refrigerating machine performance can be affected by pinch point issues.

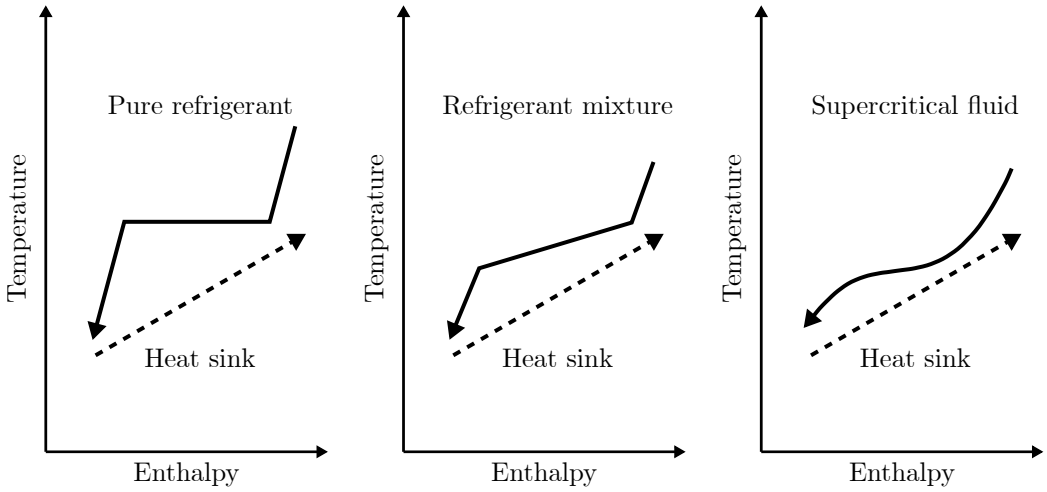

Figure 2.4 – Temperature-enthalpy diagram of the heat exchange process between a heat sink with temperature rise and different working fluids: pure refrigerant, zeotropic mixture and supercritical fluid.

According to the second law of the thermodynamics, heat flows spontaneously from a hot fluid to a cold one: $T_{hot} > T_{cold}$ in thermodynamic temperature scale. Consequently, the pinch point temperature difference must always be $\Delta T_{pp} \geq 0$. Generally, designers model heat exchangers based on a minimum allowed pinch point, because this parameter is related to the size required by the heat exchanger (NELLIS; KLEIN, 2009).

One of the most typical methods for estimating heat exchanger performance is the log-mean temperature difference (LMTD) (NELLIS; KLEIN, 2009), which relates the total heat transfer with the global conductance UA (inverse of the total thermal resistance) and the log-mean temperature difference:

$$\dot{Q} = UA\Delta T_{LMTD}. \tag{2.3}$$

This method is widely used in the solution of heat exchangers and assumes some hypotheses: heat transfer with the environment is neglected; variations of potential and

kinetic energy and axial heat exchange are also not considered; the specific heat and the global heat transfer coefficient are constants (HUNDY *et al.*, 2016). For a counter-flow heat exchanger, the total heat transfer is given by (NELLIS; KLEIN, 2009):

$$\dot{Q} = UA \left[\frac{(T_{hot,out} - T_{cold,in}) - (T_{hot,in} - T_{cold,out})}{ln\left(\frac{T_{hot,out} - T_{cold,in}}{T_{hot,in} - T_{cold,out}}\right)} \right]. \tag{2.4}$$

However, fluids that operate in the supercritical region show large variations in their thermophysical properties, which challenge the assumptions made by the logarithmic temperature difference method. To address these singularities, a local approach to the problem is proposed, whereby the heat exchanger is divided into N parts, allowing the assumptions to be applied at a local level. Therefore, each heat exchanger is discretized into N sub-sections connected in series and an energy balance is performed in each element (NELLIS; KLEIN, 2009):

$$i_{hot,j+1} = i_{hot,j} - \frac{\dot{Q}}{N\dot{m}_{hot}}, \tag{2.5}$$

$$i_{cold,j+1} = i_{cold,j} - \frac{\dot{Q}}{N\dot{m}_{cold}}. \tag{2.6}$$

The total heat transferred ($\dot{Q}$) is divided equally and distributed among the sub-heat exchangers ($\dot{Q}$/N). Assuming the pressure drop between the two streams negligible, the heat transfer is only due to the change in enthalpy. With the known inlet conditions of both streams, the temperature profiles of both fluids can be established, along with the local temperature difference:

$$T_{hot,j+1} = T(p_{hot}, i_{hot,j+1}), \tag{2.7}$$

$$T_{cold,j+1} = T(p_{cold}, i_{cold,j+1}). \tag{2.8}$$

The thermal conductance $(UA)_j$ of each sub-heat exchanger can be calculated and the overall global conductance (UA) of the heat exchanger is simply the sum of the $(UA)_j$ of all sub-heat exchangers.

The concept of pinch point can be best illustrated with an example. Figure 2.5 presents the results of a pinch point analysis in a counter-flow heat exchanger device, wherein the device was discretized into 100 elements in order to account for temperature variations in the supercritical CO_2. On the left side of Figure 2.5, the temperature profiles of water and CO_2 are displayed as a function of the number of sub-heat exchanger elements, calculated using Equations 2.5 to 2.8. On the right side, the individual conductance UA of each element of the mesh is displayed, calculated using Equation 2.4, as well as the

behaviour of the temperature difference between the hot and cold stream ($\Delta T = T_{hot,i} - T_{cold,i}$) throughout the heat exchanger. Because the maximum heat transfer corresponds to a heat exchanger with infinite conductance $UA \to \infty$, that is in the limit where CO_2 and water temperatures approach each other $\Delta T \to 0$ (NELLIS; KLEIN, 2009) it would be in the best interest to match the cold and hot streams temperature profile as close as possible. A deeper discretized analysis such as the one in Figure 2.5 can help as sanity check that second law is not being violated, specially when dealing with supercritical fluids. The drawback of increasing the heat exchanger performance by bringing the temperature profiles closer together, is the increase in UA, as shown in the left side of Figure 2.5.

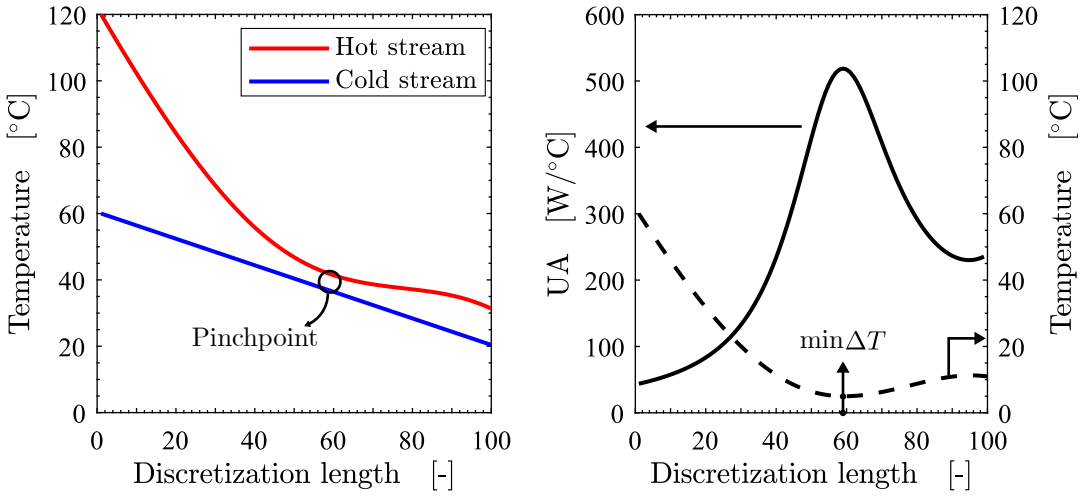

Figure 2.5 – Discretization of a heat transfer process between supercritical-CO_2 (hot fluid) and water (cold fluid). Temperature profiles of the hot and cold streams in the counter-flow heat exchanger (left). Individual conductance UA and temperature difference of each element of the discretized heat exchanger (right). Properties obtained from the Refprop library (LEMMON *et al.*, 2013).

It is worth noting that the choice of heat exchanger geometry, such as parallel, counter-flow, or cross-flow, can significantly impact the pinch point analysis. Radermacher and Hwang (2005) highlighted the advantages of using zeotropic mixtures with temperature glide in counter-flow configurations. Counter-flow heat exchanger reduces the average temperature difference between the two streams, allowing the cycle to approach a Lorenz cycle. This results in a reduction of thermodynamic irreversibility and a higher heat exchange efficiency. Still referencing Radermacher and Hwang (2005), three heat exchanger geometries (cross-flow, parallel, and counter-flow) were compared for both pure R22 (HCFC) and the zeotropic mixture R407c. Results showed that when using R-407C the combination of temperature glide and a parallel flow heat exchanger could degrade performance by up to 8.3% compared to a cross-flow configuration. On the other hand, with a pure counter-flow heat exchanger instead of a cross-flow heat exchanger, the capacity can be improved by 4.4% under typical heat pump operating conditions.

2.3 STATE-OF-THE-ART

The selection of a refrigerant fluid is crucial in designing heat pumps that are both efficient and viable economically and environmentally. This work focuses on water-to-water cycles, which both heat sink and source secondary fluids are water.

Due to restriction of high environmental impact refrigerants, such as CFCs and HCFCs, numerous studies have been conducted using CO_2 (NEKSÅ, 2002; STENE, 2005; LORENTZEN, 1994). However, due to its low critical temperature of 30.9 °C (LEMMON *et al.*, 2013), water heat pumps require a transcritical operation, as the heat sink average temperature is higher (NEKSÅ, 2002). Therefore, a strategy to control the discharge pressure to an optimal level is required to achieve the best COP (GOSNEY, 1982). Nekså (2002) demonstrated that an increase in high-side pressure leads to an increase in heating capacity until it reaches a plateau, after which the increase in discharge pressure no longer offsets the increase in compression work (as shown in Figure 2.6). In addition to its environmentally friendly properties, CO_2 also offers a volumetric capacity that is 5 to 10 times greater than other alternatives, allowing for reduced component size (NEKSÅ, 2002). Its heat transfer characteristics in the supercritical region, such as thermal conductivity and isobaric specific heat, also enable the use of compact heat exchangers (NEKSÅ, 2002; KIM, 2004).

However, the use of CO_2 as a refrigerant is associated with certain drawbacks, such as higher pressure levels (NEKSÅ, 2002; KIM, 2004), throttling losses (KIM, 2004), and reductions in specific refrigerating effect (GOSNEY, 1982) during transcritical operation. To address these obstacles, researchers have explored strategies, such as, including the use of work-recovery devices during the expansion process (SARKAR, 2008), intermediate heat exchangers (CHEN; GU, 2005; YU *et al.*, 2010), and the investigation of natural refrigerants such as hydrocarbons and their mixtures (DAI *et al.*, 2015; YU *et al.*, 2010; ZHANG *et al.*, 2017; JU *et al.*, 2018; HAKKAKI-FARD *et al.*, 2014; HAKKAKI-FARD *et al.*, 2015).

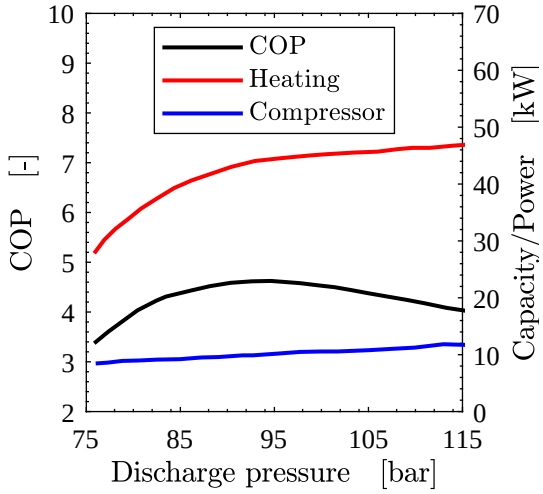

Figure 2.6 – Optimum high-side pressure for CO_2 heat pump operation. Adapted from Nekså (2002).

Yu *et al.* (2010) studied the feasibility of using a propane and R32 (HFC) mixture in a small heat pump system that operates on a transcritical cycle. The system was designed to heat water at high temperatures, ≈ 90 °C, and was evaluated at various evaporating temperatures, compressor discharge pressures, and gas cooler outlet temperatures. The thermodynamic model used air as a heat source and water as a heat sink. The authors proposed an azeotropic mixture with a 70% (R32) and 30% (R290) mass fraction concentrations. They compared its performance with CO_2 and R125. The authors found that the mixture's coefficient of performance was higher than that of pure CO_2, particularly at lower evaporating temperatures. However, the volumetric heating capacity of CO_2 was shown to be superior. In terms of the system's discharge pressure, CO_2 operation exhibited higher levels than R125 and R32/R290, which showed similar results.

In their study, Ju *et al.* (2018) conducted both experimental and theoretical investigations on a water heat pump that used mixtures of CO_2/R290. The system employed water as both the heat source and heat sink. The study aimed to examine the effect of a component mass fraction on the mixture — which varied from 0.08 to 0.16 for CO_2 — on the COP system, on the discharge pressure, and on the condenser outlet temperature. The authors identified an optimal mixture composition that maximized COP, consisting of 12% CO_2 and 88% R290. They compared the performance of the mixture to that of R22 in pure operation. Based on both experimental and theoretical results, the optimal mixture enhanced the system COP by an average of 14.5% under nominal conditions, which involved a total temperature lift of 40 °C in the heat sink. The authors attributed the improvement in COP to a reduction in irreversibilities in the condenser due to the large temperature glide of the mixture. The study also examined the effects of heat sink temperature rise and heat source inlet temperature. The optimal mixture of CO_2/R290 demonstrated improved COP and heating capacity values for heat sink temperature lifts ranging from 30 °C to 50 °C. In terms of heat source temperature, the optimal mixture

showed enhanced COP values at the highest inlet temperature investigated of 30 °C, but this was accompanied by higher discharge pressure levels.

Several works have examined the use of CO_2-based refrigerant mixtures with low GWP. Sánchez and Silva (2018) focused on employing mixtures in Rankine cycles and considered both technical and environmental aspects. The results indicated that, from a technical standpoint, a CO_2-poor mixture is preferred. However, when environmental impact is taken into account, a CO_2-rich mixture is a better option. Another comprehensive study focused on heat pump applications and is described in the work of Dai *et al.* (2015). The authors used thermodynamic modeling to evaluate a water-to-water heat pump and found that there is an optimal discharge pressure when using zeotropic mixtures with thermal glide. By analyzing T-s diagrams, the authors determined that the COP is maximized when two pinch points appear in the heat exchangers. They also noted that a good thermal match between the working and secondary fluids in the heat exchangers can enhance the COP of the system. The study also investigated the effect of mixture composition on several figures of merit. Generally, intermediate values of mixture concentration (i.e., ≈ 0.5) reduce COP due to excessive glide values, which do not match the temperature rise in the condenser/evaporator. Additionally, the results showed that the addition of CO_2 to the mixture increases the discharge pressure, and that some mixtures can switch from subcritical to transcritical operation when CO_2 concentration levels are increased.

In the context of heat pump applications in severe cold climates, the studies by Hakkaki-Fard *et al.* (2014) and Hakkaki-Fard *et al.* (2015) focused on air-to-air heat pumps. The former utilized a numerical model to investigate the performance of refrigerant mixtures with thermal glide in air heat pumps designed for cold climates — outside air temperatures ranging from -20 °C to 10 °C. The authors found that propane and its mixtures (R290) had the highest COP but the lowest heating capacity, leading them to rule out R290 for further investigation. On the other hand, the mixture of R32/CO_2 (80/20) showed the best heating capacity, even better than R410A, and offered the advantages of both CO_2 and R32 while minimizing their drawbacks. This mixture can increase the heating capacity of a conventional heat pump that runs on R410A by 30%, and its GWP is only 25% of that of R410A. This paper highlights the potential of using zeotropic refrigerant mixtures in conventional heat pumps with minimal changes in the cycle components to achieve significant performance improvements under cold climate conditions. In Hakkaki-Fard *et al.* (2015), the authors investigated the R32/CO_2 mixture (by varying its composition) in a hybrid air-to-air heat pump that comprises a backup electric heater. Based on building load and weather data of Canadian cities, the authors assessed the seasonal performance of the system. They found that increasing CO_2 mass fraction leads to an increase in heating capacity due to the elevated density of carbon dioxide at lower temperatures. However, CO_2 addition can also impair COP due to the high pressure of

CO_2 that can demand more compression work and reduce the system's efficiency. The authors demonstrated that it is possible to save up to 23% of seasonal energy consumption by using a mixture control system with 10% increments with the CO_2/R32 mixture designed to change the mixture composition based on the heat loads required.

Concerning combined heat pumps, an earlier study by Stene (2005) proposed a compression-based cycle to match the temperature profiles of different heat demands. Stene (2005) analyzed a residential CO_2 heat pump experimentally and theoretically for space heating only, hot water delivery only, and combined space and water heating. The proposed cycle allocates the gas coolers based on CO_2 temperature: high temperature one for water heating, intermediate temperature one for space heating, and low temperature one for water pre-heating.

Moreover, Brodal and Jackson (2019) investigated the number and arrangement of gas coolers in CO_2 and R410A cycles via numerical simulations, considering various operating parameters such as heat sink, heat source, and evaporating temperatures. The authors found that the space-to-water heating ratio, determined by the use of gas coolers, had the most significant impact on COP.

2.4 CONTRIBUTIONS

Previous optimization studies have analyzed CO_2 heat pumps, focusing on cycle configuration (BRODAL; JACKSON, 2019; STENE, 2005) and the ratio of space heating to domestic hot water delivery (BRODAL; JACKSON, 2019). However, none of these studies considered the impact of CO_2-based mixtures. Furthermore, literature on severe cold climates has mainly focused on air-to-air heat pumps (HAKKAKI-FARD *et al.*, 2014; HAKKAKI-FARD *et al.*, 2015). As can be seen in Table 2.1, comprehensive work on refrigerant mixtures was performed by Dai *et al.* (2015), Yu *et al.* (2010), Hakkaki-Fard *et al.* (2014) and Hakkaki-Fard *et al.* (2015). But these works only considered a single-purpose heat pump, either water heating or space heating; none of them took into consideration the influence of different heat demands in the operation range. In this context, Brodal and Jackson (2019) conducted a comparative work between pure fluid operation with CO_2 and R410A in a combined heat pump dedicated to both heating space and producing hot water, but evaporating temperatures were limited to 0 °C.

Thus, considering the general and specific objectives defined in Chapter 1 and the review of selected works, this study aims to focus on the aforementioned gaps by analyzing a combined heat pump for hot domestic water and space heating operating with low-GWP/CO_2 binary mixtures, as well as, its performance at reduced heat source temperatures to emulate cold climate zones. The main contribution of these analyses is to evaluate the performance of binary mixtures in combined heat pump systems, by improving the figures of merit of refrigerating cycles, prioritizing the technical and environmental aspects of these systems. In addition, this study aims to investigate the effects of mixture

concentration, heating demands (e.g., primary dedication to water heating or hot domestic water production) and heat source temperatures on the heat pump operation.

Table 2.1 – Brief summary of studies on the application of refrigerant mixtures in heat pumps.

Author	**Refrigerants**	**Heat source/sink**	**Heat pump type**	**Focus**
Dai *et al.* (2015)	CO_2 binary mixtures with R41, R32, R1270, R290, R161, R1234yf, R134a, RE170, R152a, R1234ze	Water/Water	Water heating	Thermodynamic analysis. Influence of mixture concentration and heat sink temperature on COP, discharge pressure and cycle irreversibilities
Yu *et al.* (2010)	CO_2, R125 and azeotropic mixture of R32/R290	Air/Water	Water heating	Thermodynamic analysis. Influence of evaporating temperature on COP, heating capacity and discharge and suction pressures. The effect of the addition of an internal heat exchanger in the cycle
Zhang *et al.* (2017)	Binary mixture of CO_2/R290	Water/Water	Water heating	Experimental investigation of various refrigerant charges, optimal discharge pressure, COP, heating capacity and heat coefficient of the gas cooler
Ju *et al.* (2018)	Binary mixture of CO_2/R290 and R22	Water/Water	Water heating	Experimental and simulations. Effects of mixture concentration and heat source and sink temperatures on COP, discharge pressure, compressor power and heating capacity
Hakkaki-Fard *et al.* (2014)	R290 and R410A. Mixtures of R290/R32, R290/CO_2, R600/R32/R125, R32/CO_2 and R290/R32/CO_2	Air/Air	Residential heating	Thermodynamic analysis. Influence of outside air temperature and mixture composition on COP, heating capacity, discharge pressure and compression ratio
Hakkaki-Fard *et al.* (2015)	R410A and binary mixtures of R32/CO_2	Air/Air	Residential heating	Thermodynamic analysis. Influence of outside air temperature and mixture composition focusing on the season performance
Brodal and Jackson (2019)	R410A and CO_2	Air/Water	Combined (water and space heating)	Thermodynamic analysis. Influence of pinch point restriction, heat sink temperature, space to water heating ratio, evaporation temperature on COP.

3 THERMODYNAMIC MODELING OF A RESIDENTIAL HEAT PUMP FOR COMBINED SPACE AND WATER HEATING USING BINARY CO_2-BASED MIXTURES

This chapter evaluates the performance of various configurations of combined heat pump systems that can provide both space heating and hot water, using refrigerant mixtures. Given the limited number of studies on this topic, the chapter investigates the impact of mixture composition and heat demand on key performance parameters of the cycle. The study is based on a manuscript – currently in the review process for publication – developed during the master thesis process.

The residential sector accounts for a significant portion of global energy consumption, with space and hot water heating contributing to the majority of this consumption. To meet the technical and environmental requirements of this sector, several alternatives for space and hot water heating were evaluated. Specifically, this study considers the use of a combined heat pump system that uses binary mixtures of CO_2 and other refrigerants. The study employs a computational model to test three cycle configurations (AB, BC and ABC), different ratios of space heating to hot water demands, and several CO_2 mass fractions in the mixture.

3.1 METHODS

This section describes the heat pump model used in this study to investigate the potential of CO_2 binary mixtures. All components are modeled using the finite control volume approach of the energy conservation equation assuming steady state regime. Pressure drop in piping and heat exchangers, as well as kinetic and potential energy losses, are not considered. Moreover, all heat exchangers within the cycle are assumed counter flow and isolated from the surroundings. To capture the temperature profile inside the equipment and avoid violating pinch point restrictions, heat exchangers were discretized into sub-heat exchangers. Details of the discretization process are presented in Subsection 3.1.2.

For conciseness, a simple heat pump configuration is described to detail operational principles and characteristics. Because CO_2 operation can occur in both subcritical and supercritical stages, a transcritical cycle is often used. Figure 3.1 shows the thermodynamic states of a hypothetical heat pump cycle with one compressor, one gas cooler, one expansion device, and one evaporator on a temperature-entropy and a pressure-enthalpy diagram. In the pressure-enthalpy diagram, CO_2 enters the compressor as saturated vapor at low pressure. The CO_2 pressure increases during the compression process until it reaches a supercritical state, as indicated by point 2 in the diagram. Note that the gas cooling process in the supercritical state is similar to the condensation in a subcritical cycle. In the gas cooler, the demand for space heating or domestic hot water is properly met. The

supercritical CO_2 then leaves the gas cooler at high pressure and low temperature, as shown by point 3 in the diagram. Next, the CO_2 pressure decreases significantly in an isenthalpic expansion device. Finally, at point 4 in the diagram, CO_2 at subcritical state is heated in the evaporator to reach the inlet conditions required by the compressor.

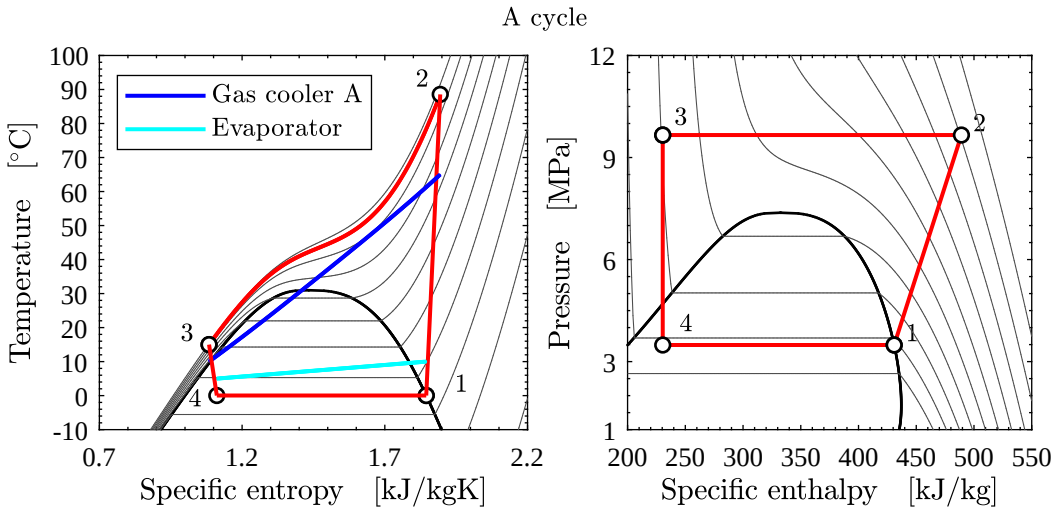

Figure 3.1 – Basic CO_2 transcritical heat pump, cycle "A"; T-s diagram (left) and profile temperatures of the secondary fluid (water) on the gas cooler and evaporator; P-h diagram (right).

3.1.1 Heat pump configurations

The term combined heat pump refers to a device designed to provide both domestic hot water and hot water for a space heating system, such as floor coils or radiators (NEKSÅ, 2002). A heat pump system that meets both these heating needs can come in two forms: as stand-alone systems, where a heat pump water heater is used alongside a separate unit for space heating, or as an integrated unit that handles both space heating and hot water. The integrated unit is often the most cost-effective option due to its compact design, resulting in lower investment and installation expenses and better overall profitability (STENE, 2007). A combined heat pump with space and domestic water heating can be controlled by means of a four-way valve and a pump (SUN *et al.*, 2013). Therefore, the combined heat pump operates with different heat sinks at different temperatures, which can be arranged in different ways to meet these heat transfer requirements. This master thesis considers three system configurations, labeled AB, BC, and ABC, based on the number of gas coolers used in each cycle. A schematic of each configuration is presented in Figure 3.2. All three configurations can be used for both space heating and domestic hot water delivery. However, configuration AB uses a low-temperature gas cooler for domestic hot water demand and a high-temperature gas cooler for space heating, whereas configuration BC is the opposite. Configuration ABC, shown in Figure 3.2c, is based on the arrangement proposed by Stene (2005). In this configuration, the low-temperature

gas cooler preheats the water that is heated in the high-temperature gas cooler, while the intermediate temperature gas cooler (B) rejects heat to the space.

For conciseness, only the modeling of configuration ABC is described, but configurations AB and BC follow a similar procedure. Regardless of the cycle configuration or the operational conditions, the following parameters were held constant:

i. Saturated vapor at evaporator outlet ($x_1 = 1$)

ii. Compressor has constant isentropic efficiency η_{isen}

iii. Mass flow rate of the refrigerant (or mixture) of 1 kgs^{-1}

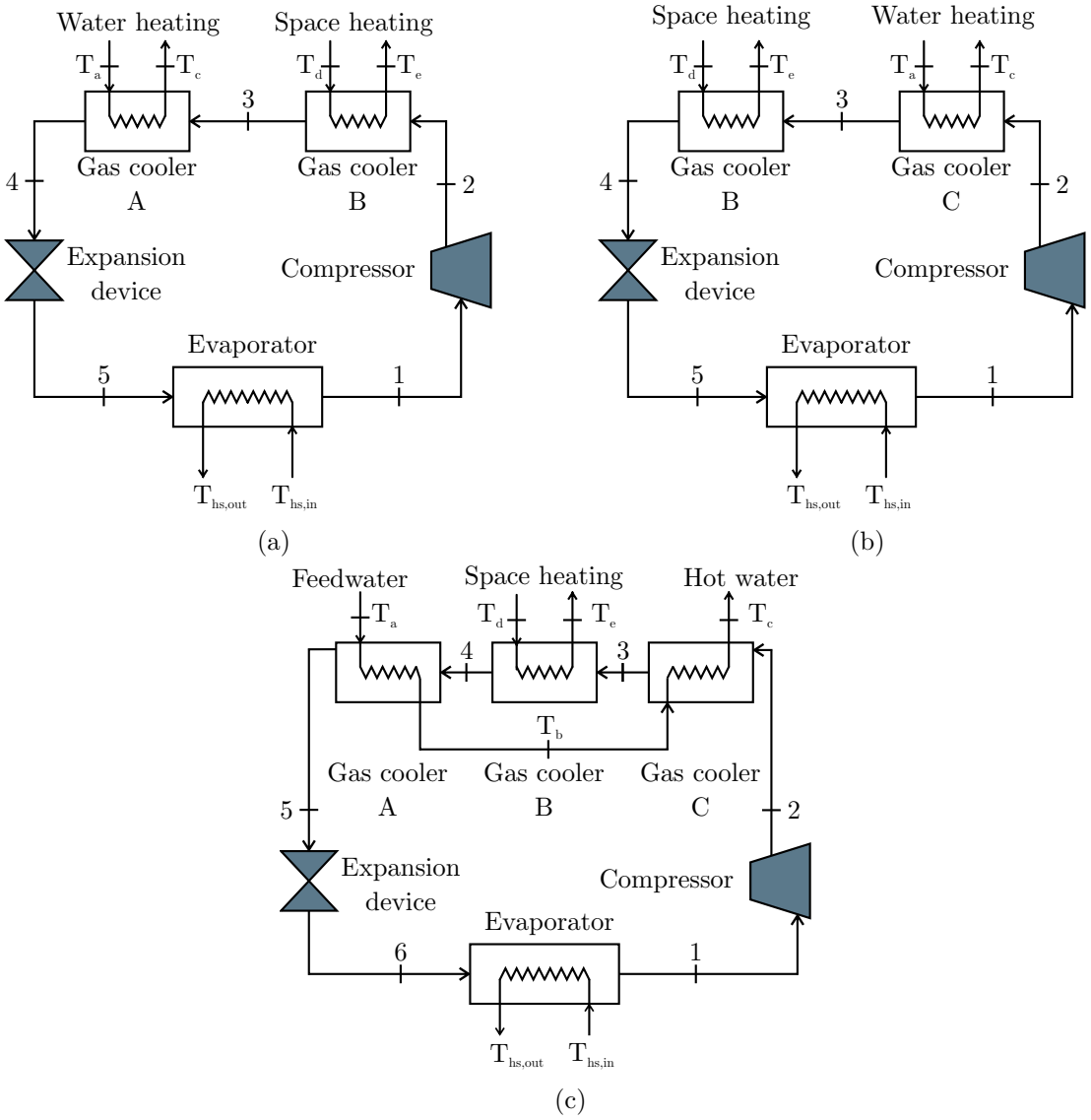

Figure 3.2 – Schematic of the combined heat pump cycles simulated. Two gas coolers and one evaporator arrangement: (a) Configuration AB; (b) Configuration BC; Three gas coolers and one evaporator: (c) Configuration ABC.

At the evaporator outlet, the saturated vapor at suction pressure (p_{low}) is compressed from state 1 to 2 as shown in Figure 3.2c. The compression of the refrigerant is defined by considering the isentropic efficiency (ÇENGEL; BOLES, 2013):

$$i_2 = i_1 + \left(\frac{i_{2,isen} - i_1}{\eta_{isen}} \right), \tag{3.1}$$

where $i_{2,iso}$ represents the enthalpy of the refrigerant mixture after compression, assuming an isentropic process, while η_{isen} represents the isentropic efficiency. Once the refrigerant mixture leaves the compressor at high pressure and temperature, it enters the gas cooler C, where it rejects heat to the water at atmospheric pressure, bringing the water to its design temperature of T_c. Next, the refrigerant mixture enters gas cooler B where it cools to temperature T_4, while heating the space from T_d to T_e. The refrigerant mixture proceeds to the gas cooler A, where it pre-heats water for the hot domestic system at temperature T_a. Finally, the refrigerant mixture expands up to a predefined pressure through an isenthalpic device, from thermodynamic states 5 to 6, reaching the suction pressure (p_{low}), where

$$i_5 = i_6, \tag{3.2}$$

considering an isenthalpic process. In the evaporator, a cold stream of the working fluid is heated by a heat source — water at atmospheric pressure entering at $T_{HS,in}$ and leaving at $T_{HS,out}$. The refrigerant is evaporated and returns to the compressor as saturated vapor at p_{low} and T_1. It is worth mentioning that the space heating circuit also uses water as the secondary fluid at atmospheric pressure.

The solution for the cycle includes a variable relevant to combined heat pumps, known as the space to water heating ratio (r_{heat}) (BRODAL; JACKSON, 2019). This ratio represents the heat demands associated with the combined heat pump operation:

$$r_{heat} = \frac{Q_B}{Q_A + Q_C}. \tag{3.3}$$

When $r_{heat} = 1$, the heating power is equally distributed between the space and domestic hot water systems; when $r_{heat} = 0$, the combined heat pump only works on hot domestic water mode; and when $r_{heat} \to \infty$, the heating is directed only towards the space.

3.1.2 Modeling of cycle components

As previously mentioned (Subsection 3.1.1), the modeling of the compressor is represented by the solution of the energy conservation equation, considering also the definition of isentropic efficiency (equation 3.1). Thus, once the state of the refrigerant fluid at the compressor inlet is known (i.e., pressure and temperature conditions), the work can be calculated using the relationship:

$$\dot{W}_{comp} = \dot{m}_{ref}(i_2 - i_1). \tag{3.4}$$

There are various methods to model compressors in vapor compression cycles, ranging from more detailed to less complex models. However, the approach based on isentropic efficiency offers independence from the specific characteristics of each compressor and refrigerant fluid (RADERMACHER; HWANG, 2005). Since this work aims to implement different fluids and their mixtures, modeling specific compressors for each refrigerant or mixture could be costly. Therefore, for this work, a model based on a constant isentropic efficiency of 70%, as described in the work of Radermacher and Hwang (2005), was chosen. Similarly, the expansion device model is based on an isenthalpic and adiabatic process (equation 3.2).

The energy balance in the evaporator and gas coolers gives the total heat transfer, provided that the inlet and outlet temperatures of the working fluid are known, as given by:

$$\dot{Q}_{evap} = \dot{m}_{ref}(i_1 - i_2) = \dot{m}_{HS}(i_{HS,in} - i_{HS,out}), \tag{3.5}$$

$$\dot{Q}_A = \dot{m}_{ref}(i_4 - i_5) = \dot{m}_{DW}(i_b - i_a), \tag{3.6}$$

$$\dot{Q}_B = \dot{m}_{ref}(i_3 - i_4) = \dot{m}_{SH}(i_e - i_d), \tag{3.7}$$

$$\dot{Q}_C = \dot{m}_{ref}(i_2 - i_3) = \dot{m}_{DW}(i_c - i_b). \tag{3.8}$$

It is important to note that in this study, we maintain constant water temperatures and a refrigerant mass flow rate of 1 kg^{-s} to simplify the optimization calculations. As a result of the energy balance, the water mass flow rates at the heat exchangers (i.e., evaporator and condensers) can vary significantly, potentially leading to increased pumping demands. In reality, these variations may not align with practical conditions. Nevertheless, this approach was chosen for the sake of practicality in conducting the calculations and optimizing the heat pump system.

Nevertheless, a discretization process is performed to account for variations in thermophysical properties by dividing each heat exchanger into N sub-heat exchangers connected in series as described previously in Subsection 2.2.4. An energy balance is performed in each of these sub-heat exchangers, where the temperature of the hot and cold stream of every j^{th} element can be determined, once pressure and enthalpy are known (following equations 2.5-2.8). The temperature difference between the hot and cold stream for each section can determined $\Delta T_j = T_{hot,j} - T_{cold,j}$. Thus, considering a minimum pinch point allowed of 5 K, the restriction $min(\Delta T_j) \geq PP_{allowed}$ must be satisfied, otherwise it is disregarded from the optimization analysis. It is essential to emphasize the significance

of the discretization procedure for each heat exchanger. This aspect takes on added importance in the context of supercritical fluids and zeotropic mixtures. In these cases, the location of the pinch point temperature difference may not necessarily occur at the entrance or outlet of the device, as is typically the case in pure fluid applications. This phenomenon was most effectively demonstrated in Section 2.2.4, as illustrated in Figure 2.5.

The overall heat transfer coefficient U is indirectly estimated using the inverse of the total thermal resistance, which is referred to as the thermal conductance UA. To calculate UA, the logarithmic mean temperature difference method is utilized (as shown in Subsection 2.2.4).

Table 3.1 presents the predefined operating parameters of the combined heat pump system. The water supply temperature (T_a) is influenced by various factors such as climate and water supply system, which means that several values are possible. In the literature, different studies have adopted different values for T_a, Wang *et al.* (2019) used 17 °C, Xu *et al.* (2021) 9 °C, and Brodal and Jackson (2019) and Stene (2005) 6.5 °C. Therefore, this master thesis has considered an average value of 10 °C. Following reference Stene (2005), the water circulation temperatures of the space heating systems (T_d/T_e) were adopted as 30/35 °C. The desired temperature for hot water (T_c) may vary depending on its intended use (Cube1981). While some heat pumps are designed to provide high-temperature water (PAN *et al.*, 2011), the typical hot water temperature for domestic use is 65 °C (WANG *et al.*, 2019; XU *et al.*, 2021). As a result, this master thesis has adopted $T_c = 65$ °C. The temperature of the heat source ($T_{HS,in}/T_{HS,out}$) was determined based on Dai *et al.* (2015).

Table 3.1 – Combined heat pump operating parameters.

Variable	Value [Unit]
η_{isen}	0.7
x_1	1
$PP_{allowed}$	5 °C
T_a	10 °C
T_c	65 °C
T_d	30 °C
T_e	35 °C
$T_{HS,in}$	10 °C
$T_{HS,out}$	5 °C
$\dot{m}_{ref}$	1 kgs^{-1}
$\dot{x}_{CO_2}$	0 to 1
r_{heat}	0.1, 0.5, 1.0, 2.0, 10

3.1.3 Fluid selection

The combined heat pump model evaluated various binary combinations of refrigerants with different fractions of CO_2, prioritizing low-GWP, zero ODP, suitability to the heat pumps, and compatibility with CO_2. The selection of potential refrigerant fluids was limited to hydrocarbons (HCs) and hydrofluorocarbons (HFCs). HCs have minimal GWP values and zero ODP but are flammable (SÁNCHEZ *et al.*, 2018), while HFCs are suitable to heat pumps, but contribute significantly to the greenhouse effect (RADERMACHER; HWANG, 2005). Binary combinations of these fluids can be beneficial when the thermodynamic properties are exploited and the problems of flammability and GWP are simultaneously mitigated (SÁNCHEZ *et al.*, 2018). The selected refrigerants and their critical pressure and temperature, and environmental indicators are presented in Table 3.2. Moreover, this study avoided mixtures with a glide greater than 60 °C to prevent compromising the system's operation by leading to mixture separation (RADERMACHER; HWANG, 2005), which is a common practice in studies dealing with mixtures (DAI *et al.*, 2014; SÁNCHEZ; SILVA, 2018).

Table 3.2 – Data and characteristics of the selected fluids for the mixture used in the combined heat pump.

Refrigerant	**T_{crit} [°C]**	**p_{crit} [MPa]**	**GWP* (100 years)**	**$T_{boiling}$ at 1 atm [ºC]**
R744 (CO_2)	31.0	7.4	1	-78.5
R41	44.1	5.9	92	-78.3
R32	78.2	5.8	675	-51.6
R1270	91.1	4.5	3	-47.6
R1234yf	94.7	3.8	4	-29.5
R290	96.2	4.2	3	-42.1
R134a	101.1	4.1	1430	-26.1
R1234ze	109.4	3.6	6	-19.0
R152a	113.3	4.5	124	-24.0
R410A	71.3	4.9	2088	-51.4

*Reference values from CoolProp 6.4.1 (BELL *et al.*, 2014).

3.1.4 Optimization routine

The heat pump models are solved through optimization aiming at maximizing the coefficient of performance while ensuring the pinch point in each sub-heat exchanger within the allowed limit ($PP_{allowed}$). The model was implemented in Matlab using a multivariable constrained optimization process with a non-linear solver (*fmincon*) (MATLAB, 2019). The properties of the refrigerant mixtures were determined using the Refprop 9.1 library (LEMMON *et al.*, 2013). A flowchart of the optimization algorithm solution is presented in Figure 3.3, where the inputs are those provided in Table 3.1 and the four independent variables are: suction (p_{low}) and discharge pressures (p_{high}), refrigerant outlet temperature of gas cooler C and A, T_3 and T_5, respectively. These variables determine the refrigerant thermodynamic state at the compressor's inlet and outlet, as well as the high and low temperature gas cooler outlets (C and A), respectively. Note that, from the algorithm and by establishing r_{heat}, one could calculate the heating power of each gas cooler by an energy balance. The refrigerant pressure and temperature at the outlet of the intermediate gas cooler B and at the outlet of the expansion device are determined once all the thermodynamic states of the cycle are defined. Then, pinch point is verified through the temperature profiles of the discretized gas coolers and evaporator. If the criteria are met, the coefficient of performance is determined, and the routine ends.

The optimization problem is therefore established by determining the input data (variables in Table 3.1), the independent variables and the objective and constrain functions (3.3).

Variables	p_{low}
	p_{high}
	T_3
	T_5
Constraints	$PP_A \leq PP_{allowed}$
	$PP_B \leq PP_{allowed}$
	$PP_C \leq PP_{allowed}$
	$PP_{evap} \leq PP_{allowed}$
Objective	maximize COP

Table 3.3 – Optmization problem premise for the combined cycle ABC.

3.1.5 Verification

To ensure that the heat pump model represents accurately the system's behavior for the parametric optimization analyses — optimization problem solved as a function of parameters that are outside of the control of the designer, it was required to verify its mesh independency and compare its preliminary results to other studies. Since all heat exchangers were discretized along their length, mesh verification was required. To accomplish this, cycle A (shown in Figure 3.1) was modeled using a single gas cooler and evaporator, since this scenario represented the most challenging condition to ensure that the energy balance was correct. Thus, the gas cooler and evaporator were analyzed with respect to their one-dimensional mesh. For mesh verification purposes, cycle A was modeled for binary mixtures of CO_2 and three other fluids (R32, R290, and R1234yf), while considering mass fractions varying between 0 and 1 in intervals of 0.2 and the most extreme cases the heat pump system could be exposed to. For instance, cycle A has three independent variables, the suction and discharge pressure values, p_{low} and p_{high}, respectively, and the outlet temperature of the gas cooler, T_3; the upper and lower limits of these three variables are reported in Table 3.4.

Table 3.4 – Operation limits considered for the mesh independency verification of cycle A.

	Subcritical		**Transcritical**	
	Low	High	Low	High
p_{low}	p_{sat}(-5 °C)	p_{sat}(5 °C)	p_{sat}(-5 °C)	p_{sat}(5 °C)
p_{high}	1 [MPa]	p_{crit}−0.1[MPa]	p_{crit}+0.1[MPa]	12 [MPa]
T_3	15 °C	65 °C	15 °C	65 °C

Notice in Table 3.4 above that p_{low} is limited by the saturation pressure at -5 ºC and 5 ºC, with the latter being determined as the difference between the temperature of the heat source and the allowed pitch point of 5 ºC. The limits of p_{high} depend on the CO_2 content of the mixture. For instance, for mixtures with CO_2 mass fractions of 0.8 or higher (i.e., pure CO_2), which tend to operate as a transcritical process, the lower bound

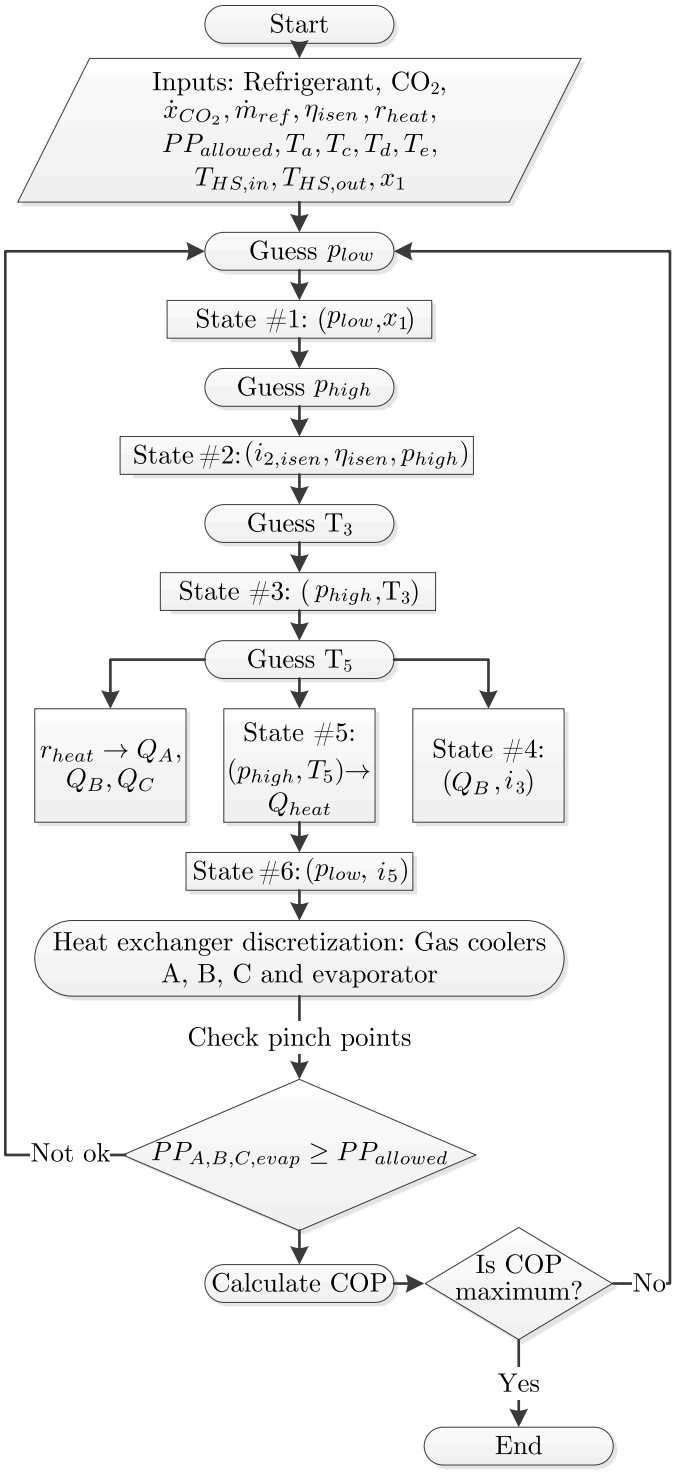

Figure 3.3 – Optimization routine

pressure was set as the critical pressure plus 0.1 MPa aiming to avoid numerical difficulties within the critical point; the upper limit was set at 12 MPa. As for mixtures with mass fraction below the 0.8, p high went from 1 MPa to 0.1 MPa — p_{crit}. T_3 was limited the between the heat sink temperature (10 °C) plus the pitch point of 5 °C and 65 °C. In total, eight different combinations for the parameters shown in Table 3.4 were tested, which can be seen in Table 3.5. A set of 14 mesh densities ranging from 10 to 900 elements (i.e., sub-heat exchangers) was employed. To establish mesh independency, the temperature was used as the figure of merit, and an absolute error lower than 0.4 K was required. Figure 3.4 shows the temperature absolute error for the different meshes analyzed. As the number of elements per mesh increased, the error decreased. Based on this figure of merit, gas coolers were modeled with 200 sub-heat exchangers and evaporators with 150.

Table 3.5 – Simulated cases for different mesh sizes of the gas cooler and evaporator for cycle A.

	$\mathbf{p_{low}}$	$\mathbf{p_{high}}$	$\mathbf{T_3}$
Case 1	High	High	High
Case 2	High	High	Low
Case 3	Low	High	Low
Case 4	Low	Low	Low
Case 5	Low	Low	High
Case 6	High	Low	High
Case 7	Low	High	High
Case 8	High	Low	Low

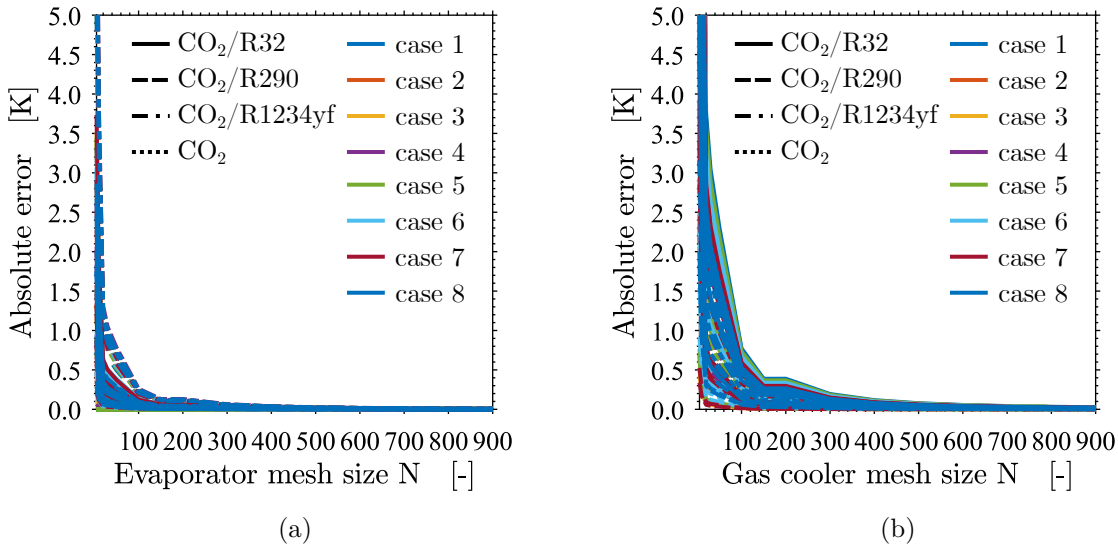

(a) (b)

Figure 3.4 – Variation of temperature absolute error in relation to the number of elements in each mesh of (a) evaporator and (b) gas cooler A.

The second verification procedure compared the implemented model with studies available in the literature (BRODAL; JACKSON, 2019; DAI *et al.*, 2015). Since the model

represents a combined heat pump with CO_2 binary mixtures, two studies were considered — one to verify the cycle configuration using pure CO_2 (BRODAL; JACKSON, 2019) and the other for the mixtures (DAI *et al.*, 2015).

Brodal and Jackson (2019) presented a model of a combined heat pump with three gas coolers, using CO_2 as a refrigerant without considering any mixtures. They optimized the process and reported the COP in relation to the ratio of space heating to domestic hot water, which is presented in Figure 3.5a and compared with the present study. The relative error to the reference model was within ± 5%, which is considered acceptable.

The proposed model was also evaluated in terms of its acceptance of mixtures as refrigerants. Since no configuration similar to that of cycle ABC was found, a heat pump with a single gas cooler model was used for this part of the verification. In a study by Dai *et al.* (2015), several compositions of low-GWP refrigerants and CO_2 were explored in a heat pump designed for water heating. Figure 3.5b shows the COP for different mixture compositions considered by Dai *et al.* (2015) as well as the present study. Relative error to the reference was found to be within 5% deviation.

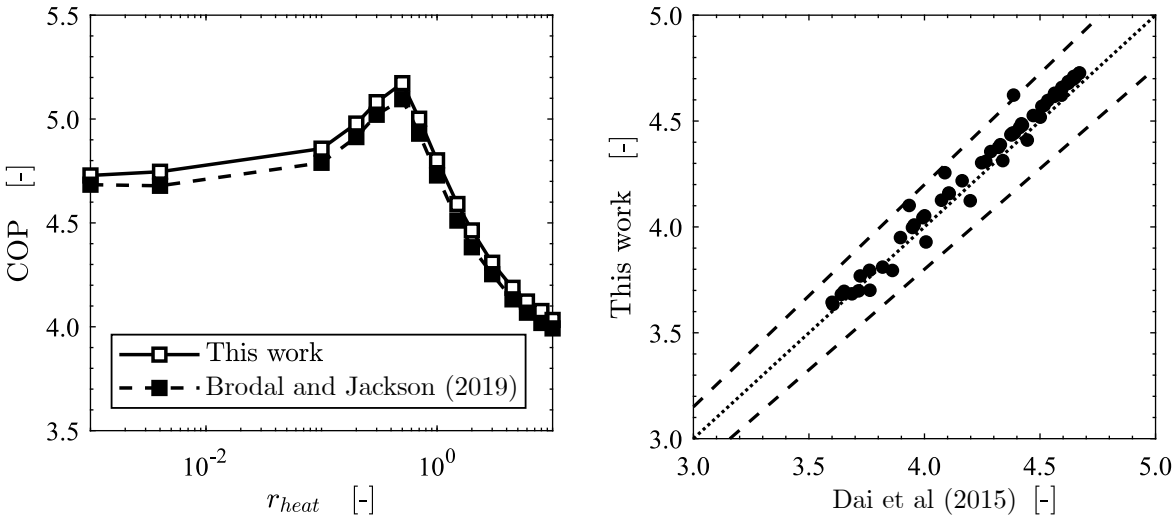

Figure 3.5 – (a) Comparison of the coefficient of performance for different ratios of space heating to domestic hot water supply for the proposed model and Brodal and Jackson (2019). (b) Coefficient of performance of the low-GWP CO_2 mixtures of Dai *et al.* (2015) versus the COP obtained with the proposed model.

3.2 RESULTS

This master thesis explores several configurations of a combined heat pump system for domestic hot water and space heating, which vary in terms of the quantity and arrangement of gas coolers, the ratio of space heating to domestic hot water (r_{heat}), the mixture fractions ($\dot{x}_{CO_2}$), and the types of secondary refrigerants used in a binary mixture. These configurations are optimized to maximize the coefficient of performance, each study

is computationally costly and time-consuming. To mitigate these costs, four secondary components of the binary mixture were considered, as presented in Table 3.2: R32, R290, R410A, and R1234yf. Each refrigerant was chosen to represent a group of refrigerants: R32 represents hydrofluorocarbons, R290 represents hydrocarbons, R1234yf represents hydrofluorolefins, and R410A serves as a standard for comparison.

3.2.1 Configuration AB

The first configuration analyzed used a high-temperature gas cooler for space heating and a low-temperature gas cooler for domestic hot water. Based on the optimization procedure described in Section 3.2, the coefficient of performance was optimized for different mixture fractions and for three ratios of space heating to domestic hot water (r_{heat} = 0.1, 1.0, and 10). For a r_{heat} value of 0.1, the demand for domestic hot water on gas cooler A is ten times higher than that of space heating; for a r_{heat} value of 1, the demands are equal; and for a r_{heat} value of 10, space heating requires 10 times more delivered heat (in this case to gas cooler B). Figures 3.6a to 3.6c show the variation of COP for the three r_{heat} values while considering several mixtures at different CO_2 mass fractions.

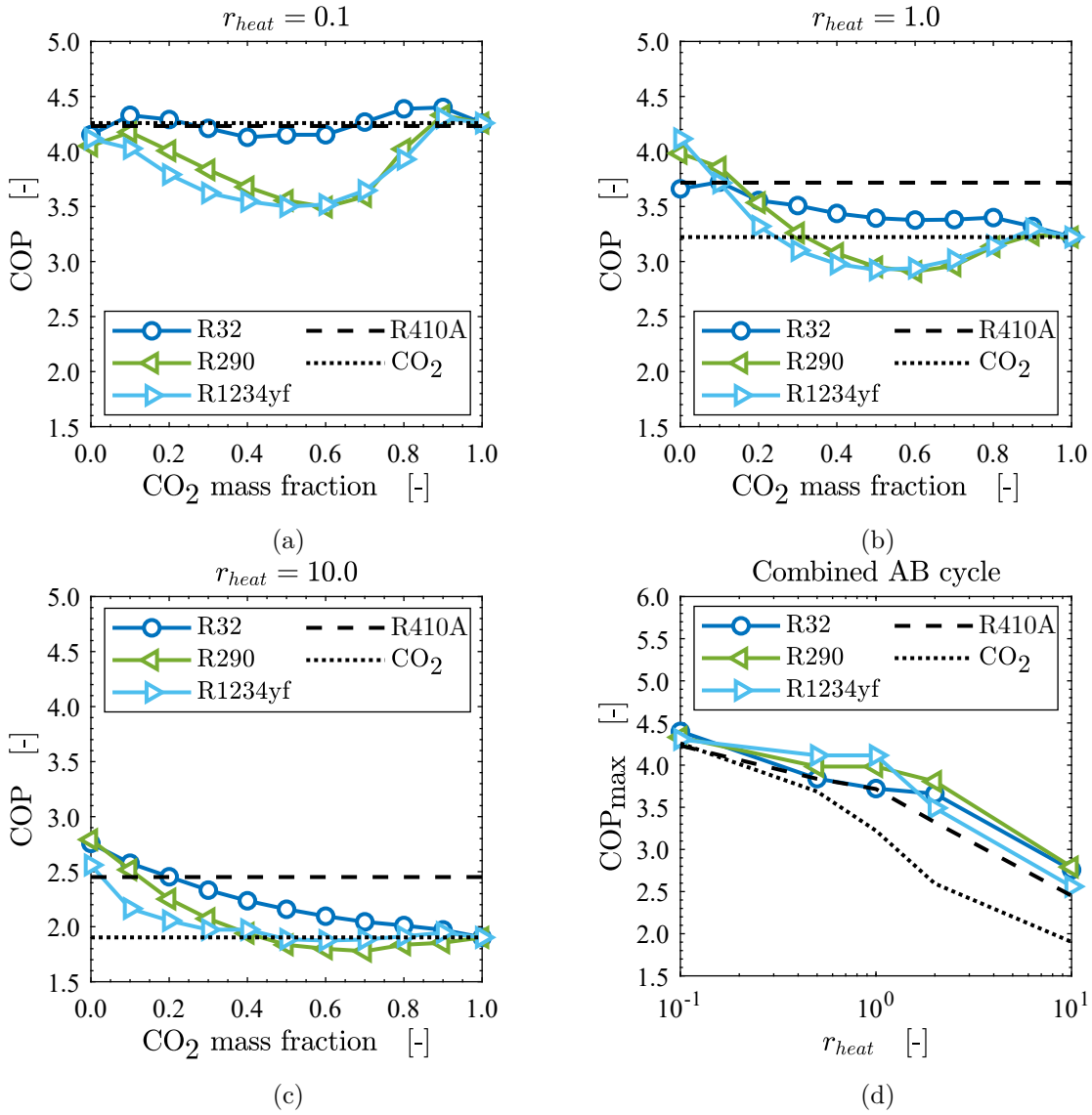

Figure 3.6 – Carbon dioxide mass fraction effects in the refrigerant mixture focusing on the coefficient of performance for the ratio of space heating to domestic hot water of 0.1 (a), 1.0 (b), and 10 (c) considering all the refrigerants presented in Table 2 employed in the AB cycle. The maximum coefficient of performance for each refrigerant curve as a function of r_{heat} (d).

From these three frames, it can be observed that the r_{heat} value of 0.1, presented in Figure 3.6a, is the only ratio where all refrigerants have a CO_2 mass fraction in which a mixture performs better than a pure fluid. In fact, it can be noticed that the CO_2 mass fractions of 10% and 90% have higher COPs, while the intermediate concentrations (approximately 50%) have the worst. One factor that might contribute to this poor performance is the excessive glide for 50/50 compositions, as previously indicated by Dai *et al.* (2015). For the other two r_{heat} values, the highest COP is observed for different pure refrigerants other than CO_2, while the lowest values are observed for roughly a 60/40 composition.

To better understand the behavior shown in Figures 3.6a to 3.6c, Figure 3.7 presents

an enthalpy-temperature diagram for the gas cooling and evaporation process. The diagram shows the heat sink fluid, the heat source fluid, and the refrigerant mixture of R32/CO_2 with mass fractions of 10%, 50%, and 90%. For example, by examining the curve slope, one can see that the highest glide during evaporation occurs for the refrigerant mixture with a mass fraction of 50%, i.e. the middle frame. This means that the performance is the worst for the highest glide, however, it is worth noting that a certain amount of glide can actually improve performance, as seen in the left and right frames. Dai *et al.* (2015) found that a modest glide helps to match the temperature profile and, consequently, enhances the coefficient of performance.

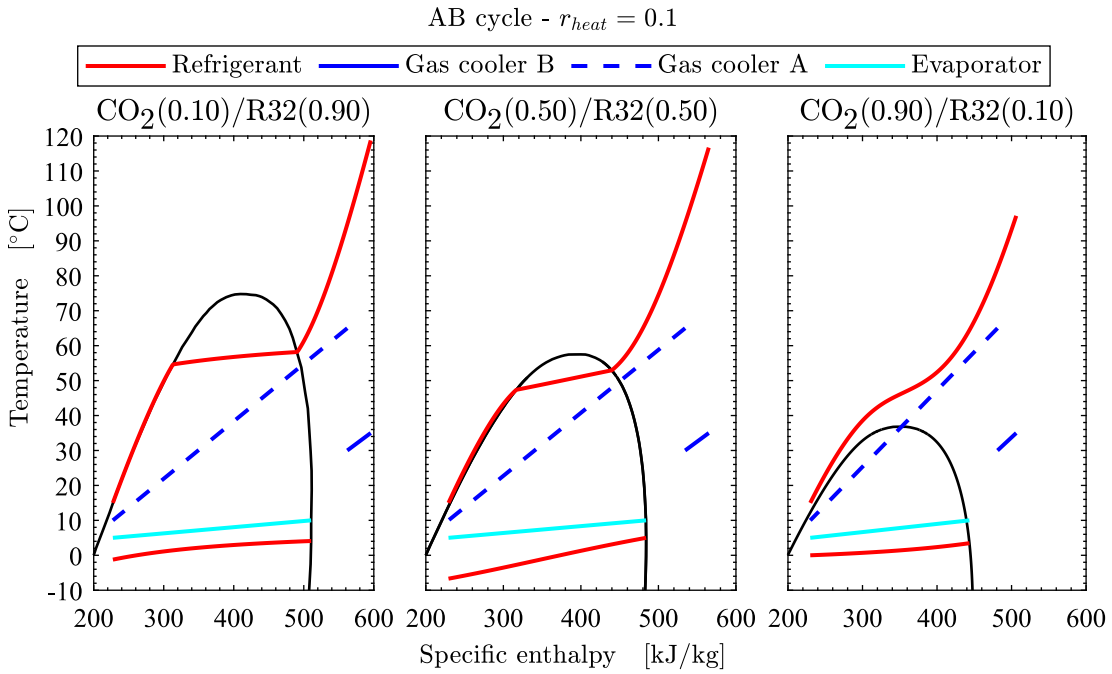

Figure 3.7 – Temperature-enthalpy curves of the R32/CO_2 binary mixture, the heat source fluid, and the heat sink fluids during evaporation and gas cooling processes for various CO_2 mass fractions considering the AB configuration operating with 0.1 of space to water heating ratio.

As the demand for space heating increases (in comparison to that of domestic hot water) greater COPs are achieved with pure fluids than with mixtures, as shown in Figures 3.6a to 3.6c. This is because space heating only requires a low temperature rise of the heat sink fluid – from 30 °C to 35 °C – and an excessive temperature glide may not be necessary, which could be a reason for pure fluids performing better. For instance, Figure 3.8 presents the temperature-enthalpy diagram for the 80%CO_2/20%R32 mixture for r_{heat} values of 0.1 and 10, as well as the heat sink fluid curves. The figure indicates that the refrigerant glide suits better a greater temperature rise demand, i.e., domestic hot water and small r_{heat} values. Additionally, Figures 3.6a to 3.6d show that pure CO_2 has performance as the ratio of space heating to domestic hot water (r_{heat}) decreases, i.e., as the heat sink fluid demands a greater rise in temperature, from 10 °C to 65 °C.

According to Austin and Sumathy (2011), the temperature gradient during gas cooling is higher than during condensation, and arranging the temperature curves of CO_2 and the heat sink fluid can improve performance.

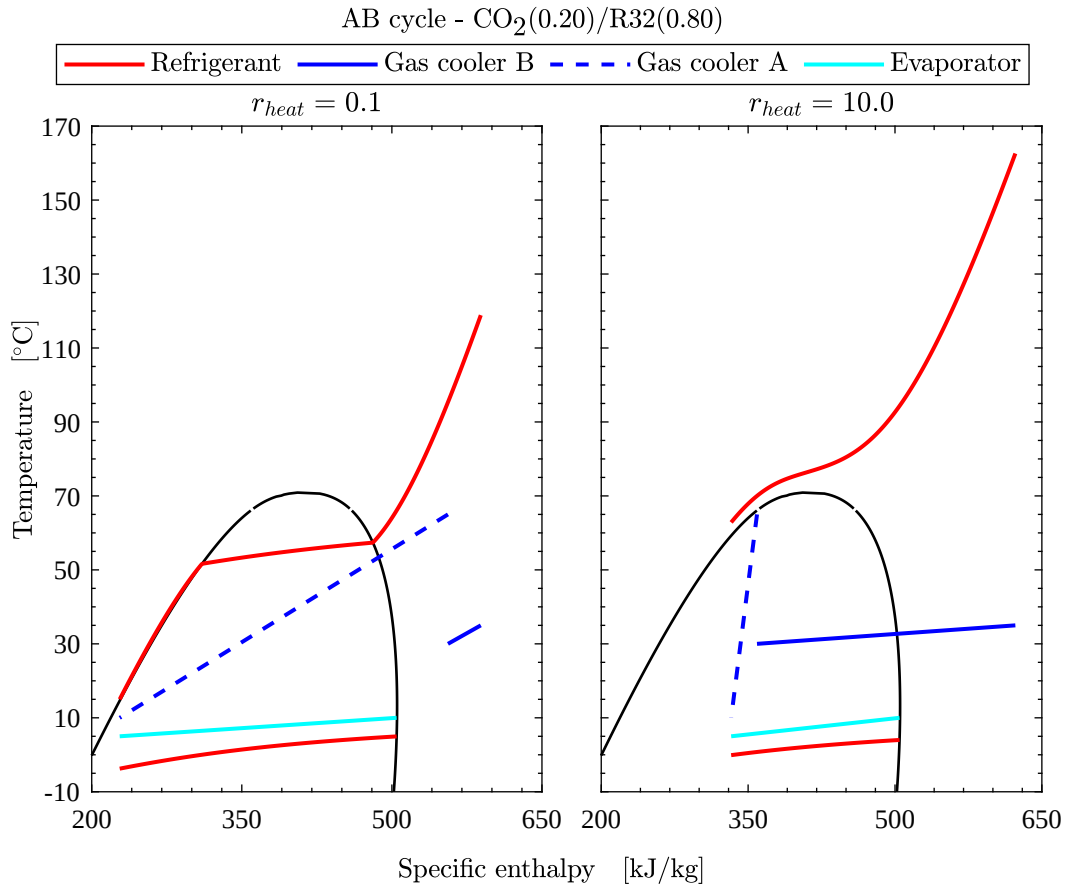

Figure 3.8 – Temperature-enthalpy diagram of the evaporation and heat rejection processes of the refrigerant CO_2/R32 with 80%/20% mixture composition for different heat demands of r_{heat} 0.1 and 10 on the combined AB cycle.

Lastly, Figure 3.6d shows the maximum COP for each working fluid at different r_{heat} values. Since the influence of CO_2 mass fraction on the COP was investigated previously, Figure 3.6d does not differentiate between pure fluids or mixtures (i.e., it reports the highest COP regardless of whether it was produced by a pure fluid or a mixture). However, the focus, here, is to investigate the influence of the demands on the coefficient of performance. Figure 3.6d shows that configuration AB benefits from low r_{heat} values since the COP increases as r_{heat} decreases. Therefore, this heat pump configuration might be suitable for hot water demands greater than space heating.

3.2.2 Configuration BC

In this configuration, the high-temperature gas cooler is dedicated to domestic hot water, while the low-temperature one is used for space heating. Figures 3.9a to 3.9c

show the effect of CO_2 mass fractions on the coefficient of performance for several binary mixtures at different ratios of space heating to domestic hot water (r_{heat}). Some mixtures exhibit an M-shaped curve of performance, with the highest COPs achieved at CO_2 mass fractions of around 10% and 90% approximately, and the lowest at 50%. As discussed previously, this behavior may be influenced by the temperature glide of the binary mixture, which can improve or deteriorate the heat pump performance. Unlike configuration AB, where the M-shaped profile only appears for small r_{heat}, for configuration BC, the M-shaped profile is noticeable for all the ratios of space heating to domestic hot water tested. In addition, Figures 3.9a to 3.9c show that there is, at least, one binary mixture performing better than the pure fluid that composes them.

Furthermore, for configuration BC, the COP of pure fluids varies significantly. The COP of pure CO_2 is the lowest among the pure fluids, indicating the advantage in terms of performance of mixing it with another refrigerant. Similar to configuration AB, Figure 3.9d presents the maximum COP for each refrigerant (pure or binary mixture) at different ratios of space heating to domestic hot water (r_{heat}). Compared to Figure 6d, configuration BC yields higher COP and favors higher demands of space heating compared to domestic hot water (r_{heat} higher than 1).

3.2.3 Configuration ABC

The last configuration presents three gas coolers, in which the low-temperature gas cooler (A, the closest to the expansion device) is used to preheat the feedwater; the intermediate-temperature gas cooler (B) is dedicated to space heating; and the high-temperature gas cooler (C, the closest to the compressor) heats the preheated feedwater. The coefficient of performance of the heat pump using this arrangement is shown in Figures 3.10a to 3.10c for different ratios of space heating to domestic hot water. Each subfigure presents the COP according to the CO_2 mass fraction on the refrigerant for all binary mixtures considering the refrigerants in Table 3.2.

Figures 3.10a to 3.10c also indicate how unequal content mixtures, such as 10% of CO_2 or the other refrigerant, can enhance the coefficient of performance due to the moderate glide associated with them. This phenomenon occurs for mixtures of CO_2 and R32 or R1270. Differences in the performances of the mixtures in relation to the pure fluids might be justified considering the refrigerant behavior in the evaporator. Pure fluids present constant pressure and temperature during phase change. Consequently, the refrigerant temperature within the evaporator is limited by its own saturation temperature. However, the heat source fluid — the fluid that transfers heat to the refrigerant in the evaporator — enters the equipment with a temperature of 10 °C and leaves with a temperature of 5 °C, according to the operating parameters in Table 3.1. Since the evaporator is modeled as a counterflow heat exchanger using a minimum pinch point allowed of 5 °C, as shown in Table 3.1, the pure fluid saturation temperature is equal to 0 °C, and the pinch point occurs

at the refrigerant inlet of the evaporator. By using mixtures with a temperature glide, a better match between the heat source temperature and the binary mixture temperature could be achieved in the evaporator, and the pinch point would not be limited to the inlet. Higher evaporating pressures could be obtained, and consequently, low pressure ratio and low compression work.

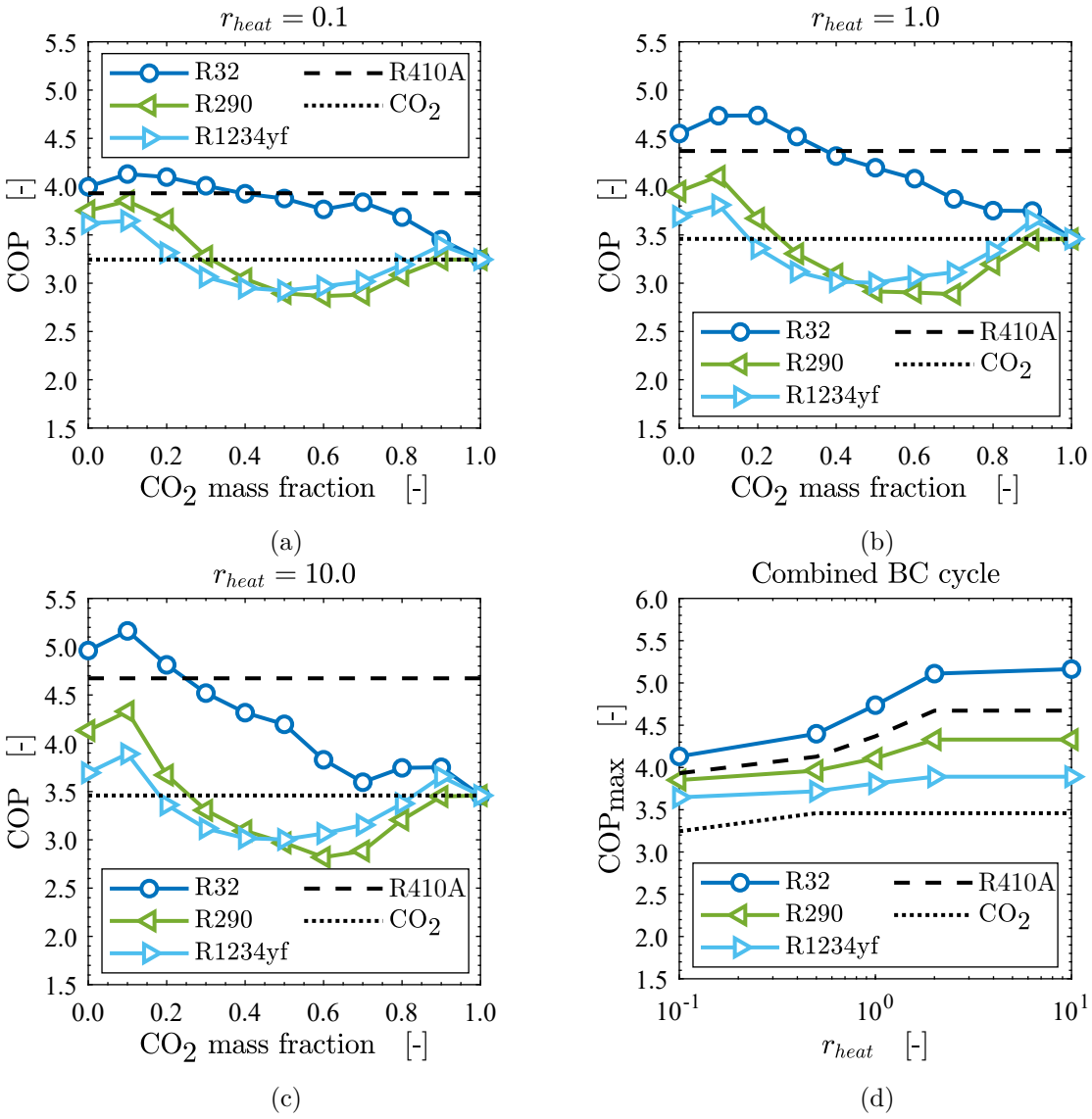

Figure 3.9 – Effects of the CO_2 mass fraction on the coefficient of performance of several binary mixtures at the cycle BC and at r_{heat} of 0.1 (a), 1 (b), and 10 (c). Variation of the maximum COP at the configuration BC according to ratio of space heating to domestic hot water for fluids analyzed on items (a) to (c).

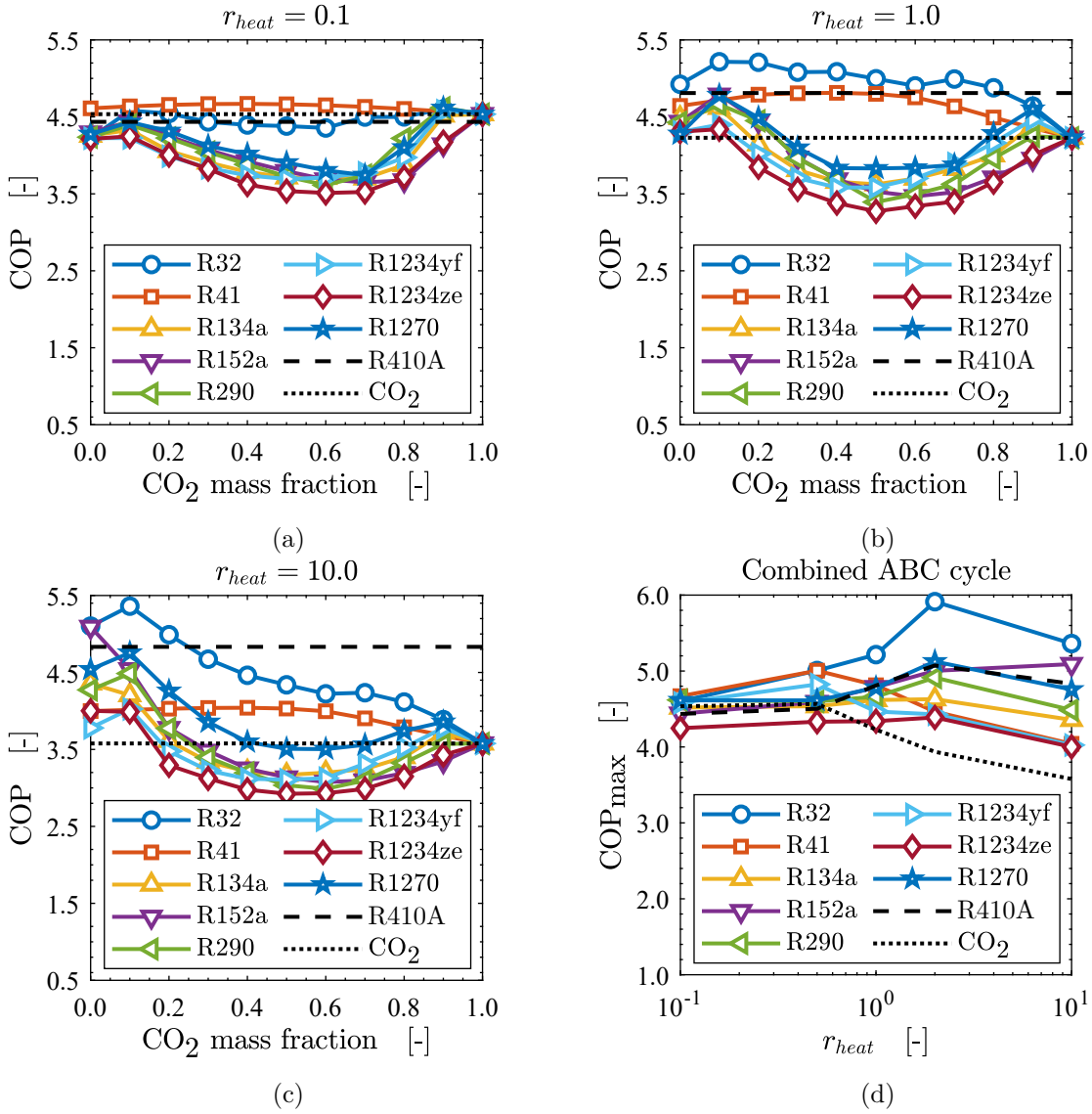

Figure 3.10 – Effects of the CO_2 mass fraction on the coefficient of performance of several binary mixtures at the cycle ABC and at r_{heat} of 0.1 (a), 1 (b), and 10 (c). Variation of the maximum COP at the configuration ABC according to ratio of space heating to domestic hot water for fluids analyzed on items (a) to (c).

It can be observed that most mixtures composed by equal parts of CO_2 and another refrigerant impair the COP, which may be related to the difference in boiling temperatures between the two refrigerants. Specifically, mixtures containing CO_2 and R123ze, R123yf, or R152a exhibit the highest glides and fail to match the temperature profiles of the heat sink and heat source fluids. However, as shown in Figures 3.10a to 3.10c, most of the refrigerants studied benefit from mixtures with certain CO_2 mass fractions. Moreover, for space heating and domestic hot water demands, mixtures with limited CO_2 compositions (around 10%) favor space heating with high r_{heat} values. In contrast, for higher demands of domestic hot water, low r_{heat} values, the best performance is achieved with mixtures containing mostly CO_2 (roughly 90%).

In terms of the performance of binary mixtures focusing on their components,

low-GWP mixtures exhibit comparable (and in some cases, even superior) performance to conventional refrigerants such as R410A and R134a for low r_{heat} values. Additionally, mixtures with R41 or R1234yf reach a maximum COP at $r_{heat} = 0.5$, indicating an optimal ratio between the demands of space heating and domestic hot water. For higher demands of space heating (high r_{heat}), low-GWP mixtures of CO_2 and R1270, R290, or R152a are a better option, and optimal values for mixtures with R290 or R1270 are achieved at $r_{heat} = 2.0$.

Figure 3.10d illustrates the maximum coefficient of performance (COP) for each binary mixture according to the ratio of space heating to domestic hot water demand. Compared to the previously configurations shown in Figures 3.6d and 3.9d, configuration ABC has the best COP range — which is between 3.5 to 6 comparing to 1.9 to 4.4 for AB configuration and 3.3 to 5 for BC arrangement. In addition, as discussed in Sections 3.2.1 and 3.2.2, AB configuration suits better domestic hot water demands, while BC configuration the space heating. In contrast, for configuration ABC, the mixtures seem to have an optimal ratio of space heating to domestic hot water demand that maximizes the COP. This observation is consistent with the idea that configuration ABC is a combination of the previous two configurations.

3.2.4 Discharge pressure

The feasibility of the heat pump cycle is influenced by various factors, including the compressor's discharge pressure, which can impact the equipment's dimensions. Figures 3.11a to 3.11c illustrate the discharge pressure for several binary mixtures at different ratios of space heating to domestic hot water demands, based on the CO_2 mass fraction. Knowing that CO_2 water heat pumps typically operate at high pressure levels (NEKSÅ, 2002) an increase in the CO_2 mass fraction in the refrigerant binary mixture leads to a higher discharge pressure, as shown in the figures and also supported by Dai *et al.* (2015).

Furthermore, Figure 3.11d shows that there is a sudden decrease in the discharge pressure as r_{heat} (the ratio of space heating to domestic hot water demands) increases. This observation aligns with the earlier discussion: as mixtures rich in CO_2 perform better for low r_{heat} (resulting in higher discharge pressure), while poorer mixtures in CO_2 suit high r_{heat} (leading to a sharp decrease in the discharge pressure).

3.2.5 Heat exchangers size

In addition to discharge pressure, the feasibility of a heat pump system can be assessed based on the size of the heat exchangers used. This is an important factor to consider because an equipment of large dimensions would demand a space that is coherent with its size. Moreover, the size of the heat exchangers is a critical aspect of the overall dimensions of the system. Therefore in this section, the thermal conductance (UA) is used as a parameter to determine the system's size and is calculated as the sum of the

thermal conductance of each heat exchanger (evaporator and gas coolers A, B, and C) (BEJAN, 2000). Each thermal conductance is calculated by the log-mean temperature difference for counter-flow heat exchangers, using the sub-heat exchanger discretization method explained in Subsection 3.1.2, following the approach described by Nellis and Klein (2009).

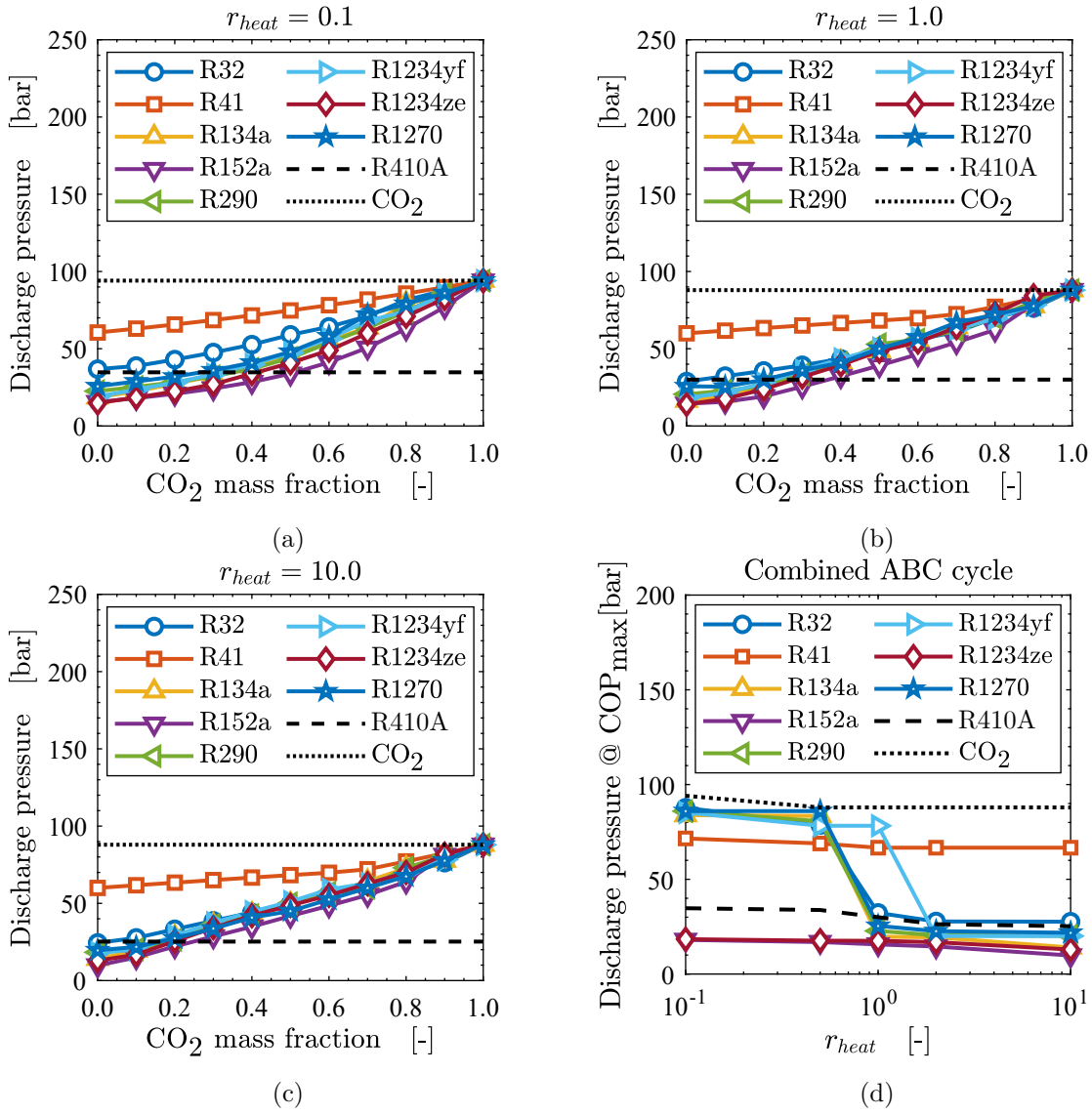

Figure 3.11 – Discharge pressure of the refrigerants shown in Table 2 as a function of the variation of $\dot{x}_{CO_2}$ for the configuration ABC and r_{heat} equals to 0.1 (a), 1 (b), and 10 (c). (d) Discharge pressure associated to the maximum coefficient of performance for the refrigerants tested as a function of the ratio of space heating to domestic hot water.

Figures 3.12a to 3.12c display the thermal conductance variation with respect to the mass fraction of CO_2 in refrigerant binary mixtures for several refrigerants and ratios of space heating to domestic hot water. In addition, Figure 3.12d presents the thermal conductance associated with the maximum coefficient of performance (COP) for different ratios of space heating to domestic hot water. As shown in the figures, the effect of

modifying the CO_2 fraction in the mixture is not the same for all refrigerants: for mixtures containing R134a, R1234yf, or R1234ze, the addition of CO_2 leads to a higher thermal conductance; however, for most fluids tested — including R32, R41, R152a, R290, and R1270 — the opposite effect occurs. Nonetheless, the figures also indicate that mixtures containing approximately 10% or 90% CO_2 exhibit higher conductance, i.e., systems using mixture with a moderate glide have the best COP are the ones that need more space for their heat exchangers. The thermal conductance can also be related to another figure of merit that combines the performance of the system to its size, COP/UA. Previous studies, such as those by Sánchez and Silva (2018) and Battisti *et al.* (2015), have evaluated the net power produced and the first-law efficiency per unit of UA for transcritical Rankine cycles that use carbon dioxide as a working fluid. COP/UA incorporates data from Figures 3.10 and 3.12, but is more influenced by conductance. The ratio highlights differences between two sets of fluids in 3.12: those in which adding CO_2 to the mixture increases COP/UA (R32, R41, R152a, R290, and R1270), and those in which the opposite effect occurs (R134a, R1234yf, and R1234ze). For brevity, the variation of COP/UA with CO_2 mass fraction was not included.

In summary, two groups show improved performance: one with about 90% CO_2 and 10% of other refrigerants, suitable for low heat demands, and another with roughly 10% CO_2 and 90% of certain refrigerants, recommended for high space heating. Mixtures with CO_2 mass fractions of 0.1 or 0.9 have better heat exchanger properties, suggesting potential optimization for both COP and thermal conductance in future studies. Further research can explore additional constraints relevant to the system, such as those for power cycles, compressor parameters, and variations in evaporator inlet temperature due to changing environmental conditions. Detailed studies may involve modeling heat transfer phenomena within heat exchangers and determining heat transfer coefficients using available correlations.

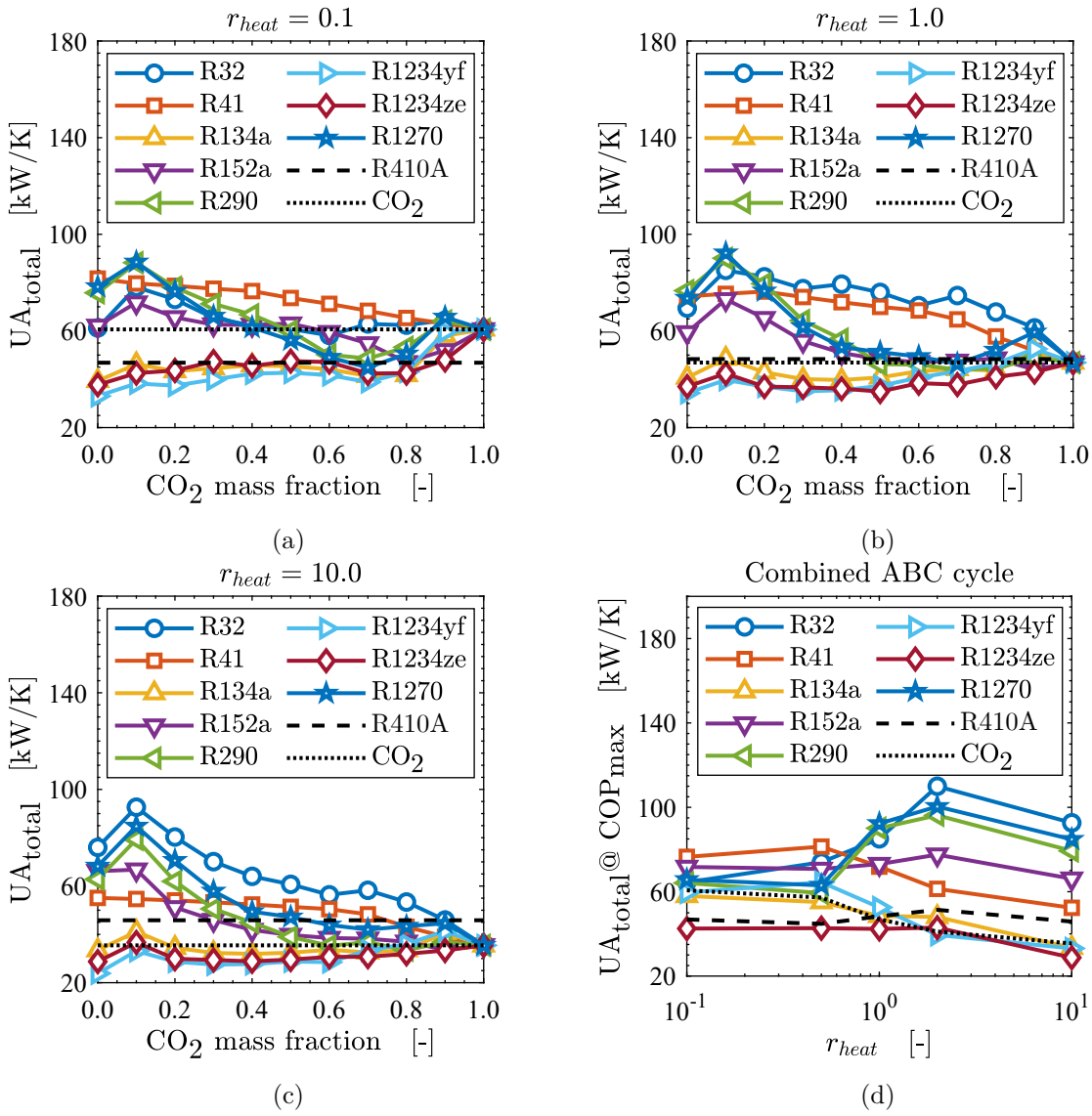

Figure 3.12 – Total global conductance of the cycle as a function of the variation of $\dot{x}_{CO_2}$ for the configuration ABC and r_{heat} equals to 0.1 (a), 1 (b), and 10 (c). (d) Total global conductance associated to the maximum coefficient of performance for the refrigerants tested as a function of the ratio of space heating to domestic hot water.

4 EVALUATING CO_2-BASED HEAT PUMPS FOR RESIDENTIAL HEATING IN DIFFERENT CLIMATES

This chapter is based on manuscript — currently in preparation for submission — that aims to evaluate the performance of refrigerant mixtures in a combined heat pump that provides both space heating and hot water in cold climates. Due to the limited research on this topic, this chapter investigates the impact of heat demand and heat source temperature on key performance parameters of the cycle. As aforementioned, the residential sector consumes a significant portion of global energy, with space and hot water heating being major contributors. During winter, the outside air temperature in cities like Quebec, Tokyo, and Stockholm can range from -5 °C to -28 °C (SENGUPTA *et al.*, 2018). To meet the technical and environmental requirements of this sector, this study focuses on a combined heat pump system that utilizes binary mixtures of CO_2 and low-GWP refrigerants, operating with heat sources with reduced temperatures. A computational model is utilized to evaluate the performance of the proposed heat pump running on different ratios of space-to-water heating, and varying the inlet and outlet temperatures of the heat source, emulating various cold climate conditions.

4.1 METHODOLOGY AND MODELLING

To assess the impacts of the temperature of the heat source and the space-to-water heating ratio, a combined heat pump model was used. The model was based on the ABC configuration described in detail on Subsection 3.1.1 and whose arrangement of equipment was initially conceptualized by Stene (2005). Figures 4.1a and 4.1b show the proposed configuration scheme and the simulated cycle operating with pure R410A in a T-s diagram, respectively. As can be seen, the proposed configuration comprises an evaporator, a compressor, condensers (or gas coolers) and an expansion device. In the T-s diagram, the temperature profiles of the heat source and heat sinks are also presented to better visualize the cycle. The diagram shows that the R410A cools the secondary fluid from $T_{HS,in}$ to $T_{HS,out}$ in the evaporator and leaves as saturated vapor (state 1). After being compressed (from 1 to 2), R410A at high pressure and temperature transfers heat to the secondary fluid in condensers C, B and A. Heat transfer on the high side of the cycle is characterized by first a desuperheating; then, a condensation; and finally, a subcooling process. The fluid leaves condenser A at high pressure and low temperature (5). Next, the pressure of R410A decreases through an isenthalpic expansion until state 6, i.e., the evaporator inlet. Notwithstanding, this study also explores refrigerant mixtures with lower critical pressures, especially those rich in CO_2, which require transcritical operation. In that case, a gas cooling process within the supercritical state takes place instead of a condensation.

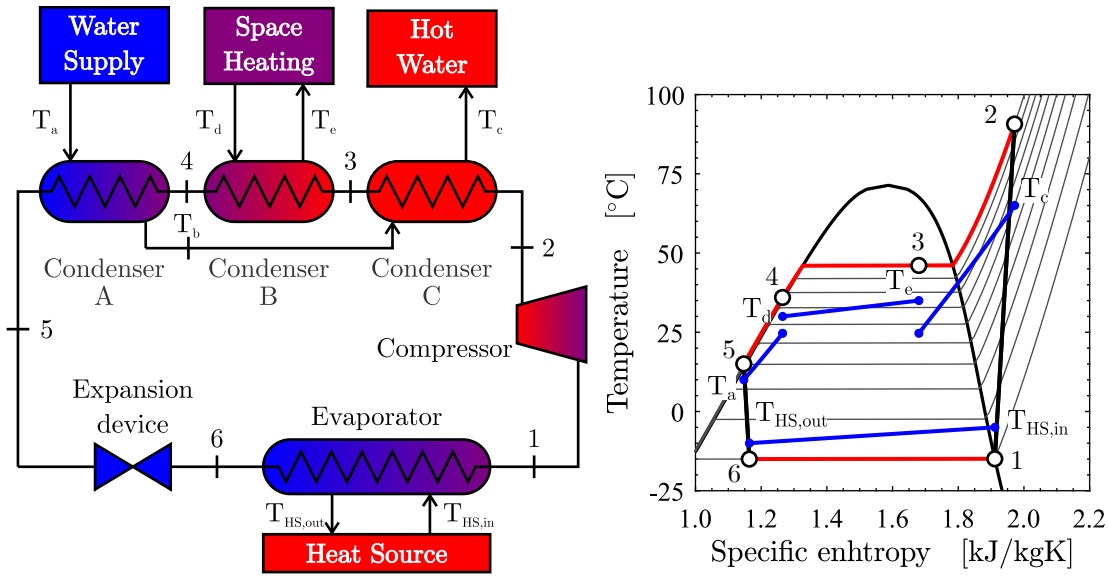

Figure 4.1 – (a) Schematic of the combined heat pump analyzed (b) Temperature-entropy diagram of the heat pump cycle using R410A as refrigerant, and of water and water(50%)/propylene glycol(50%) as the secondary fluids in the heat sink and source, respectively.

4.1.1 Thermodynamic assumptions and component modelling

The cycle was modeled considering steady-state operation based on principles of mass and energy conservation established by the first law of thermodynamics, which was previously described in Section 3.1. The evaporator is discretized into 150 elements, and each gas cooler (or condenser) is divided into 200 elements along its length, following the mesh verification process described in Subsection 3.1.5.

As the heat source temperature can vary greatly based on geographical location and weather conditions, this study considers four sets of $T_{HS,in}/T_{HS,out}$, with a temperature decrease of 5 °C (DAI *et al.*, 2015). The range of investigated heat source temperatures is presented in Table 4.1. It is important to clarify that source temperature is inherently tied to the outdoor ambient temperature. While some geographical locations around the world may experience extremely low temperatures during winter, such as -25°C (SENGUPTA *et al.*, 2018), it's relatively rare for heat pumps to operate under such extreme conditions for extended periods. In practice, heat pumps are typically designed to function within a more moderate range of source temperatures. Nevertheless, conducting research on heat pump behavior under these extreme conditions can yield valuable insights into their performance capabilities and contribute to a better understanding of their behavior.

In terms of secondary fluids, the heat sink is water, whereas in the heat source, since temperatures are bellow the water freezing point, an aqueous solution with propylene glycol was employed. The concentration of the water/propylene glycol mixture was 0.5 to 0.5 (BAHMAN *et al.*, 2022) and its properties are modeled according to the freeware

library CoolProp (BELL *et al.*, 2014).

Other operational parameters, including the heat sink temperatures, the minimum allowed pinch point, compressor isentropic efficiency, remained consistent with the previous analysis in Chapter 3 and can be found in Table 3.1.

Table 4.1 – Combination of heat source inlet and outlet temperatures investigated.

Description	**Variable**	**Value [Unit]**
Heat source	$T_{HS,in}/T_{HS,out}$	-25/-30 °C
		-15/-20 °C
		-5/-10 °C
		5/0 °C

4.1.2 Working fluids

The present work focuses on selecting refrigerants that when mixed with CO_2 are able to mitigate environmental impacts. Thus, three binary mixtures with CO_2 are considered in this study: R32, R1234yf, and R290; along with pure R410A as a baseline for comparison. For these mixtures two concentration values are considered, $\dot{x}_{CO_2} = 0.1$ and $\dot{x}_{CO_2} = 0.9$ — because these mass fractions were able to enhance the COP system compared to pure fluid operation. Furthermore, these three fluids summarize three classes of working fluids: hydrofluorcarbons (HFC), hydrofluorolefins (HFO) and hydrocarbons (HC), all alternatives with no ODP. More information regarding the refrigerants evaluated in this work is presented in Table 4.2.

Table 4.2 – Thermophysical and environmental data of the selected fluids.

Refrigerant	**T_{crit} [°C]**	**p_{crit} [MPa]**	**GWP* (100 years)**	**ODP**	**Chemical composition**	**ASHRAE flammability**
R744 (CO_2)	31.0	7.4	1	0	CO_2	No
R32	78.2	5.8	675	0	CH_2F_2	Yes (lower flammability)
R1234yf	94.7	3.8	4	0	$C_3H_2F_4$	Yes (lower flammability)
R290	96.2	4.2	3	0	C_3H_8	Yes (higher flammability)
R410A	71.3	4.9	2088	0	R32(0.5)/R125(0.5)	No

4.1.3 Optmization procedure

The combined brine-to-water heat pump model comprises four independent variables: p_{low}, p_{high}, T_3, and T_5, and the solution of the cycle is accomplished through a non-linear optimization process similar to that presented in Chapter 3 in Subsection 3.1.4. The optimization procedure follows the same steps as the ones presented in Figure 3.3, with the exception of the energy balance in the evaporator, which now accounts for an aqueous solution with propylene glycol. The algorithm aims to maximize COP while respecting the pinch point restrictions in the heat exchangers.

4.1.4 Model verification

Before proceeding with the analysis, the numerical model was compared with published data to ensure the correctness of it. The accuracy of the combined water-to-water heat pump was already evaluated in the previous chapter at Subsection 3.1.5. However, in this case, an aqueous solution of water (0.5) and propylene glycol (0.5) was used instead of water as the secondary fluid in the evaporator. The results of the numerical model were compared with Bobbo *et al.* (2019), which performed a thermodynamic analysis on a ground source heat pump. The authors conceptualized a brine-to-water heat pump dedicated to heating domestic water. The COP system and the volumetric heating effect (VHE) were selected as the figures of merit for verification. It is worth mentioning that in their analysis, Bobbo *et al.* (2019) used pure R410A and R32 as refrigerants and a pair of heat source temperatures of 0/-3 °C in the evaporator. These operational parameters were used as input to the numerical model (Figure 3.3), whose results were compared to the volumetric heating effect presented by Bobbo *et al.* (2019); all shown in Figure 4.2. The divergences observed between the VHE results were no greater than 0.31%, whereas the relative error among the COP results oscillated from -0.12% to 0.62% (Table 4.3).

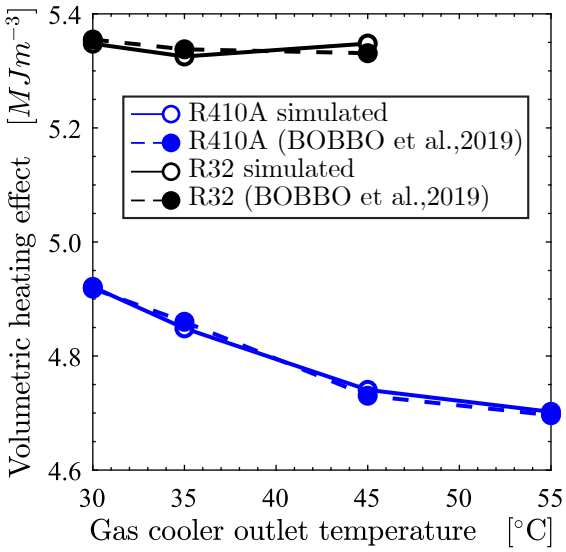

Figure 4.2 – Volumetric heating effect variation with outlet gas cooler temperature for pure working fluids R32 and R410A.

Table 4.3 – Comparison of the coefficient of performance and volumetric heating effect between the present study and Bobbo *et al.* (2019) using R-32 and R410A.

	COP [-]			**VHE** $[kJm^{-3}]$		
	This work	Bobbo *et al.* (2019)	Error	This work	Bobbo *et al.* (2019)	Error
R32	4.88	4.85	0.62%	5348	5355	-0.13%
	4.33	4.34	-0.08%	5325	5338	-0.24%
	3.39	3.40	-0.04%	5348	5331	0.31%
	This work	Bobbo *et al.* (2019)	Relative error	This work	Bobbo *et al.* (2019)	Error
R410A	4.94	4.94	0.03%	4922	4918	0.06%
	4.36	4.36	-0.06%	4849	4860	-0.24%
	3.39	3.39	0.13%	4741	4731	0.22%
	2.63	2.64	-0.12%	4702	4696	0.13%

4.2 RESULTS

This chapter explores the influence of reduced heat source temperatures and heat demand on the combined heat pump performance with CO_2-binary mixtures with low-GWP refrigerants aiming to identify refrigerant fluid alternatives that meet both technical and environmental criteria, while providing good heating performance at low temperatures for domestic water and space heating needs. Given that end-use heating accounts for a significant portion of energy consumption in buildings (EUROSTAT, 2022), this study is important, particularly in cold climate regions, where heating systems are most needed.

4.2.1 Coefficient of performance

The performance of the combined heat pump is analyzed on terms of different ratios of space to domestic hot water (r_{heat} from 0.1 to 10) aiming to establish, for each

range of heat source temperature, an optimal refrigeration in terms of fluids and their fractions.

Figures 4.3a to 4.3f show the COP variation for different values of r_{heat} as well as heat source temperatures and mixtures. The mixture CO_2(10%)/R32(90%) offers the best COP values compared to the other mixtures throughout the range of reduced heat source temperatures studied. Notably, the efficiency of the heat pump is significantly reduced as the temperature of the heat source decreases, for example, change from 5/0 °C to -25/-30 °C can cause nearly 40% decrease in COP values.

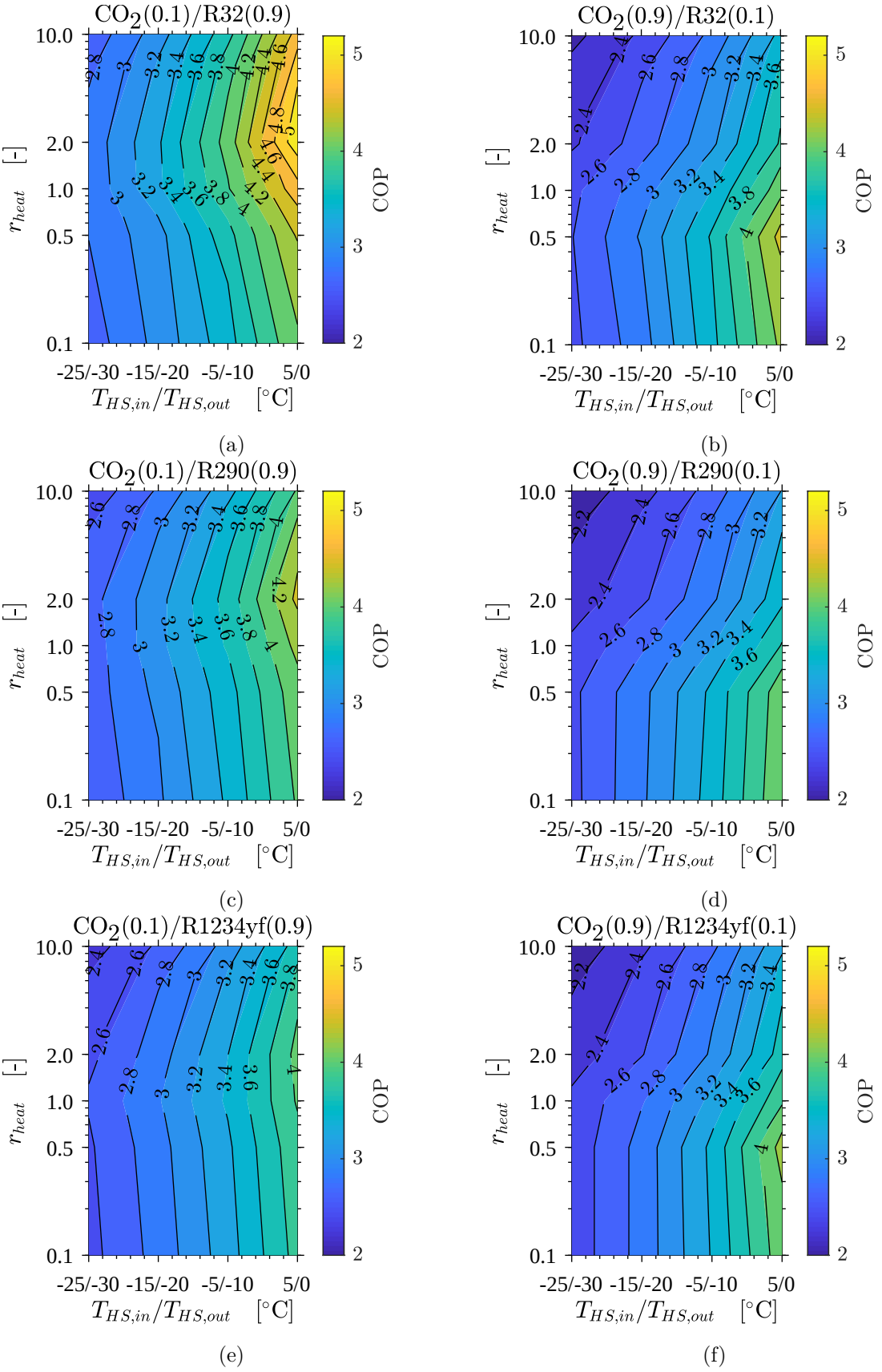

Figure 4.3 – Variation of the coefficient of performance with space-to-water heating ratio and heat source temperature considering the refrigerant mixtures with CO_2 mass fractions of 0.1 and 0.9. Results for R32 (a and b), R290 (b and c) and R1234yf (d and e).

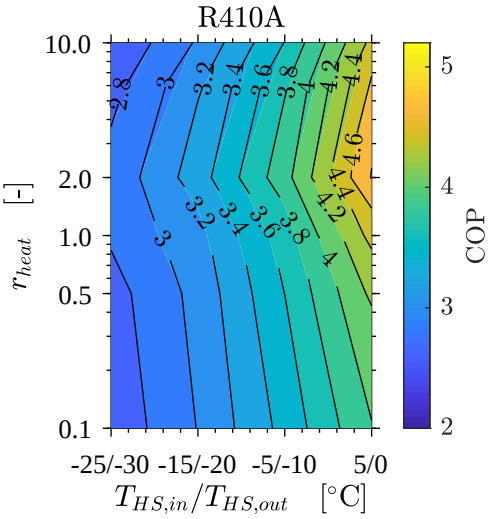

Figure 4.4 – COP results for various ratios of space to water heating demands and heat source temperatures for the pure fluid operation with R410A.

Increasing the CO_2 mass fraction on the mixture from 10% to 90% seems to change r_{heat} in which the maximum COP that can be achieved appears.For example, the mixture CO_2(10%)/R1234yf(90%) presents the best COP, approximately 4.2, for systems focused on space heating (r_{heat} close to 2) and at the higher heat source temperature. However, by changing to a CO_2-rich mixture, CO_2(90%)/R1234yf(10%), the maximum COP occurs at r_{heat} conditions close to 0.5. A similar behaviour is noted for other refrigerant mixtures, although they do not necessarily present peak performance at the same ratios of space heating to domestic hot water values, which suggests that, even in cold climates (i.e., reduced evaporating temperatures), mixtures with high CO_2 concentrations suit better systems focused on demands of domestic hot water, while mixtures with low CO_2 concentrations exhibit greater performance for demands focused on space heating.

Nevertheless, when comparing mixtures with a higher content of CO_2 and their corresponding mixture with a higher refrigerant content, the addition of CO_2 appears to impair COP, especially for heat demands focused on space heating and for lower heat source temperatures. For instance, the operation with CO_2(90%)/R290(10%) only outperforms its counterpart CO_2(10%)/R290(90%) for heat demands of $r_{heat} = 0.1$ and at heat source temperatures $T_{HS,in}/T_{HS,out}$ of -5/-10 °C and 5/0 °C. For all the other operating conditions of r_{heat} and $T_{HS,in}/T_{HS,out}$, the refrigerant-rich mixture presents higher COP values. This suggests that refrigerant-rich mixtures can be robust enough to operate under low-temperature conditions, where heat demand can vary greatly over the operating range. But, for production of dometic hot water (lower r_{heat}) and higher evaporating temperatures, CO_2-rich mixtures can be employed when prioritizing the system efficiency.

Compared to the baseline operation of R410A, the CO_2(10%)/R32(90%) has higher COP for all heat source temperatures and ratios of space heating to domestic hot water investigated, as shown in Figure 4.4. The CO_2(10%)/R290(90%) mixture presents comparable COP values to R410A at low r_{heat} values (0.1 to 0.5) and; CO_2(10%)/R1234yf(90%)

at r_{heat} of 0.1 and $T_{HS,in}/T_{HS,out}$ equals to 5/0 °C. Therefore, considering the improved COP, the CO_2(10%)/R32(90%) mixture can be a suitable replacement for R410A. Besides, the addition of CO_2 to the mixture can also contribute to the mitigation of R32 flammability and GWP effects.

4.2.2 Suction line pressure and pressure ratio

The design of heat pump for extremely cold applications (lower than -25 °C) should account for the large temperature difference between the evaporator and the condenser. This leads to high pressure ratios. $\pi = p_{high}/p_{low}$, during compressor operation, which can reduce volumetric efficiency (GOSNEY, 1982). Additionally, some fluids may operate at very low suction pressures, resulting in air and moisture ingress when the suction pressure falls below atmospheric pressure (GOSNEY, 1982). Therefore, the relationship between the refrigerant mixtures and pressure ratio should be assessed.

Figures 4.5a to 4.5f present the pressure ratio for different CO_2 and refrigerant-rich mixtures, the right-hand side ordinate represents the ratio π, while the left-hand side represents the suction pressure (p_{low}). Data is presented for several heat demands of r_{heat} values, where solid lines represent the suction pressure, and dashed lines represent the pressure ratio. The baseline operation with R410A is shown for comparison in Figure 4.6.

As observed in Figures 4.5a-4.5f and 4.6, the suction pressure is strongly correlated with the heat source temperature. While the suction pressure is also related to the normal boiling point of the refrigerants, mixtures rich in CO_2 operate at much higher suction pressures due to the lower normal boiling point of the main component of the mixture. The CO_2(10%)/R1234yf(90%) mixture presented the lowest suction pressure, notably at the lowest simulated heat source of -25/-30 ° C. The value is close to atmospheric pressure, approximately 1.22 bar. Based on the analysis conducted in this work, none of the alternatives pose a risk of compromising the heat pump operation due to issues related to suction pressures below atmospheric pressure, particularly for heat source temperatures as low as -25/-30 °C.

According to Figures 4.5a-4.5f and 4.6, the evaporating pressure of the cycle appears unaffected by the ratio of heating demand r_{heat}, which seems reasonable, as heat demand is related to changes in the heat sink temperatures — the high-side of the cycle. However, the heat demand influences the pressure levels of the cycle, which can be seen by comparing the different π values for the same heat source temperature. Figures 4.5a-4.5f and 4.6 show that the heat demand is responsible for increasing the optimal discharge pressure of the cycle: for lower r_{heat} values, the discharge pressure p_{high} increases and so does the pressure ratio π. Therefore, an increase in the optimal discharge pressure is expected to cover the high-temperature heating demand associated with hot domestic water production. This is consistent with the findings of Brodal and Jackson (2019), who observed that the optimal p_{high} increases as r_{heat} decreases for CO_2 combined heat pump systems.

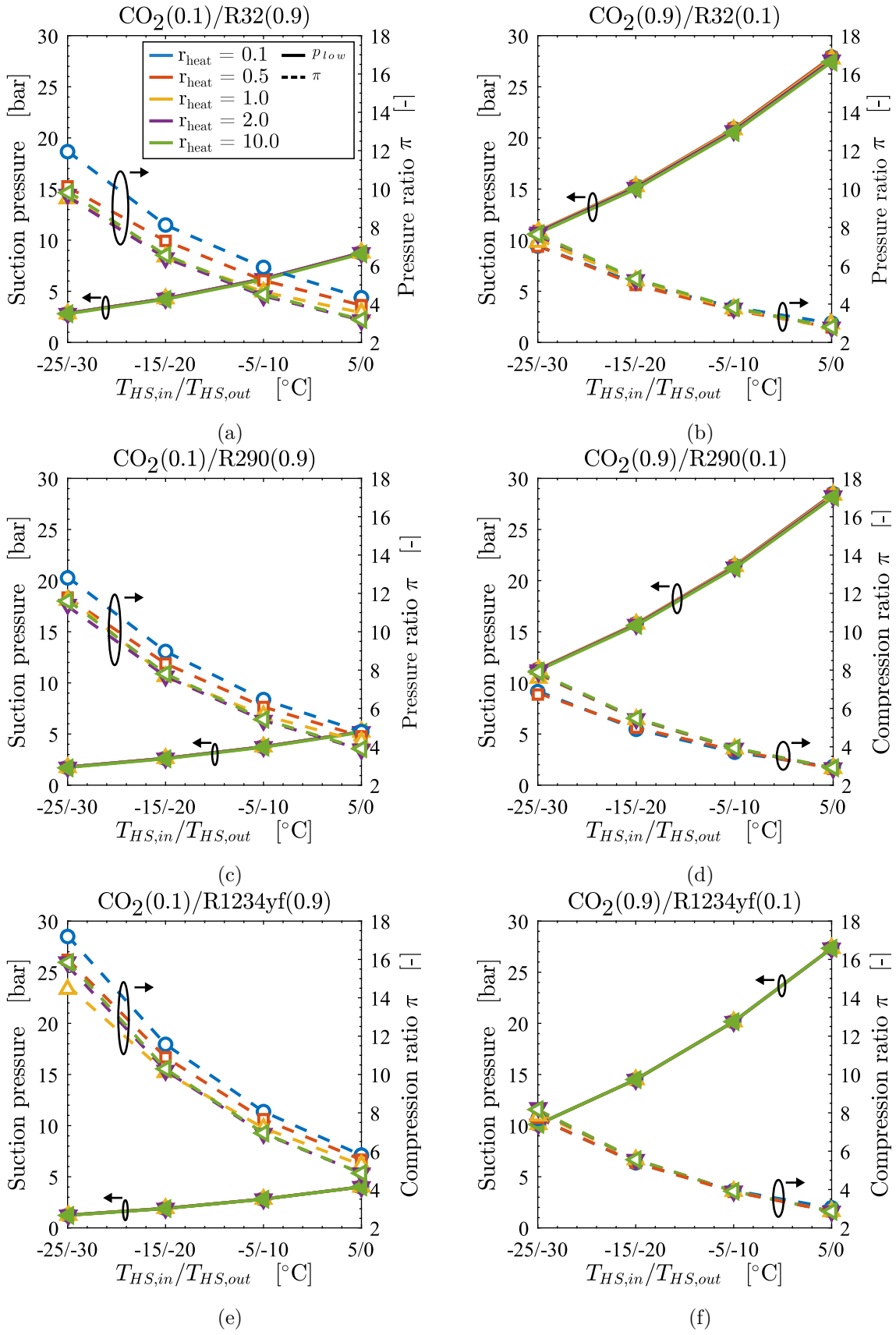

Figure 4.5 – Suction pressure and pressure ratio π of several refrigerant mixtures as a function of heat source temperature $T_{HS,in}/T_{HS,out}$.

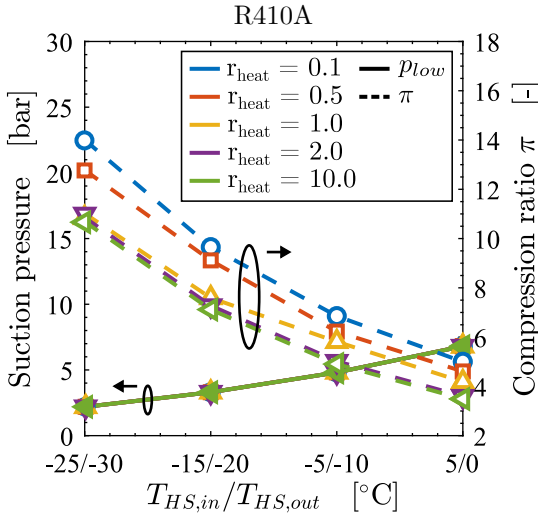

Figure 4.6 – Suction pressure and pressure ratio π as a function of heat source temperature $T_{HS,in}/T_{HS,out}$ of the baseline operation with R410A.

Heat sink conditions of the heat pump cycle are fixed in all simulations, i.e., the design temperatures of the hot domestic water and the space heating system remain unchanged. Consequently, decreasing the heat source temperature results in an increase of the temperature difference between the high and low sides of the heat pump cycle. As a result, the pressure ratio also increases, as shown in Figures 4.5a-4.5f and 4.6. In addition, knowing that the pressure ratio π tends to increase with the refrigerant boiling point (GOSNEY, 1982), mixtures rich in R1234yf and R290 (which have the highest boiling points) exhibit the highest pressure ratios, as shown in Figures 4.5c and 4.5e. However, adding CO_2 to the mixtures can help reduce excessive pressure ratios. For example, when changing the CO_2 concentration to 90%, the pressure ratio values of the CO_2-binary mixtures poor in CO_2 — CO_2(10%)/R1234yf(90%) and CO_2(10%)/R290(90%) — can be reduced to reasonable levels ranging from 2 to 10, compared to the values of 4.8-17.3 and 3.8-12.9 obtained earlier. High pressure ratios can compromise compressor operation, particularly in reciprocating types, and reduce volumetric efficiency (GOSNEY, 1982). Thus, the feasibility of the heat pump in cold climates can also be assessed in terms of the required pressure ratio. Based on the values obtained in this work, operation with the mixture CO_2(10%)/R1234yf(90%) may require a cascade system or a multi-stage cycle to overcome such excessive pressure ratio. CO_2-rich mixtures appear to benefit the most from reduced heat source temperatures in terms of pressure ratio values, as they have lower values of π than all other mixtures and the pure fluid (R410A) investigated.

4.2.3 Size of the system

In addition to the environmental and performance requirements, other technical issues, such as space and quantity of heat needed, should be addressed when designing a heat pump. Here, the volumetric heating effect (VHE) is used to express the relationship

between the total heat delivered and the space required. VHE can be expressed as a function of the refrigerant mass flow rate $\dot{m}_{ref}$, the specific volume at the compressor outlet v_1 (Figure 4.1a), and the specific heating effect $(i_5 - i_2)$ (Figure 4.1a) (GOSNEY, 1982):

$$VHE = \dot{m}_{ref}\frac{(i_5 - i_2)}{v_1} = \dot{V}_1(i_5 - i_2) = \frac{\dot{Q}_{heat}}{v_1}. \tag{4.1}$$

The specific volume at the compressor inlet (v_1), which is taken as saturated vapor in this work, depends on the suction line pressure (p_{low}) and, notably, on the refrigerant or mixture. Figures 4.7a-4.7d show the Volumetric heating effect (VHE) as a function of r_{heat} in megawatts per cubic meter (MWm^{-3}). Data is presented for several $T_{HS,in}/T_{HS,out}$ values and for CO_2-rich mixtures (dashed lines), for other refrigerant-rich mixtures (solid lines), and for R410A. As shown in these figures, the VHE was higher for all mixtures of R32, R290, and R1234yf with CO_2 concentrations of $\dot{x}_{CO_2} = 0.9$, compared to their respective mixtures of $\dot{x}_{CO_2} = 0.1$. This result is consistent with findings described by Hakkaki-Fard *et al.* (2015), which state that an increase in CO_2 mass fraction in R32 mixture leads to an increase in heating capacity due to elevated density of carbon dioxide. Since VHE is related to the specific volume of the refrigerant at the compressor inlet, mixtures with higher concentrations of CO_2 benefit from the high densities of the natural refrigerant at low temperatures. Therefore, according to Figures 4.7a to 4.7c, mixtures of R32, R290 and R1234yf poor in CO_2 ($\dot{x}_{CO_2} = 0.1$) require more swept volume from the compressor to produce the same heat capacity as their respective CO_2-rich mixtures. Consequently, heat pumps designed to heat both space and water at low temperatures, based on CO_2-binary mixtures rich in other refrigerants, may be larger and more expensive compared to CO_2-rich mixtures.

Figures 4.7a-4.7d indirectly related the compressor size (that is, the linear dimensions of the machine) and the total heat delivered by the heat pump when operating with refrigerant mixtures and low heat source temperatures. The size of other components, such as heat exchangers, which are arguably the largest contributor to the plant footprint (BEJAN, 2000), is evaluated based on the total thermal conductance of the cycle. As the heat exchangers are discretized, the UA of each heat exchanger could be calculated using the log-mean temperature difference (LMTD) method (NELLIS; KLEIN, 2009). By taking into consideration the total UA of the cycle (sum of the evaporator and all the gas coolers or condensers), one can evaluate the scale of the plant (BEJAN, 2000). Therefore, Figures 4.8a-4.8f and 4.9 present the total heat delivered by the combined heat pump (that is, the sum of the total heat transfer of the gas coolers A, B, and C) normalized by the heat exchanger size of the plant (i.e., sum of the UA from evaporator and gas coolers A, B, and C).

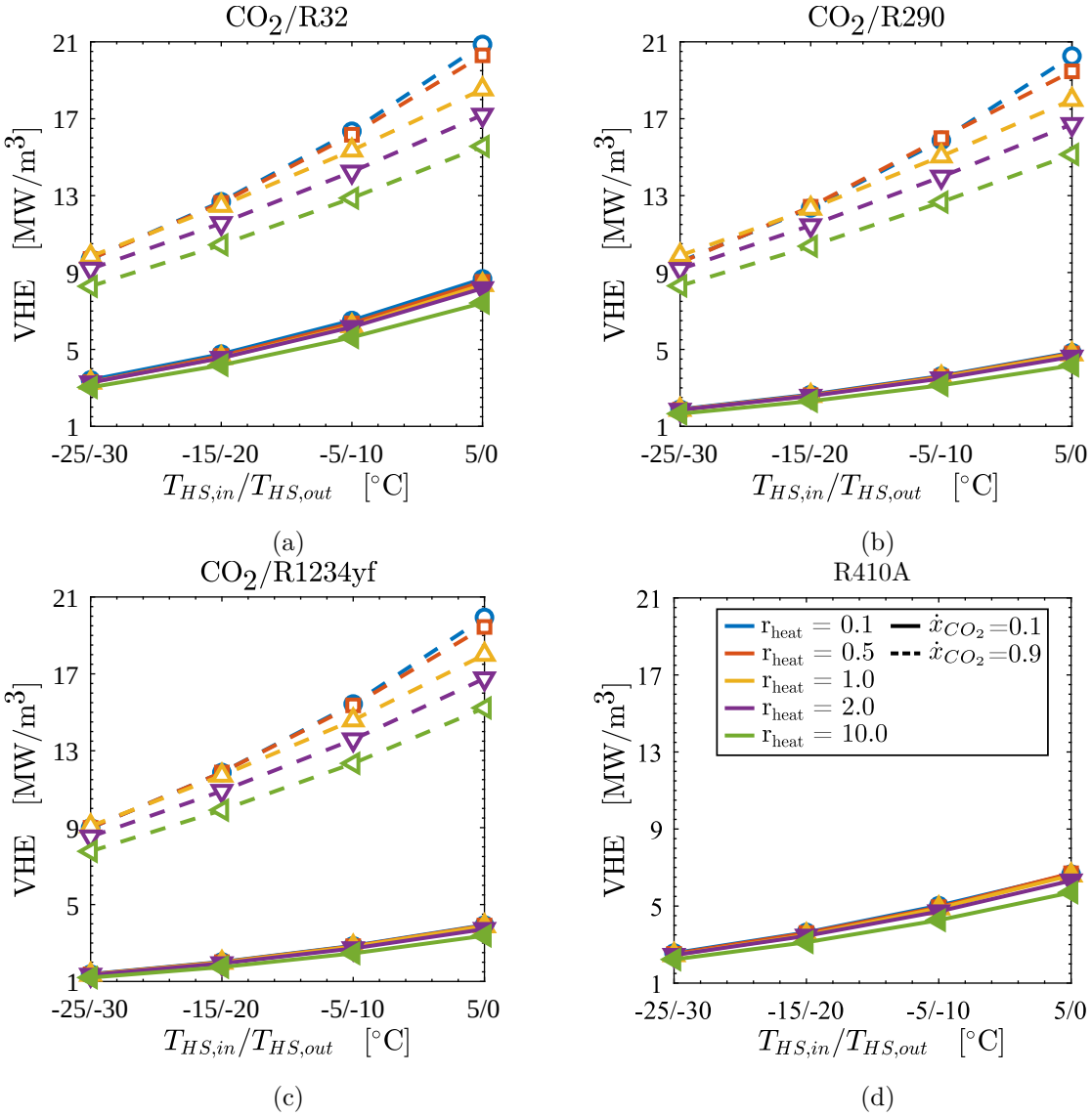

Figure 4.7 – Volumetric heating effect as a function of heat source temperature. Solid-lines represent mixtures with $\dot{x}_{CO_2} = 0.1$ and dashed-lines $\dot{x}_{CO_2} = 0.9$. Results for the CO_2-binary mixtures with R32 (a), R290 (b) and R1234yf, and pure fluid operation with R410A (d).

The figure of merit $\dot{Q}_{heat}/(UA)_{total}$ relates the the expected heat pump performance to the size of the heat exchangers and the physical dimensions of the heat pumps footprint. Since higher values of $\dot{Q}_{heat}$ and lower values of UA_{total} are preferable, the figure of merit $\dot{Q}_{heat}/(UA)_{total}$ reflects the compactness of the heat pump, with higher values indicating that the refrigerant mixture can more efficiently use the available footprint space (heat exchanger area) to produce heat.

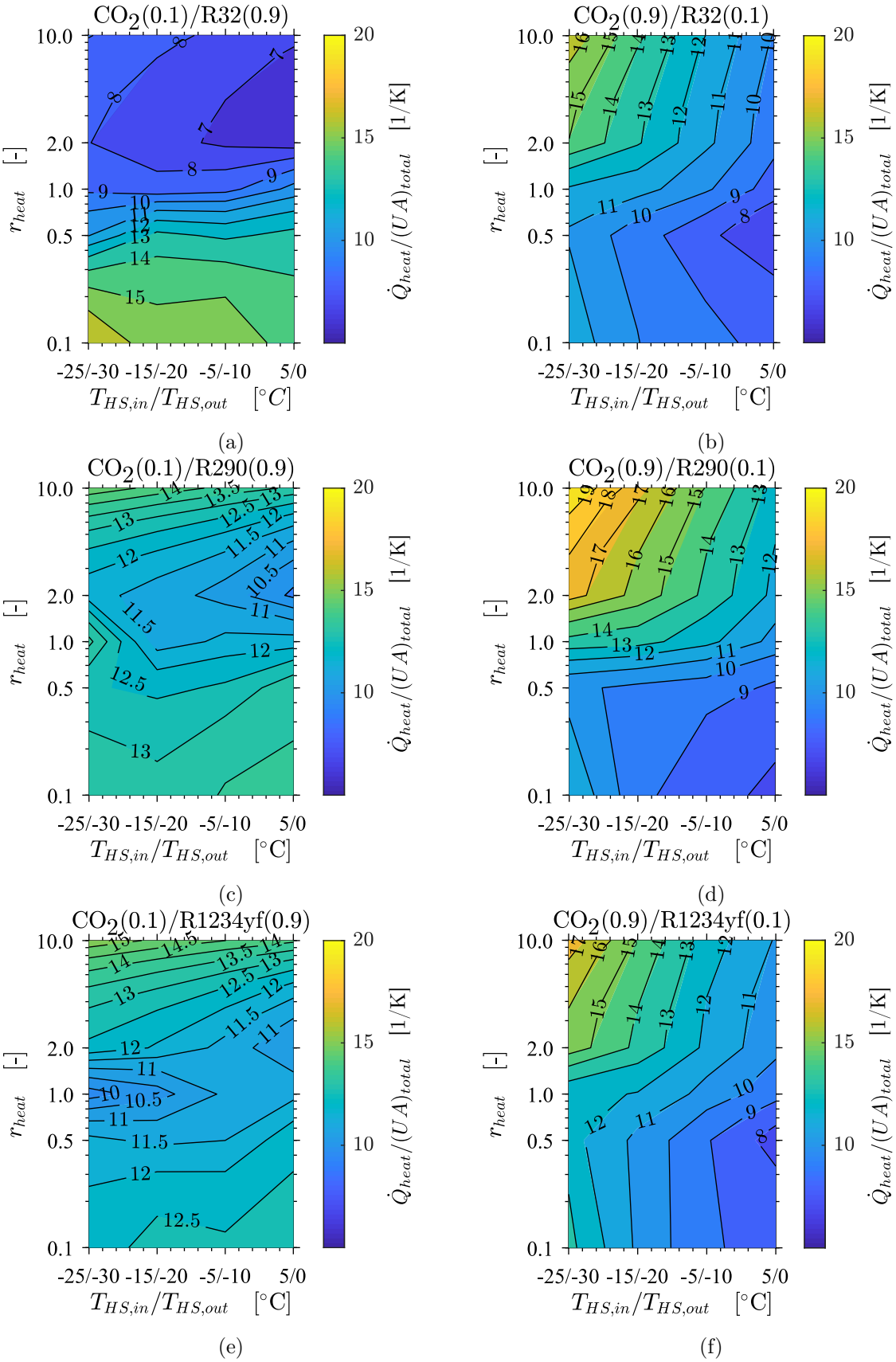

Figure 4.8 – Influence of heat demand (r_{heat}) and heat source temperature ($T_{HS,in}/T_{HS,out}$) on the normalized figure of merit $\dot{Q}_{heat}/(UA)_{total}$. Results for CO_2-binary mixtures with R32 (a and b), R290 (c and d) and R1234yf (e and f).

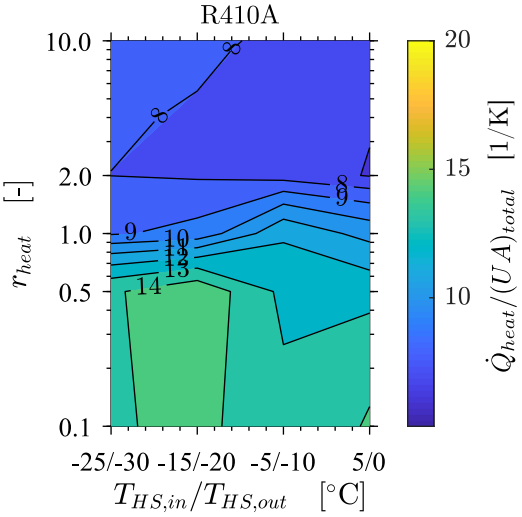

Figure 4.9 – $\dot{Q}_{heat}/(UA)_{total}$ results for the pure fluid operation with R410.

One can notice that the reduced values of $\dot{Q}_{heat}/(UA)_{total}$ in Figures 4.8a, 4.8b, 4.8c, 4.8d, 4.8f and 4.9 seem to match the the highest COP values observed for these working fluids as pointed out in Subsection 4.2.1. As discussed in the literature by Dai *et al.* (2015) and in this master thesis in the Chapter 3, heat pump performance (COP) can be improved by correctly matching the temperature profiles in the heat exchangers. In addition, as presented in Subsection 2.2.4 — Pinch point and heat exchanger design — closer temperature profiles of refrigerant and secondary fluid in the heat exchangers (evaporator and gas coolers) can result in an increase of the thermal conductance (UA) of the device (Figure 2.5). Thus, there is a practical penalty for promoting COP — by using mixture-glide to match temperature profiles in the heat exchanger — which is a larger surface is required for the device or greater heat transfer coefficient (UA).

The CO_2-rich mixtures achieved the highest $\dot{Q}_{heat}/(UA)_{total}$ values at the lowest heat source temperature and higher space heating demands ($r_{heat} = 10$). In contrast to the performance analysis of Subsection 4.2.1, where CO_2-rich mixtures performed poorly, the evaluation based on the $\dot{Q}_{heat}/(UA)_{total}$ criteria allows CO_2-rich mixtures to be more competitive.

In summary, adding CO_2 to mixtures can reduce COP, especially at low-temperature heat sources. In colder climates (below -5 °C), mixtures with 10% CO_2, like R32, R410A, and R290, perform better. CO_2-rich mixtures maintain lower pressure ratios, improving efficiency. Refrigerant-rich mixtures need more compressor volume to produce the same heat as CO_2-rich ones. Using mixture-glide to match temperatures can boost COP but requires a larger surface area or higher heat transfer coefficient (UA). CO_2-rich mixtures achieve the highest $\dot{Q}_{heat}/(UA)_{total}$ values at lower heat source temperatures and for higher space heating demands.

5 CONCLUSIONS

This master thesis aimed to analyzed refrigerant mixtures composed by CO_2 and low-GWP fluids performing in a heat pump system dedicated to space heating and domestic hot water.

This master thesis proposed a new thermodynamic analysis of the use of low-GWP refrigerant mixtures, more specifically CO_2-binary mixtures, for heating plants dedicated to water and space heating. Through a thermodynamic model, several heat pump configurations, heat demands and heat source temperatures were presented and thoroughly discussed. Based on the above, this work proposed and collaborated in two aspects: combined heat pump analysis focused on (i) cycle configuration, type of secondary refrigerant, heat demand and CO_2 mass fraction, (ii) reduced evaporating temperatures and plant scale.

i. Thermodynamic analysis explored the use of CO_2-binary mixtures with low-GWP refrigerants and the effects of mixture composition and heat demand. Three system configurations were considered (AB, BC, and ABC) based on the number of gas coolers used in each cycle. Configuration AB uses a low-temperature gas cooler for domestic hot water and a high-temperature gas cooler for space heating, while configuration BC is the opposite. In configuration ABC, the low-temperature gas cooler preheats water for the high-temperature gas cooler, while an intermediate temperature gas cooler rejects heat to the space. For the AB configuration, pure fluids perform better when the space to water heating ratio (r_{heat}) is equal to or greater than 1. However, for higher demands of domestic hot water (low r_{heat}), the COP of the heat pump is higher when using mixtures, indicating the benefit of using them. In the second configuration, BC, the COP varies with the CO_2 mass fraction in an M-shaped pattern. The best performances are achieved for mass fractions of 10% and 90%, while the worst performances are achieved for roughly 50%. This behavior illustrates that moderate glide can improve the heat pump performance up to a certain point. Unlike cycle AB, all r_{heat} values benefit from using mixtures to some extent, and the highest COP values are obtained in cycles that focus on space heating (high r_{heat}). Lastly, configuration ABC shows the highest range of COP, which is coherent since it is a combination of the two previous configurations. Additionnaly, similar to configuration BC, configuration ABC shows that binary mixtures can improve the COP for all r_{heat} values for, at least, one mass fraction of CO_2 in the refrigerant mixture. Regarding it, two groups with enhanced performance were identified: the first one composed of mixtures of roughly 90% CO_2 and 10% of R41, R1234yf, R1270, or R290, which is recommended for low r_{heat} values: the second one composed of mixtures of approximately 10% CO_2 and 90% R1270, R290, or R152a which is indicated for high demands of space heating. In addition, mixtures

with CO_2 mass fractions of 0.1 or 0.9 have greater thermal conductance properties in the heat exchangers, indicating a multi-objective optimization for increasing the COP and decreasing thermal conductance as future work.

ii. In addition to the exploratory study about mixture composition effects and cycle configurations, a complementary study was conducted to investigate the impact of heat source temperature on combined heat pumps. The performance analysis showed that adding CO_2 can reduce COP, especially at low-temperature heat sources. In contrast to the previous study, where CO_2-rich mixtures demonstrated improved COP values for heat demands focused on water heating, mixtures with higher CO_2 content outperformed their counterparts only at conditions of higher heat source temperatures (5/0 and 0/-5 °C) and lower r_{heat} (0.1 and 0.5). Therefore, in cold climate regions with mean temperatures around 0 °C that require hot water production, CO_2-rich mixtures can enhance system efficiency. However, in even colder climate conditions (below -5 ° C), refrigerant-rich mixtures with 10% (mass basis) of CO_2 have better performance, especially those composed by R32, followed by R410A and R290. The results also showed that, in terms of space heating requirements, refrigerant-rich mixtures with CO_2 mass fractions of 10% (mass basis) yield improved COP values for all heat source temperatures investigated. The results also showed that the heat source temperature strongly impacts the suction pressure and pressure ratio. CO_2-rich mixtures were able to maintain lower pressure ratio compared to all other mixtures and the baseline operation with R410A. Additionally, a volumetric analysis of the heat pump capacity showed that refrigerant-rich mixtures require more swept volume from the compressor to produce the same heat than CO_2-rich mixtures. The impact of the size of the heat exchanger on the performance of the heat pump was also considered. The analysis showed that using mixture-glide to match temperature profiles increase the COP, but demands larger surface area or a greater heat transfer coefficient (UA). Furthermore, CO_2-rich mixtures achieved the highest $\dot{Q}_{heat}/(UA)_{total}$ values at the lowest heat source temperature and for higher space heating demands, making them more competitive when evaluated based on the $\dot{Q}_{heat}/(UA)_{total}$ criterion.

In summary, this study has offered valuable theoretical insights into the utilization of refrigerant mixtures in heat pumps. Nevertheless, it is imperative to acknowledge the inherent limitations in the approach employed. Several simplifying assumptions, such as a fixed refrigerant mass flow rate, were made to facilitate the parametrical optimizations and assessments conducted. Although these assumptions were regarded as crucial for laying the theoretical groundwork of the research, they might not entirely address the details present in real-world heat pump systems, which introduce added complexity through factors such as variable refrigerant mass flow rates and fluctuating heat source temperatures.

Furthermore, phenomena like frost formation on cold surfaces were not addressed in-depth within this study. The study recognizes that the design of heat pumps for extreme conditions, such as a heat source temperature of -25 °C, may not align with practical considerations, as such conditions are rarely sustained over extended periods. Nonetheless, this research offers valuable insights within the defined scope of these limitations.

5.1 FUTURE WORKS

This master thesis highly suggests that future efforts should be directed towards developing additional objective functions, in addition to COP. As demonstrated in this study, heat pump performance (COP) and thermal conductance (UA) are two competing factors; thus, a multi-objective optimization approach that considers both of these metrics could be performed. Furthermore, a cost analysis would provide valuable insight for the preliminary analysis performed in this work, which could be incorporated to a multi-criterion analysis that considers cost, performance, and environmental impact (GPW) with reasonable weights for each objective, helping the decision-making process of heat pump design.

BIBLIOGRAPHY

ANDRESEN, T. **Mathematical modeling of CO_2 based heat pumping systems**. 1-150 p. Thesis (phd) — Norwegian University of Science and Technology, 2009.

AUSTIN, B. T.; SUMATHY, K. Transcritical carbon dioxide heat pump systems: A review. **Renewable and Sustainable Energy Reviews**, v. 15, p. 4013–4029, 10 2011. ISSN 13640321. Available from Internet: <https://linkinghub.elsevier.com/retrieve/pii/S1364032111002607>.

BAHMAN, A. M.; PARIKHANI, T.; ZIVIANI, D. Multi-objective optimization of a cold-climate two-stage economized heat pump for residential heating applications. **Journal of Building Engineering**, Elsevier Ltd, v. 46, p. 103799, 4 2022. ISSN 23527102. Available from Internet: <https://linkinghub.elsevier.com/retrieve/pii/S2352710221016570>.

BATTISTI, F. G.; CARDEMIL, J. M.; MILLER, F. M.; SILVA, A. K. da. Normalized performance optimization of supercritical, CO_2-based power cycles. **Energy**, Elsevier Ltd, v. 82, p. 108–118, 3 2015. ISSN 03605442. Available from Internet: <https://linkinghub.elsevier.com/retrieve/pii/S0360544215000122>.

BEJAN, A. **Shape and Structure: From Engineering to Nature**. [S.l.]: Cambridge University Press, 2000.

BEJAN, A. **Advanced Engineering Thermodynamics**. 3. ed. [S.l.]: John Wiley & Sons, 2006. ISBN 0471677639.

BELL, I. H.; WRONSKI, J.; QUOILIN, S.; LEMORT, V. Pure and pseudo-pure fluid thermophysical property evaluation and the open-source thermophysical property library coolprop. **Industrial & Engineering Chemistry Research**, v. 53, p. 2498–2508, 2 2014. ISSN 0888-5885. Available from Internet: <https://pubs.acs.org/doi/10.1021/ie4033999>.

BOBBO, S.; FEDELE, L.; CURCIO, M.; BET, A.; CARLI, M. D.; EMMI, G.; POLETTO, F.; TARABOTTI, A.; MENDRINOS, D.; MEZZASALMA, G.; BERNARDI, A. Energetic and exergetic analysis of low global warming potential refrigerants as substitutes for R410A in ground source heat pumps. **Energies**, MDPI AG, v. 12, p. 3538, 9 2019. ISSN 1996-1073. Available from Internet: <https://www.mdpi.com/1996-1073/12/18/3538>.

BRODAL, E.; JACKSON, S. A comparative study of CO_2 heat pump performance for combined space and hot water heating. **International Journal of Refrigeration**, Elsevier Ltd, v. 108, p. 234–245, 12 2019. ISSN 01407007. Available from Internet: <https://linkinghub.elsevier.com/retrieve/pii/S0140700719303688>.

ÇENGEL, Y. A.; BOLES, M. A. **Termodinâmica**. 7. ed. [S.l.]: McGraw Hill, 2013. -1080 p. ISBN 9788580552003.

CHANG, Y.; KIM, M.; RO, S. Performance and heat transfer characteristics of hydrocarbon refrigerants in a heat pump system. **International Journal of Refrigeration**, v. 23, p. 232–242, 5 2000. ISSN 01407007. Available from Internet: <https://linkinghub.elsevier.com/retrieve/pii/S0140700799000420>.

CHEN, Y.; GU, J. The optimum high pressure for CO_2 transcritical refrigeration systems with internal heat exchangers. **International Journal of Refrigeration**, v. 28, p. 1238–1249, 12 2005. ISSN 01407007.

CUBE, H. L. von.; STEIMLE, F.; GOODALL, E. G. A. **Heat pump technology**. [S.l.]: Butterworths, 1981. 379 p. ISBN 0408004975.

DAI, B.; DANG, C.; LI, M.; TIAN, H.; MA, Y. Thermodynamic performance assessment of carbon dioxide blends with low-global warming potential (gwp) working fluids for a heat pump water heater. **International Journal of Refrigeration**, v. 56, p. 1–14, 8 2015. ISSN 01407007.

DAI, B.; LI, M.; MA, Y. Thermodynamic analysis of carbon dioxide blends with low gwp (global warming potential) working fluids-based transcritical rankine cycles for low-grade heat energy recovery. **Energy**, v. 64, p. 942–952, 1 2014. ISSN 03605442.

EUROSTAT. **Energy consumption in households Statistics Explained**. 2022. Available from Internet: <https://ec.europa.eu/eurostat/statistics-explained/index.php?title=Energy_consumption_in_households#Energy_consumption_in_households_by_type_of_end-use>.

GOSNEY, W. B. **Principles of Refrigeration**. 1. ed. [S.l.]: Cambridge University Press, 1982.

GRASSI, W. **Heat Pumps**. Springer International Publishing, 2018. ISBN 978-3-319-62198-2. Available from Internet: <http://link.springer.com/10.1007/978-3-319-62199-9>.

HAKKAKI-FARD, A.; AIDOUN, Z.; OUZZANE, M. Applying refrigerant mixtures with thermal glide in cold climate air-source heat pumps. **Applied Thermal Engineering**, v. 62, p. 714–722, 1 2014. ISSN 13594311.

HAKKAKI-FARD, A.; AIDOUN, Z.; OUZZANE, M. Improving cold climate air-source heat pump performance with refrigerant mixtures. **Applied Thermal Engineering**, v. 78, p. 695–703, 3 2015. ISSN 13594311.

HALL, W. Heat transfer near the critical point. p. 1–86, 1971. Available from Internet: <https://linkinghub.elsevier.com/retrieve/pii/S0065271708700169>.

HUNDY, G. F.; TROTT, A. R.; WELCH, T. C. **REFRIGERATION, AIR CONDITIONING AND HEAT PUMPS**. 5. ed. [S.l.]: Butterworth-Heinemann, 2016. ISBN 978-0-08-100647-4.

IEA. **Key World Energy Statistics 2021**. 2021. Available from Internet: <https://www.iea.org/reports/key-world-energy-statistics-2021>.

IEA. **World Energy Outlook Special Report: The Future of Heat Pumps**. 2022. Available from Internet: <www.iea.org>.

IEA. CO_2 emissions in 2022. **IEA Publications**, 2023.

JU, F.; FAN, X.; CHEN, Y.; OUYANG, H.; KUANG, A.; MA, S.; WANG, F. Experiment and simulation study on performances of heat pump water heater using blend of R744/R290. **Energy and Buildings**, v. 169, p. 148–156, 6 2018. ISSN 03787788.

KIM, M. Fundamental process and system design issues in CO_2 vapor compression systems. **Progress in Energy and Combustion Science**, Elsevier Ltd, v. 30, p. 119–174, 2004. ISSN 03601285. Available from Internet: <https://linkinghub.elsevier.com/retrieve/pii/S0360128503000765>.

LECOMPTE, S.; NTAVOU, E.; TCHANCHE, B.; KOSMADAKIS, G.; PILLAI, A.; MANOLAKOS, D.; PAEPE, M. D. Review of experimental research on supercritical and transcritical thermodynamic cycles designed for heat recovery application. **Applied Sciences**, MDPI, v. 9, n. 12, p. 2571, 2019.

LEMMON, E. W.; HUBER, M. L.; MCLINDEN, M. O. Nist standard reference database 23: Reference fluid thermodynamic and transport properties-refprop, version 9.1. **Standard Reference Data Program, Gaithersburg**, National Institute of Standards and Technology (NIST), 2013. Available from Internet: <https://tsapps.nist.gov/publication/get_pdf.cfm?pub_id=912382>.

LIU, R.; GAO, F.; LIANG, K.; WANG, L.; WANG, M.; MI, G.; LI, Y. Thermodynamic evaluation of transcritical co 2 heat pump considering temperature matching under the constraint of heat transfer pinch point. **Journal of Thermal Science**, Springer, v. 30, p. 869–879, 2021.

LORENTZEN, G. Revival of carbon dioxide as a refrigerant. **International Journal of Refrigeration**, v. 17, p. 292–301, 1 1994. ISSN 01407007. Available from Internet: <https://linkinghub.elsevier.com/retrieve/pii/0140700794900590>.

MATLAB. **MATLAB version 9.7.0.1319299 (R2019b)**. [S.l.]: The MathWorks Inc., 2019.

MONTAGNER, G. P. **Um estudo da aplicação de ciclos transcríticos de CO_2**. Thesis (phd) — Federal University of Santa Catarina, 2013.

MUZAYANAH, I. F. U.; LEAN, H. H.; HARTONO, D.; INDRASWARI, K. D.; PARTAMA, R. Population density and energy consumption: A study in indonesian provinces. **Heliyon**, v. 8, p. e10634, 9 2022. ISSN 24058440.

NEKSÅ, P. CO_2 heat pump systems. **International Journal of Refrigeration**, v. 25, p. 421–427, 6 2002. ISSN 01407007. Available from Internet: <https://linkinghub.elsevier.com/retrieve/pii/S0140700701000330>.

NELLIS, G.; KLEIN, S. A. **Heat transfer**. [S.l.]: Cambridge University Press, 2009. 1107 p. ISBN 9780521881074.

OLIVEIRA, R. N. de. **MODELO DINÂMICO E ESTUDO EXPERIMENTAL PARA UM RESFRIADOR DE UMA BOMBA DE CALOR OPERANDO COM CO_2 PARA AQUECIMENTO DE ÁGUA RESIDENCIAL**. 2013. 1-111 p. Available from Internet: <www.demec.ufmg.br>.

PAN, L.; WANG, H.; CHEN, Q.; CHEN, C. Theoretical and experimental study on several refrigerants of moderately high temperature heat pump. **Applied Thermal Engineering**, v. 31, p. 1886–1893, 8 2011. ISSN 13594311. Available from Internet: <https://linkinghub.elsevier.com/retrieve/pii/S1359431111001165>.

RADERMACHER, R.; HWANG, Y. **Vapor compression heat pumps with refrigerant mixes**. [S.l.]: Taylor & Francis, 2005. 307 p. ISBN 0849334896.

SÁNCHEZ, C. J.; SILVA, A. K. da. Technical and environmental analysis of transcritical rankine cycles operating with numerous CO_2 mixtures. **Energy**, v. 142, p. 180–190, 1 2018. ISSN 03605442.

SÁNCHEZ, C. J. N. *et al.* Análise de misturas de fluidos orgânicos e dióxido de carbono para aplicação em ciclos de potência. 2018.

SARKAR, J. Optimization of ejector-expansion transcritical CO_2 heat pump cycle. **Energy**, v. 33, p. 1399–1406, 9 2008. ISSN 03605442.

SENGUPTA, M.; XIE, Y.; LOPEZ, A.; HABTE, A.; MACLAURIN, G.; SHELBY, J. The national solar radiation data base (nsrdb). **Renewable and Sustainable Energy Reviews**, v. 89, p. 51–60, 6 2018. ISSN 13640321.

STENE, J. Residential CO_2 heat pump system for combined space heating and hot water heating. **International Journal of Refrigeration**, v. 28, p. 1259–1265, 12 2005. ISSN 01407007. Available from Internet: <https://linkinghub.elsevier.com/retrieve/pii/S0140700705001775>.

STENE, J. Integrated co2 heat pump systems for space heating and hot water heating in low-energy houses and passive houses. **International Energy Agency (IEA) Heat Pump Programme–Annex**, Citeseer, v. 32, 2007.

SUN, X.; WU, J.; WANG, R. Exergy analysis and comparison of multi-functional heat pump and conventional heat pump systems. **Energy conversion and management**, Elsevier, v. 73, p. 51–56, 2013.

WANG, D.; LIU, Y.; KOU, Z.; YAO, L.; LU, Y.; TAO, L.; XIA, P. Energy and exergy analysis of an air-source heat pump water heater system using CO_2/r170 mixture as an azeotropy refrigerant for sustainable development. **International Journal of Refrigeration**, Elsevier Ltd, v. 106, p. 628–638, 10 2019. ISSN 01407007. Available from Internet: <https://linkinghub.elsevier.com/retrieve/pii/S0140700719301069>.

XU, Y.; MAO, C.; HUANG, Y.; SHEN, X.; XU, X.; CHEN, G. Performance evaluation and multi-objective optimization of a low-temperature CO_2 heat pump water heater based on artificial neural network and new economic analysis. **Energy**, Elsevier Ltd, v. 216, p. 119232, 2 2021. ISSN 03605442. Available from Internet: <https://linkinghub.elsevier.com/retrieve/pii/S0360544220323392>.

YAN, L. **China Energy Efficiency Report**. 1. ed. [S.l.: s.n.], 2018. ISBN 9789059482036.

YU, J.; XU, Z.; TIAN, G. A thermodynamic analysis of a transcritical cycle with refrigerant mixture r32/R290 for a small heat pump water heater. **Energy and Buildings**, v. 42, p. 2431–2436, 12 2010. ISSN 03787788. Available from Internet: <https://linkinghub.elsevier.com/retrieve/pii/S0378778810002914>.

ZHANG, X.; WANG, F.; FAN, X.; DUAN, H.; ZHU, F. An investigation of a heat pump system using co/propane mixture as a working fluid. **International Journal of Green Energy**, Taylor and Francis Inc., v. 14, p. 105–111, 1 2017. ISSN 1543-5075. Available from Internet: <https://www.tandfonline.com/doi/full/10.1080/15435075.2016.1253577>.

Appendix

APPENDIX A – ILLUSTRATIVE SAMPLE CALCULATION

To provide further insights into the optimization process described in Section 3.1.4, a step-by-step calculation for the optimized cycles (AB, BC, and ABC) was conducted.

A.1 AB CYCLE

The flowchart outlining the calculation process for cycle AB is presented in Figure A.1.

This calculation begins with the specification of fixed input variables, as outlined in Table 3.3. These variables comprehensively define a specific operational condition for the combined heat pump:

- **Inputs:**
  $Refrigerant = R410A$, $\dot{x}_{CO_2}$ =0, $\dot{m}_{ref} = 1 kgs^{-1}$, $\eta_{isen} = 0.7$, $r_{heat} = 0.5$, $PP_{allowed} = 5$°C, $T_a = = 10$°C, $T_c = 65$ °C, $T_d = 30$ °C, $T_e = 35$ °C, $T_{hs,in} = 10$ °C, $T_{hs,out} = 5$°C

Subsequently, the suction and discharge pressures, along with the gas cooler outlet temperature (T_4) are specified. These parameters significantly influence heat pump performance and define thermodynamic states #1, #2, and #4:

- State #1: $p_{low} = 800.5$ kPa & x_1=1 $\rightarrow i_1 = 421.4$ kJ/kg, $s_1 = 1.8$ kJ/kgK, $T_1 = 0$ °C
- State #2: $p_{high} = 4681.7$ kPa & $\eta_{isen} = 0.7 \rightarrow i_{2,isen} = i_2(p_{high}, s_2 = s_1)$, $i_2 = i_1 + \dfrac{(i_{2,isen} - i_1)}{\eta_{isen}} = 491.3$ kJ/kg, $s_2 = 1.9$ kJ/kgK, $T_2 = 112$ °C
- State #4: $T_4 = 15$ °C & $p_{high} \rightarrow i_4 = 264.0$ kJ/kg, $s_4 = 1.2$ kJ/kgK

The thermodynamic state #3 and the performance characteristics of gas coolers A and B can be determined once the heat distribution, denoted as r_{heat} in the inputs, is specified:

- $r_{heat} = 0.5$ & $\dot{Q}_{heat} = \dot{m}_{ref}\,(i_2 - i_4) = 487.3$ kW $\rightarrow \dot{Q}_B = \left(\dfrac{r_{heat}}{1 + r_{heat}}\right) \dot{Q}_{heat} = 75.7$ kW, $\dot{Q}_A = \dot{Q}_{heat} - \dot{Q}_B = 151.5$ kW
- State #3: $i_3 = i_2 - \dfrac{\dot{Q}_B}{\dot{m}_{ref}} = 415.6$ kJ/kg, $s_3 = 1.66$ kJ/kgK, $T_3 = 72.5$ °C

With an isenthalpic expansion device in place, we can calculate thermodynamic state #5 and evaluate the evaporator's performance:

- State #5: $i_5 = i_4 = 264.0$ kJ/kg, $s_5 = 1.23$ kJ/kgK, $T_5 = 0$ °C

- $\dot{Q}_{evap} = \dot{m}_{ref}\,(i_1 - i_5) = 157.4$ kW

Next, we employ a discretization process along the length of each heat exchanger, as outlined in Section 2.2.4, to determine the pinch point temperature difference and the total thermal conductance (UA) of the heat exchangers within the cycle:

- $PP_B = 42.5$ °C
- $PP_A = 7.5$ °C
- $PP_{evap} = 5$ °C
- $UA_B = 1.4$ kW/K
- $UA_A = 7.2$ kW/K
- $UA_{evap} = 21.9$ kW/K

The maximum COP value, as illustrated in Figure 3.6d for the AB cycle with R410A under the heating condition of $r_{heat} = 0.5$, is achieved with $p_{low} = 800.5$ kPa, $p_{high} = 4681.7$ kPa and $T_4 = 15$ °C. Consequently, the optimization of cycle AB is conducted for the set of independent variables (p_{low}, p_{high} and T_3) that maximizes the COP. These results, along with other data for the AB reference cycle with R410A, can be found in Figure A.2.

- $\text{COP} = \dfrac{\dot{Q}_{heat}}{\dot{Q}_{evap}} = \dfrac{i_2 - i_4}{(i_2 - i_4) - (i_1 - i_5)} = 3.84$

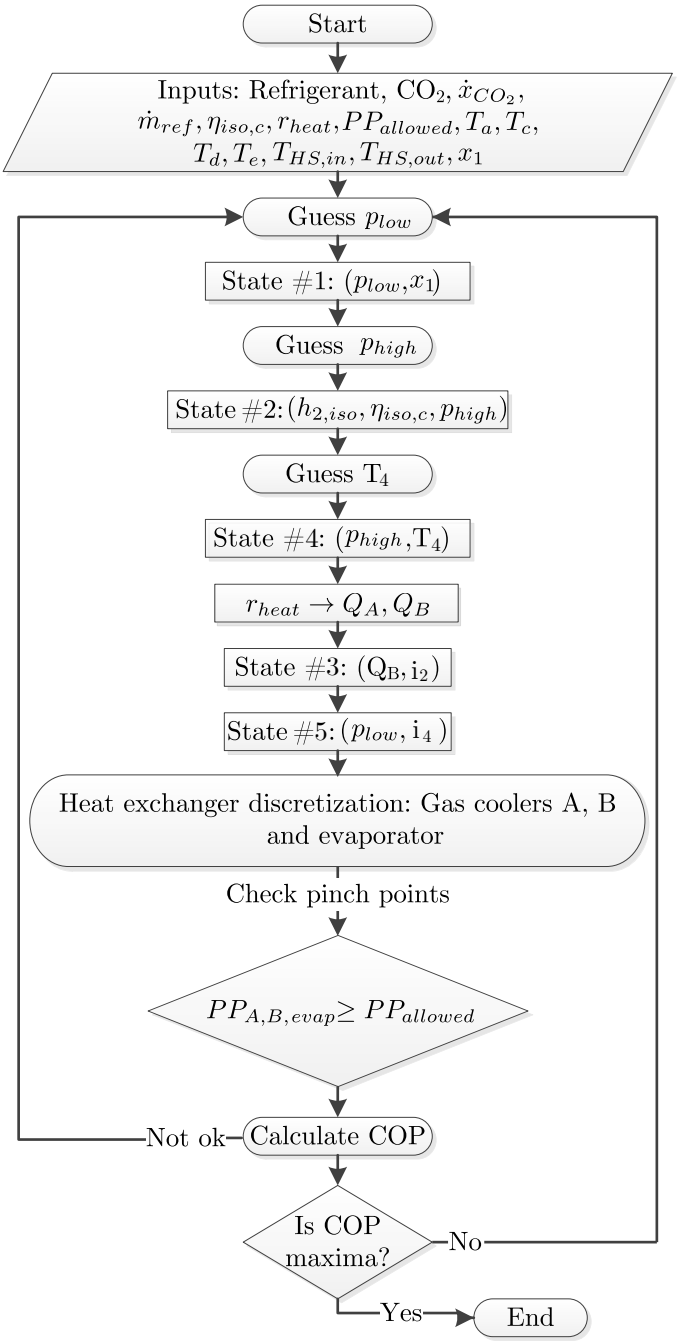

Figure A.1 – Flowchart for the Combined AB cycle displayed in Figure 3.2a.

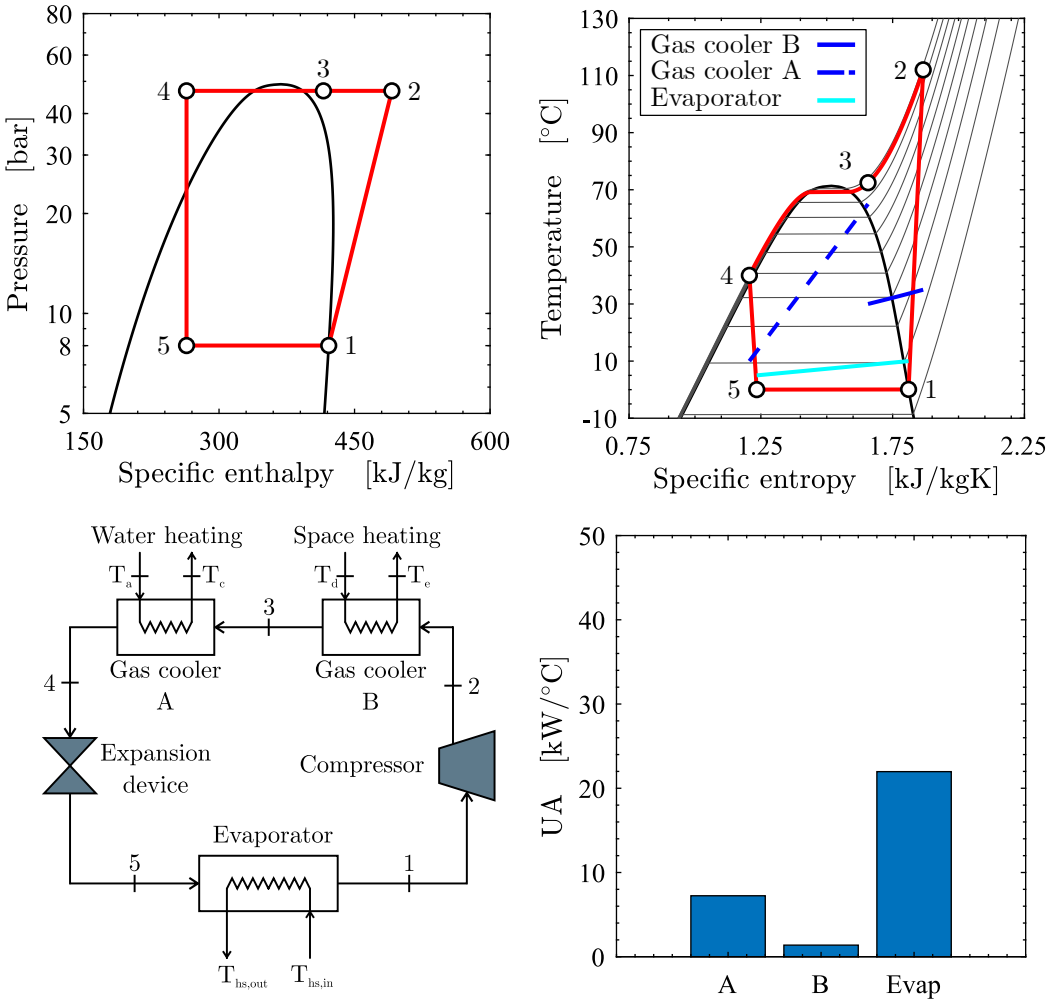

Figure A.2 – Optimized AB cycle for R410A operation.

A.2 BC CYCLE

Figure A.3 illustrates the flowchart of the calculation procedure for cycle BC.

The calculation procedure initiates with the specification of input variables, as referenced in Table 3.3. These parameters remain constant throughout the optimization process, fully defining the specific operating condition for the combined heat pump:

- **Inputs:**
  $Refrigerant = R410A$, $\dot{x}_{CO_2}$ =0, $\dot{m}_{ref} = 1kgs^{-1}$, $\eta_{isen} = 0.7$, $r_{heat} = 0.5$, $PP_{allowed} = 5$°C, $T_a = = 10$°C, $T_c = 65$ °C, $T_d = 30$ °C, $T_e = 35$ °C, $T_{hs,in} = 10$ °C, $T_{hs,out} = 5$°C

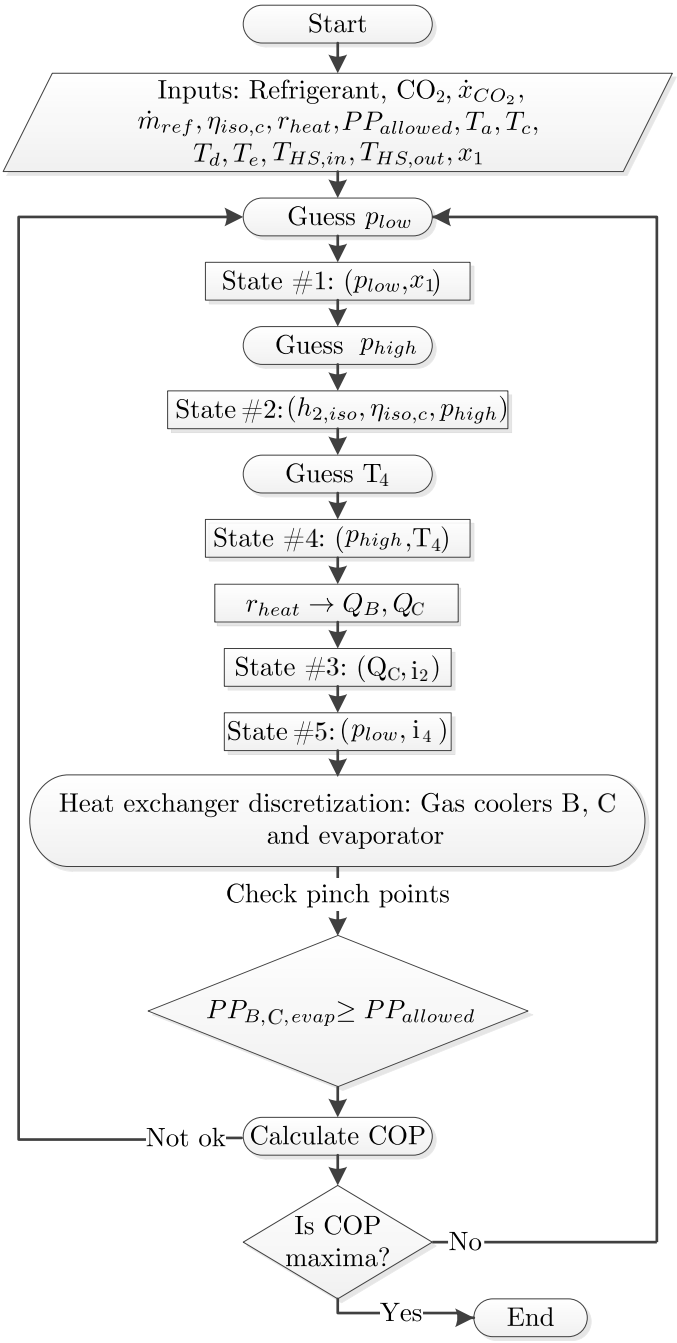

Figure A.3 – Flowchart for the Combined BC cycle displayed in Figure 3.2b.

Subsequently, we determine suction and discharge pressures, along with the gas cooler outlet temperature (T_4), allowing to define states #1, #2, and #4 accordingly:

- State #1: p_{low} = 800.1 kPa & x_1=1 $\rightarrow$ i_1 = 421.4 kJ/kg, s_1 = 1.8 kJ/kgK, T_1 = 0 °C
- State #2: p_{high} = 3071.9 kPa & η_{isen} = 0.7 $\rightarrow$ $i_{2,isen} = i_2(p_{high}, s_2 = s_1)$, $i_2 = i_1 + \dfrac{(i_{2,isen} - i_1)}{\eta_{isen}}$ = 474.1 kJ/kg, s_2 = 1.85 kJ/kgK, T_2 = 83 °C

- State #4: $T_4 = 35$ °C & $p_{high} \rightarrow i_4 = 256.4$ kJ/kg, $s_4 = 1.2$ kJ/kgK

By specifying the space to water heating ratio (r_{heat}) as part of the inputs, we can calculate thermodynamic state #3 and assess the performance of gas coolers B and C:

- $r_{heat} = 0.5$ & $\dot{Q}_{heat} = \dot{m}_{ref}\,(i_2 - i_4) = 217.7$ kW $\rightarrow \dot{Q}_B = \left(\dfrac{r_{heat}}{1 + r_{heat}}\right) \dot{Q}_{heat} = 72.6$ kW, $\dot{Q}_C = \dot{Q}_{heat} - \dot{Q}_B = 145.2$ kW
- State #3: $i_3 = i_2 - \dfrac{\dot{Q}_B}{\dot{m}_{ref}} = 401.5$ kJ/kg, $s_3 = 1.64$ kJ/kgK, $T_3 = 50.1$ °C

Upon considering the expansion device as isenthalpic, we can calculate thermodynamic state #5 and evaluate the evaporator's performance:

- State #5: $i_5 = i_4 = 256.4$ kJ/kg, $s_5 = 1.21$ kJ/kgK, $T_5 = 0$ °C
- $\dot{Q}_{evap} = \dot{m}_{ref}\,(i_1 - i_5) = 165.0$ kW

We then move on to a discretization process for each heat exchanger length, as outlined in Section 2.2.4, enabling us to determine the pinch point temperature difference and to calculate (UA) for each heat exchanger within the cycle:

- $PP_C = 5.0$ °C
- $PP_B = 15.1$ °C
- $PP_{evap} = 5.0$ °C
- $UA_C = 11.7$ kW/K
- $UA_B = 4.1$ kW/K
- $UA_{evap} = 23.0$ kW/K

Therefore, the optimization of cycle BC — previously as illustrated in Figure 3.9d — regarding the coefficient of performance yields:

- $\text{COP} = \dfrac{\dot{Q}_{heat}}{\dot{Q}_{evap}} = \dfrac{i_2 - i_4}{(i_2 - i_4) - (i_1 - i_5)} = 4.13$

Additional results for the reference cycle with R410A can be found in Figure A.4.

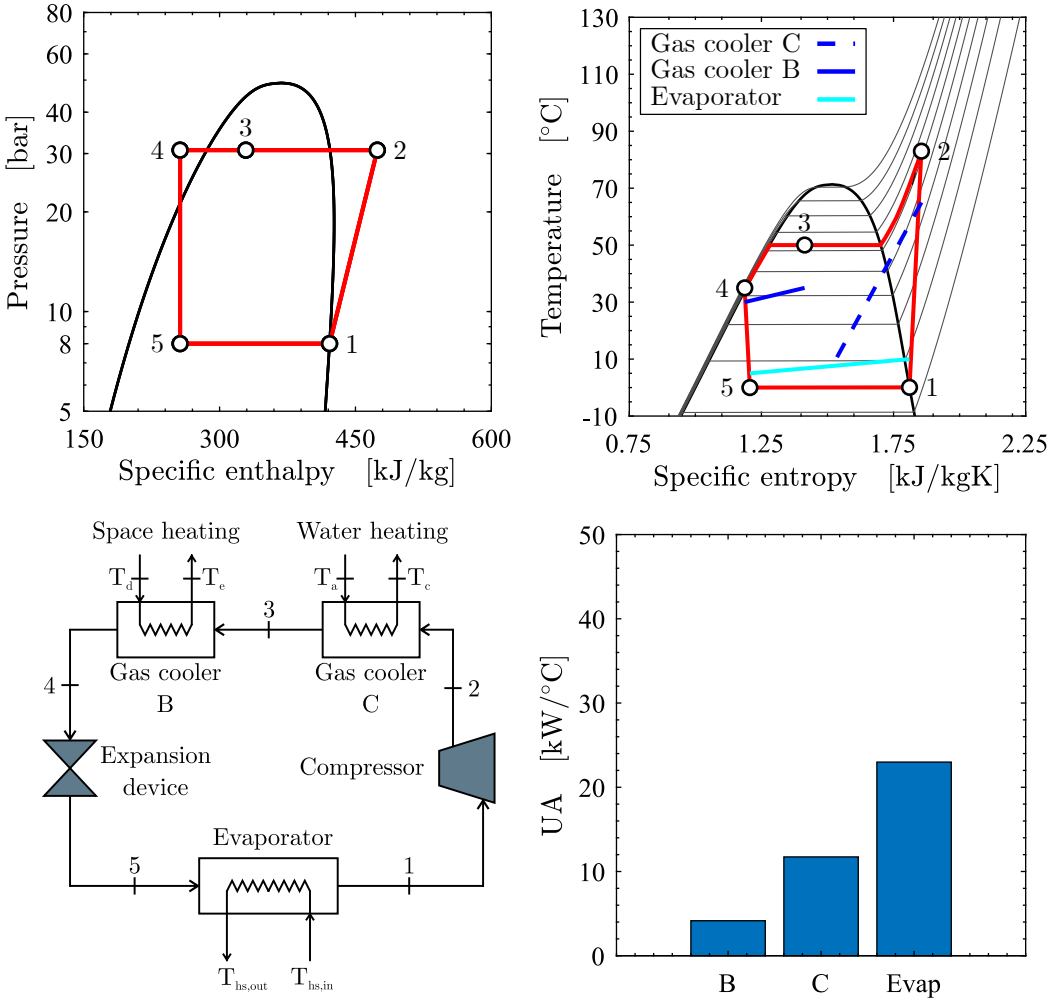

Figure A.4 – Optimized BC cycle for R410A operation.

A.3 ABC CYCLE

The calculation process flowchart for cycle ABC was previously presented in Figure 3.3. The calculation initiates with the specification of fixed input variables, as referenced in Table 3.3. These variables completely define a given operating condition for the combined heat pump:

- **Inputs:**
  $Refrigerant = R410A$, $\dot{x}_{CO_2}$ =0, $\dot{m}_{ref} = 1 kgs^{-1}$, $\eta_{isen} = 0.7$, $r_{heat} = 0.5$, $PP_{allowed} = 5$°C, $T_a = = 10$°C, $T_c = 65$ °C, $T_d = 30$ °C, $T_e = 35$ °C, $T_{hs,in} = 10$ °C, $T_{hs,out} = 5$°C

Following this, suction and discharge pressures, along with the gas cooler outlet temperature (T_5), must be determined:

- State #1: $p_{low} = 800.5$ kPa & x_1=1 $\rightarrow i_1 = 421.4$ kJ/kg, $s_1 = 1.8$ kJ/kgK, $T_1 = 0$ °C

- State #2: p_{high} = 3379.9 kPa & $\eta_{isen} = 0.7 \rightarrow i_{2,isen} = i_2(p_{high}, s_2 = s_1)$, $i_2 = i_1 + \dfrac{(i_{2,isen} - i_1)}{\eta_{isen}} = 478.0$ kJ/kg, $s_2 = 1.86$ kJ/kgK, $T_2 = 89.4$ °C
- State #5: $T_5 = 15$ °C & $p_{high} \rightarrow i_5 = 223.0$ kJ/kg, $s_5 = 1.1$ kJ/kgK
- $\dot{Q}_{heat} = \dot{m}_{ref}\,(i_2 - i_5) = 254.9$ kW

Thermodynamic state #3 hinges on specifying the gas cooler C outlet temperature (T_3), which affects $\dot{Q}_C$, and subsequently, $\dot{Q}_A$ and $\dot{Q}_B$, considering that r_{heat} is already set:

- State #3: $T_3 = 54.3$ °C & $p_{high} \rightarrow i_3 = 421.8$ kJ/kg, $s_3 = 1.7$ kJ/kgK
- $\dot{Q}_C = \dot{m}_{ref}\,(i_2 - i_3) = 56.1$ kW
- r_{heat} =0.5 & $\dot{Q}_{heat} \rightarrow \dot{Q}_B = \left(\dfrac{r_{heat}}{1 + r_{heat}}\right)\dot{Q}_{heat} = 85.0$ kW
- $\dot{Q}_A = \dot{Q}_{heat} - \left(\dot{Q}_B + \dot{Q}_C\right) = 113.8$ kW
- State #4: $i_4 = i_3 - \dfrac{\dot{Q}_B}{\dot{m}_{ref}} = 336.9$ kJ/kg, $s_4 = 1.4$ kJ/kgK, $T_4 = 54.2$ °C

Considering an expansion device as isenthalpic the thermodynamic state #6 and the evaporator performance can be calculated:

- State #6: $i_6 = i_5 = 223.0$ kJ/kg, $s_6 = 1.08$ kJ/kgK, $T_6 = 0$ °C
- $\dot{Q}_{evap} = \dot{m}_{ref}\,(i_1 - i_6) = 198.4$ kW

Next, a discretization process is performed along the length of each heat exchanger to obtain the pinch point temperature difference and to determine (UA) for each of the heat exchangers within the cycle:

- $PP_C = 8.5$ °C
- $PP_B = 19.3$ °C
- $PP_A = 5.0$ °C
- $PP_{evap} = 5.0$ °C
- $UA_C = 4.2$ kW/K
- $UA_B = 3.9$ kW/K
- $UA_B = 9.0$ kW/K
- $UA_{evap} = 27.6$ kW/K

The maximal COP value, as depicted in Figure 3.10d for the ABC cycle using R410A at the heating condition of $r_{heat} = 0.5$, is achieved when $p_{low} = 800.1$ kPa, $p_{high} = 3071.9$ kPa, $T_3 = 54.3$ °C and $T_5 = 35$ °C. In Figure A.5, the optimization of cycle ABC is demonstrated for the set of independent variables that maximizes COP, alongside other results for the reference cycle with R410A.

- $\text{COP} = \dfrac{\dot{Q}_{heat}}{\dot{Q}_{evap}} = \dfrac{i_2 - i_5}{(i_2 - i_5) - (i_1 - i_6)} = 4.50$

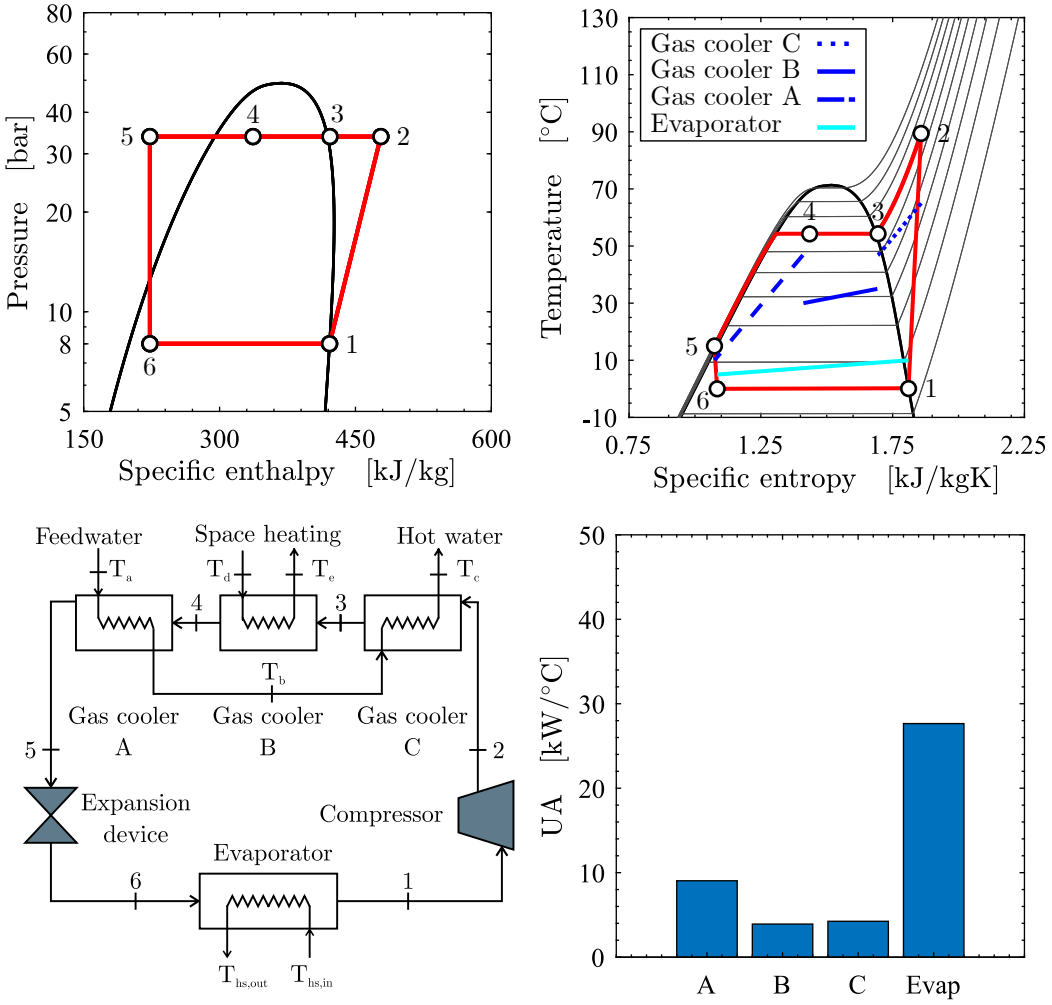

Figure A.5 – Optimized ABC cycle for R410A operation.

Following a similar procedure the optmization of ABC cycle operating with pure CO_2 for r_{heat} condition of 0.5 yields a COP of 4.57 (Figure 3.10d). The reference ABC cycle (i.e., the optimized cycle which produces the maximum COP) is presented in more details in Figure A.6. By taking a closer look it is possible to observe how pinch point can occur in the middle of the heat exchanger — in the gas cooler C the pinch point occurs within a temperature difference of 7 °C when CO_2 temperature is approximately 53 °C and the water temperature is 46 °C.

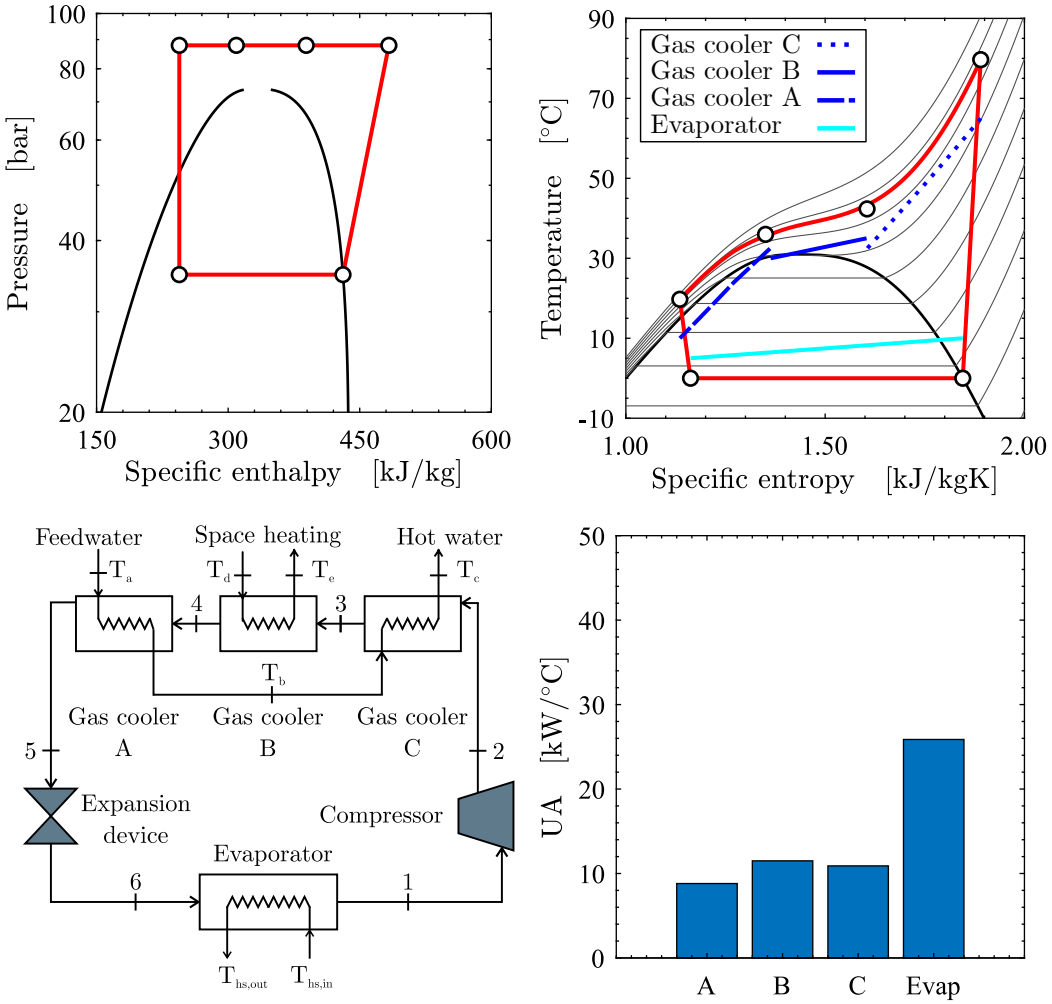

Figure A.6 – Optimized ABC cycle for CO_2 operation.

Therefore, as demonstrated in this appendix using these reference cycles, the singularity of the solution is found in the maximization of COP through the careful selection of the appropriate set of independent variables (p_{low}, p_{high}, T_3 and T_5), which must also satisfy the constraints imposed by the pinch point requirements.